ARCHIVES OF MECHANICS **Appears since 1949**



## Aims and Scope

ARCHIVES OF MECHANICS provides a forum for original research on mechanics of solids, fluids and discrete systems, including the development of mathematical methods for solving mechanical problems. The journal encompasses all aspects of the field, with the emphasis placed on:

- mechanics of materials: elasticity, plasticity, time-dependent phenomena, phase transformation, damage, fracture; physical and experimental foundations, micromechanics, thermodynamics, instabilities
- methods and problems in continuum mechanics: general theory and novel applications, thermomechanics, structural analysis, porous media, contact problems
- dynamics of material systems
- fluid flows and interactions with solids



Address of the Editorial Office:
Institute of Fundamental Technological Research
Świętokrzyska 21
PL 00-049 Warsaw, Poland

Tel.: (48-22) 826 60 22, Fax: (48-22) 826 98 15, E-mail: publikac@ippt.gov.pl

## Abstracted/indexed in:

Applied Mechanics Reviews, Current Mathematical Publications, Mathematical Reviews, MathSci, Zentralblatt für Mathematik, UnCover.

Polish Academy of Sciences

Institute of Fundamental Technological Research



# Archives of Mechanics

## Archiwum Mechaniki Stosowanej

volume 53 issue 1

Agencja Reklamowo-Wydawnicza A. Grzegorczyk
Warszawa 2001

# SUBSCRIPTIONS

Address of the Editorial Office: Archives of Mechanics
Institute of Fundamental Technological Research, Świętokrzyska 21
PL 00-049 Warsaw, Poland
Tel.: (48-22) 826 60 22, Fax: (48-22) 826 98 15, E-mail: publikac@ippt.gov.pl

**Subscription orders for all journals edited by IFTR may be sent directly to the Editorial Office of the Institute of Fundamental Technological Research**

**Subscription rates**

Annual subscription rate (2001) including postage is US $ 210.
Please transfer the subscription fee to our bank account: Payee: IPPT PAN,
Bank: PKO SA. IV O/Warszawa,
Account no: 12401053-40054492-3000-401112-001.

All journals edited by IFTR are available also through:

- Foreign Trade Enterprise ARS POLONA Krakowskie Przedmieście 7, 00-068 Warszawa, Poland fax: (48-22) 826 86 73
- RUCH S.A. ul. Towarowa 28, 00-958 Warszawa, Poland fax:(48-22) 620 17 62
- Agencja Reklamowo-Wydawnicza A. Grzegorczyk, Bitwy Warszawskiej 1920r. 3, 00-973 Warszawa, Poland tel./fax: (48-22) 822 49 36

---

# Warunki prenumeraty

**Redakcja przyjmuje prenumeratę na wszystkie czasopisma wydawane przez IPPT PAN. Bieżące numery można nabyć a także zaprenumerować roczne wydanie Archiwum Mechaniki Stosowanej bezpośrednio w Dziale Wydawnictw IPPT PAN, Świętokrzyska 21, 00-049 Warszawa, Tel.: (48-22) 826 60 22; Fax: (48-22) 826 98 15.**
Cena rocznej prenumeraty z bonifikatą (na rok 2001) dla krajowego odbiorcy wynosi 180 zł

Również można je nabyć, a także zamówić (przesyłka za zaliczeniem pocztowym) we Wzorcowni Ośrodka Rozpowszechniania Wydawnictw Naukowych PAN,
00-818 Warszawa, ul. Twarda 51/55, tel. (48-22) 697 88 35.
Wpłaty na prenumeratę przyjmują także jednostki kolportażowe RUCH S.A. Oddział Krajowej Dystrybucji Prasy, 00-958 Warszawa, ul. Towarowa 28. Konto: PBK.S.A. XIII Oddział Warszawa nr 11101053-16551-2700-1-67. Dostawa odbywa się pocztą zwykłą w ramach opłaconej prenumeraty z wyjątkiem zlecenia dostawy pocztą lotniczą, której koszt w pełni pokrywa zleceniodawca. Tel.: (48-22) 620 10 39, fax: (48-22) 620 17 62

---

Arkuszy wydawniczych 6. Arkuszy drukarskich 7.3/A5.
Papier offset. kl III 70 g. B1.
Oddano do składania w styczniu 2001 r. Druk ukończono w lutym 2001 r.
Skład i łamanie: G. Wasilewska. Druk i oprawa: Drukarnia OMIKRON, Stare Babice ul. Kutrzeby 15.

---

Arch. Mech., **53**, 1, pp. 3–21, Warszawa 2001

# An inhomogeneous variational model applied to predict the behaviour of isotropic polycrystalline ice [1]

O. GAGLIARDINI (*) [1)], M. ARMINJON (**) and D. IMBAULT (**)

(*) *Laboratoire de Glacialogie et Géophysique de l'Environnement, CNRS, UJF-Grenoble I, BP 96, F-38402 Saint-Martin d'Hères cedex, France*

(**) *Laboratoire Sols, Solides, Structures, CNRS, UJF, INPG, Domaine Universitaire, BP 53, F-38041 Grenoble cedex 9, France*

A MODEL FOR THE PREDICTION of the viscoplastic behaviour of polycrystalline ice is presented. This model is based on the minimization of the dissipation energy under the principle of minimal heterogeneity. The grain is supposed to behave as a linear transversely isotropic medium depending on one anisotropy parameter. Anisotropic textures can be considered, but the present numerical results are for an isotropic texture. The model then predicts a linear isotropic behaviour involving an effective viscosity. The latter depends on the prescribed value for the strain-rate heterogeneity and on the grain anisotropy parameter. The present model is compared with a self-consistent model built under the same assumptions for the grain behaviour. The deviation from the no-correlation condition is studied.

## 1. Introduction

IN ORDER TO UNDERSTAND the evolution of the polar ice sheets and their response to climatic changes, it is necessary to build thermomechanical models of the flow of ice sheet under gravity. Due to the large depth, the internal layers of the sheet are subjected to very large compression strains that lead to the development of a strong crystallographic texture (or "fabric") in the polycrystalline ice. Moreover, the anisotropy of the constituent crystals is rather extreme: the rate of creep of a single crystal by basal glide is roughly $10^4$ times faster, at a given stress, than that of a single crystal oriented such that the resolved shear stress on the basal plane is negligible [1]. The single crystal of ice deforms mainly by dislocation glide on the basal plane, normal to the hexagonal symmetry $c-$axis. This makes the textured polycrystal strongly anisotropic. As shown by MANGENEY *et al.* [2, 3], this macroscopic anisotropy must be accounted for in the mechanical model, because it strongly influences the flow of the sheet. But, since the macroscopic anisotropy is due to the texture development, hence to the flow itself, one should

[1] This work was done at Laboratoire Sols, Solides, Structures.

include the polycrystal texture and its evolution in the constitutive equation – in other words, it seems that one should use a micro-macro approach for the constitutive relation. One is then faced with the important computation cost needed to implement a polycrystal model in a finite element code. For this reason, a finite-element thermomechanical model of an ice sheet has been based on the "static" model, that assumes a uniform stress in a volume element of polycrystal [4]. The use of the static model for ice, as opposed to using the Taylor model that assumes uniform strain-rate, was suggested by a comparison between "static" and "self-consistent" predictions, due to CASTELNAU *et al.* [5].

It is, however, useful to first use the more complex and more exact models to predict the constitutive relation and the texture evolution for a given deformation history. This also has a short-term benefit, which is to assess the error involved in using the simpler (static) model.

In the present paper, a recently proposed micro-macro model is used [6, 7]. It is based on a minimum problem with two constraints and allows a continuous transition between the extreme models (Voigt-Taylor and "static"), see Sec. 3.1 for a motivation of using that model. In the present work, the model is adapted to a linear viscoplastic grain, which allows analytical developments (see Sec. 2). A new numerical approach is used (see Sec. 3.4) to solve the minimization problem.

The numerical results of the present study are restricted to the prediction of the effective potential of an isotropic polycrystal, i.e., a randomly textured polycrystal is considered. However, the present implementation of the micro-macro model allows also to consider textured polycrystals [8], as observed in ice sheets.

## 2. Single crystal behaviour

Since the ice crystal is incompressible, both strain-rate and deviatoric stress tensors can be expressed as vectors in a 5-D space, respectively $\mathbf{D}^g$ and $\mathbf{S}^g$ [9, 10]. Here we shall use the transformation proposed by LEQUEU *et al.* [10]:

$$\mathbf{X} = [(X_{22} - X_{11})/\sqrt{2}, \sqrt{3/2}X_{33}, \sqrt{2}X_{23}, \sqrt{2}X_{31}, \sqrt{2}X_{12}]. \tag{2.1}$$

Because the crystal of ice has an hexagonal symmetry axis, it is assumed to behave as a transversely isotropic medium. At low temperature (lower than $-10°C$) and for the deviatoric stress magnitude typical in polar ice (less than 0.05 MPa), there are some indications from data analysis for a behaviour close to linear behaviour [11]. Therefore, following MEYSSONNIER and PHILIP [12], we will assume in what follows that the ice crystal behaves as a linear transversely isotropic medium.

In the case of power-law viscoplastic behaviour with rate-sensitivity $m$, the potential $\Phi_D^g$ giving the stress as function of the strain-rate is given by

$$\Phi_D^g = W^g(\mathbf{D}^g)/(m+1), \tag{2.2}$$

where $W^g(\mathbf{D}^g)$ is the energy dissipation per unit volume and unit time due to the viscous deformation, defined as

$$W^g = \mathbf{D}^g \cdot \mathbf{S}^g . \tag{2.3}$$

In the particular case of the linear behaviour envisaged here ($m = 1$), the energy dissipation is twice as much as the dissipation potential $\Phi_D^g(\mathbf{D}^g)$. The deviatoric stress derives from $\Phi_D^g(\mathbf{D}^g)$ as

$$\mathbf{S}^g = \frac{\partial \Phi_D^g}{\partial \mathbf{D}^g} . \tag{2.4}$$

Since the grain is transversely isotropic, only the direction $x_3$ of its rotational symmetry axis needs to be defined in order to fixe the grain reference frame relative to the fixed global reference frame. This is done by using two angles, the co-latitude $\theta$ and the longitude $\varphi$. The simplest expression for the dissipation potential $\Phi_D^g(\mathbf{D}^g)$, when expressed in the grain reference frame with rotational symmetry axis along the $x_3$ direction, is given by

$$\Phi_D^g = \frac{1}{2} W^g = \frac{\eta}{\beta} \left[ D_1^{g2} + D_2^{g2} + \beta \left( D_3^{g2} + D_4^{g2} \right) + D_5^{g2} \right] , \tag{2.5}$$

where $\eta$ is the viscosity for shear in the planes perpendicular to the plane of isotropy $(x_1, x_2)$ ($\eta = 1/\psi$ in [13, 14], because the inverse law was used in the latter works) and $\beta$ is the ratio of the shear viscosity in the planes perpendicular to the basal plane to that in the basal plane. The parameter $\beta$ should be regarded as a measure of the grain anisotropy: when $\beta = 0$ the grain can deform only by basal glide, while $\beta = 1$ corresponds to an isotropic grain.

In the global reference frame, the relation (2.4) becomes

$$\mathbf{S}^g = \boldsymbol{\eta}^g(\theta, \varphi)\mathbf{D}^g , \tag{2.6}$$

where $\boldsymbol{\eta}^g$ is a 6-D fourth order tensor, symmetric, and with the dimension of a viscosity. Its expression can be inferred from Eqs. (2.4), (2.5) and by using the rotation matrix to pass from the grain reference frame to the global reference frame.

## 3. Polycrystal behaviour

### 3.1. Motivation of the micro-macro model under consideration

A well-known approach to defining more accurate models than the extreme models is the self-consistent approach, initiated almost fifty years ago for lin-

early elastic aggregates by HERSHEY [15] and independently by KRÖNER [16]. These models start from the consideration of an ellipsoidal inclusion embedded in a space-filling matrix material, as envisaged by ESHELBY [17, 18]: in the self-consistent model, the strain and stress in a given constituent are assumed to be the same as if that constituent were an ellipsoidal inclusion embedded in a space-filling matrix endowed with the effective macroscopic behaviour which is sought. A specific feature of Eshelby's exact solution to the problem of the linear elastic inclusion [18] is the fact that the inclusion undergoes a uniform strain state, hence also a uniform stress state. If one considers, not an ellipsoidal inclusion in a homogeneous matrix, but instead an aggregate of arbitrarily-shaped constituents, it is in practice impossible that any constituent may undergo a uniform strain state. Indeed it is easy to prove the following result [19]: If the strain-rate field has the uniform value $\mathbf{D}$ in the domain $\Omega$ and the uniform value $\mathbf{D}'$ in the contiguous domain $\Omega'$, and if the boundary between $\Omega$ and $\Omega'$ is not plane, then the strain-rate field can be derived from a continuous velocity field only if $\mathbf{L} = \mathbf{L}'$, where $\mathbf{L}$ and $\mathbf{L}'$ are the (necessarily uniform) values of the velocity gradient in $\Omega$ and $\Omega'$ (thus, not merely the strain-rates but also the rotation rates must be the same in $\Omega$ and $\Omega'$). This result holds true, of course, if one substitutes "small-strain tensor" for "strain-rate tensor", and "displacement" for "velocity". It means that the strain-rate tensors $\mathbf{D}^1, ..., \mathbf{D}^N$, which are predicted in the constituents $\Omega^1, ..., \Omega^N$ of some aggregate, e.g. by a self-consistent model, have to be interpreted as volume averages of the strain-rate field in the different constituents. Accepting this interpretation for the predicted distribution $(\mathbf{L}^k)_{k=1,...,N}$ of the velocity gradient, then the "compatibility problem" may always be solved, in the sense that, given any (reasonable or unreasonable) distribution $(\mathbf{L}^k)_{k=1,...,N}$, it is always possible to construct a regular velocity field $\mathbf{V}$ such that, for all $k$, the volume average of grad $\mathbf{V}$ in domain $\Omega^k$ is $\mathbf{L}^k$ [19]. Thus no model can be preferred to another one as regards the compatibility problem for the strain distribution – except, of course for the Voigt-Taylor model: but, for the latter, the incompatibility is found in the stress distribution. In the same way, one should be able to show that the compatibility problem may always be solved for the stress distribution in the sense of the volume average.

Furthermore, the self-consistent model provides a particular solution between the extreme models of Voigt (assuming uniform strain) and of Reuss (assuming uniform stress; when extended to non-linear behaviour, this is also called the "static model"). As found by KRÖNER [20], the self-consistent model for a linearly elastic aggregate is likely to correspond to the ideal statistical situation called "perfect disorder", in which knowledge of the volume fractions of the different constituents in the aggregate is sufficient to determine the effective macroscopic behaviour, due to the vanishing of all higher-order correlations. It is unlikely that this ideal situation could always be representative for real materials. In

the present paper, it will be shown that, for an isotropic aggregate of linearly viscous ice crystals, the self-consistent solution is indeed not very close to the likely effective behaviour.

Finally, following KRÖNER [21], various extensions of the self-consistent model have been proposed for the non-linear constitutive relations that describe elasto-plastic, viscoplastic or other behaviours. These extensions use different kinds of linearizations of the constitutive relations of the constituent phases. As shown by GILORMINI [22], the most classical extension, based on an incremental linearization due to HILL [23], exceeds the tighter upper bound derived by PONTE CASTAÑEDA [24] (more precisely, this has been shown for an isotropic two-phase aggregate of incompressible power-law elastic spheres [22]. This shortcoming of the classical extensions of the self-consistent model will not be relevant in the present paper, however, because a linearly viscous behaviour will be assumed on experimental grounds).

Despite the foregoing arguments, it is acknowleged, of course, that the self-consistent approach has proved very useful in providing many micro-macro models capable of capturing observed features in real heterogeneous materials [25, 26, 27, 28]. But these arguments add appeal to a different model, namely the "inhomogeneous variational model" [6, 7]: *i*) This model is based on a rigorous statistical framework and accounts explicitly for the fact that distributions only of the volume averages of the stress and strain in the different constituents are sought [6]. *ii*) It leads to a continuous transition between the two extreme (Voigt-Taylor and "static") models. *iii*) It makes no use of any linearization nor any perturbation treatment, and it applies to any behaviour that derives from a convex potential. Thus it is likely to be appropriate for the modelling of strongly heterogeneous materials (as is polycrystalline ice), for which perturbation techniques do not seem to be best suited. These advantages must have a price, and this is the fact that the heterogeneity parameter $r$, allowing the continuous transition between the extreme bounds (see Sec. 3.2), cannot be predicted from microstructural information and instead must be phenomenologically adjusted. This does not prevent the model from exhibiting a predictive capacity, however: this has been verified already for deformation textures in steels [7] and for the overall behaviour of fiber-reinforced composites [29].

### 3.2. Formulation of the micro-macro model under consideration

The micro-macro model formulated by ARMINJON and IMBAULT [7] is based on the minimization of the average potential under the principle of minimal heterogeneity. Because of the viscoplastic linear behaviour, it is equivalent here to consider the energy dissipation $W$ instead of the potential $\Phi_D$. Let us first introduce some general definitions that are useful for the presentation of the

model. In the following, the polycrystal is assumed to be made of $N$ constituents. Each constituent $(k)$ $(k = 1, .., N)$ occupies the spatial domain $\Omega_k$ where the crystal orientation has some given value $(\theta_k, \varphi_k)$. Note that $\Omega_k$ is in general not a connected domain, i.e., the zone with given orientation is in several pieces. The texture is described in the global reference frame by the set of the orientations $(\theta_k, \varphi_k)$ and the associated volume fractions $f_k$. When some quantity $Y^k$ is defined for each constituent $(k)$, we shall denote the weighted average of the distribution $(Y^k)_{k=1,..,N}$ by:

$$Y^{\mathrm{av}} = \langle Y^k \rangle = \sum_{k=1}^{N} f_k Y^k \,. \tag{3.1}$$

The average heterogeneity function $h$ of some distribution (strain-rate, stress) $(\mathbf{Y}^k)_{k=1,..,N}$ around the macroscopic quantity $\mathbf{Y}$ is defined as

$$h((\mathbf{Y}^k)) = \left[ \sum_{k=1}^{N} f_k |\mathbf{Y}^k - \mathbf{Y}^{\mathrm{av}}|^2 \right]^{1/2} , \tag{3.2}$$

where $|\mathbf{Y}| = [\mathrm{tr}\mathbf{Y}^2]^{1/2} = [Y_i Y_i]^{1/2}$.

This micro-macro model consists in determining the distribution of the average strain-rates $\mathbf{D}^k$ (in the constituents $(k)$, $k = 1, .., N$) by solving a minimum problem with two constraints. Namely, we have to find the minimum of the average viscoplastic dissipation energy $W^{\mathrm{av}}$ under the two conditions that $(i)$ the average strain-rate $\mathbf{D}^{\mathrm{av}}$ over the $N$ constituents is the macroscopic strain-rate $\mathbf{D}$ (consistency condition) and $(ii)$ the average heterogeneity of the strain-rate distribution $h((\mathbf{D}^k))$ does not exceed a prescribed value $r$, thus:

$$W_r(\mathbf{D}) \equiv \min_{\mathbf{D}^k} \left[ \sum_{k=1}^{N} f_k W^k(\mathbf{D}^k) \right] , \tag{3.3}$$

under constraints

$$(i) \quad \sum_{k=1}^{N} f_k \mathbf{D}^k = \mathbf{D} \quad \text{and} \quad (ii) \quad h((\mathbf{D}^k)) \leq r \,. \tag{3.4}$$

In Eq. (3.3), $W^k(\mathbf{D}^k)$ is the energy dissipation (2.5) in the constituent $g = k$, assuming that the $N$ constituents of the polycrystal have the same behaviour in their respective axes ($\eta = \eta^k$ and $\beta = \beta^k$ for all $k$).

### 3.3. The lower and upper bounds in the model considered

The proposed formulation allows the passage from the upper bound to the lower bound in a continuous manner. Since the upper bound corresponds to a uniform strain-rate distribution (i.e., $\mathbf{D}^k = \mathbf{D}$ for all $k$), it appears from Eq. (3.2)

that this bound is obtained when the average strain-rate heterogeneity is null (i.e., for the heterogeneity parameter $r = 0$). ARMINJON [6] has shown that the lower bound corresponds to the static model (i.e. a uniform distribution of stress, $\mathbf{S}^k = \mathbf{S}$ for all $k$) and that this bound is obtained when the heterogeneity parameter $r$ reaches a critical value $R$. This critical value depends on the grain anisotropy parameter $\beta$.

When the polycrystal texture is isotropic, analytical expressions of the dissipation potential can be obtained for both the upper and lower bounds. This is done by using a continuous description of the texture with the, so-called, Orientation Distribution Function (ODF). The ODF $f(\theta, \varphi)$ gives the relative density of grains whose rotational symmetry axis $x_3$ have the orientation $(\theta, \varphi)$. With the use of the ODF, a macroscopic quantity $Y^{\mathrm{av}}$ is defined similar to (3.1):

$$Y^{\mathrm{av}} = \langle Y(\theta,\varphi)\rangle = \frac{1}{2\pi}\int_0^{2\pi}\int_0^{\pi/2} Y(\theta,\varphi) f(\theta,\varphi)\sin\theta d\theta d\varphi\,. \tag{3.5}$$

Using this definition for the weighted average, the average of the energy dissipation, $W^{\mathrm{av}}$, is defined as

$$W^{\mathrm{av}} = \langle W(\mathbf{D}^{\mathrm{loc}}(\theta,\varphi))\rangle\,, \tag{3.6}$$

where $W$ is given by Eq. (2.5) in the grain reference frame and $\mathbf{D}^{\mathrm{loc}} = \mathbf{D}^{\mathrm{loc}}(\theta,\varphi)$ is the distribution of the strain-rate as function of the orientation. For an isotropic texture $f(\theta,\varphi) = 1$ and, therefore, after some straightforward integrations, the analytical expression of the upper bound is found to be

$$W_{\mathrm{sup,iso}} \equiv \langle W(\mathbf{D})\rangle = \eta\frac{6+4\beta}{5\beta}\mathrm{tr}\mathbf{D}^2\,, \tag{3.7}$$

and that of the lower bound is

$$W_{\mathrm{inf,iso}} \equiv \inf(W^{\mathrm{av}};\ \langle \mathbf{D}^{\mathrm{loc}}(\theta,\varphi)\rangle = \mathbf{D}) = \eta\frac{10}{2+3\beta}\mathrm{tr}\mathbf{D}^2\,. \tag{3.8}$$

For an isotropic grain (i.e., $\beta = 1$) the two bounds are identical and $W_{\mathrm{sup,iso}} = W_{\mathrm{inf,iso}} = 2\eta\mathrm{tr}\mathbf{D}^2$. The difference between the two bounds increases as the anisotropy of the grain increases (i.e., as the anisotropy parameter $\beta$ decreases). Since $W_{\mathrm{sup,iso}} = \infty$ when $\beta = 0$, the difference between the two bounds is infinite when the grain deforms only by slide in its isotropic plane.

The analytical values of the energy dissipation (3.7) and (3.8) will be used to check the numerical implementation of the model.

### 3.4. Numerical method for the calculation of the microscopic distributions

We have to solve the convex minimum problem (3.3) involving one linear constraint (3.4) *i4andoneconvexinequality*(3.4)ii4. We use the problem formu-

lation of [30]. The linear constraint (3.4) $i$ is used to eliminate the strain-rate of the last constituent ($k = N$), so that the list of the optimization variables is $\mathbf{Y} = (\mathbf{D}^k)_{k=1,..,N-1}$ (thus $5(N-1)$ variables). From (3.4) $i$, we get

$$\mathbf{D}^N = \left( \mathbf{D} - \sum_{k=1}^{N-1} f_k \mathbf{D}^k \right) / f_N \,. \tag{3.9}$$

The function to minimize is then written as:

$$F(\mathbf{Y}) = \sum_{k=1}^{N-1} f_k W^k(\mathbf{D}^k) + f_N W^N \left[ \left( \mathbf{D} - \sum_{k=1}^{N-1} f_k \mathbf{D}^k \right) / f_N \right] , \tag{3.10}$$

and the heterogeneity function (3.2) is rewritten as a function of the list $\mathbf{Y}$:

$$h(\mathbf{Y}) = \left[ \sum_{k=1}^{N-1} f_k \left| \mathbf{D}^k - \mathbf{D} \right|^2 + \frac{1}{f_N} \left| \sum_{k=1}^{N-1} f_k (\mathbf{D}^k - \mathbf{D}) \right|^2 \right]^{1/2} . \tag{3.11}$$

The optimization problem is: find $\mathbf{Y}_0$ making $F(\mathbf{Y})$ a minimum, among the $\mathbf{Y}$'s satisfying the constraint $C(\mathbf{Y}) = h(\mathbf{Y})^2 - (r|\mathbf{D}|)^2 \leq 0$. The saddle point theorem characterizes the solution of this problem as follows:

$$\begin{aligned} &\exists \lambda \geq 0 \quad \text{such that:} \\ &(i) \qquad \nabla F(\mathbf{Y}_0) + \lambda \nabla C(\mathbf{Y}_0) = \mathbf{0} \quad \text{and} \quad (ii) \quad \lambda C(\mathbf{Y}_0) = 0 \,. \end{aligned} \tag{3.12}$$

In this work, the optimization problem is solved by seeking the saddle point $(\mathbf{Y}_0, \lambda_0)$ of the Lagrangian function

$$L(\mathbf{Y}, \lambda) = F(\mathbf{Y}) + \lambda C(\mathbf{Y}) \,, \tag{3.13}$$

instead of using a classical penalty method as in [7, 30]. This saddle point is defined as

$$L(\mathbf{Y}_0, \lambda_0) = \min_{\mathbf{Y}} L(\mathbf{Y}, \lambda_0) = \max_{\lambda} \min_{\mathbf{Y}} L(\mathbf{Y}, \lambda) \,. \tag{3.14}$$

By introducing the function $G(\lambda)$ defined as

$$G(\lambda) = \min_{\mathbf{Y}} L(\mathbf{Y}, \lambda) \,, \tag{3.15}$$

the saddle point corresponds to the maximum of $G(\lambda)$.

Numerically, for a given value of $\lambda$, the value of the function $G(\lambda)$ is obtained by using the conjugate gradient method. The maximum value of $G(\lambda)$ is then

sought by an inverse parabolic interpolation. Since the function $G(\lambda)$ is smooth, this method has been found to be more efficient than the Uzawa algorithm.

When $r \geq R$, the Lagrange multiplier $\lambda$ is equal to zero and the optimization problem reduces to finding the minimum of the function $F(\mathbf{Y})$. To obtain convergence of the algorithm in the case $r \geq R$, the function $G(\lambda)$ (3.15) is transformed into:

$$G(\lambda) = \begin{cases} \min_{\mathbf{Y}} [F(\mathbf{Y}) + \lambda C(\mathbf{Y})] & \text{if} \quad \lambda > 0 \\ \min_{\mathbf{Y}} [F(\mathbf{Y})] - \lambda & \text{if} \quad \lambda \leq 0, \end{cases} \tag{3.16}$$

## 4. Results

### 4.1. Numerical tests of the saddle point solution

In Fig. 1 is presented the evolution of the function $G(\lambda) = L(\mathbf{Y}_0(\lambda), \lambda)$ Eq. (3.16) for a given grain anisotropy parameter $\beta = 0.01$ and a given heterogeneity parameter $r = 0.5$. The condition (3.12) $i$ is verified for every $\lambda$ (for each $\lambda$, it is verified with the solution $\mathbf{Y}_0(\lambda)$ of the minimization problem (3.15), but it appears in this figure that the condition (3.12) $ii$ (i.e., $\lambda C(\mathbf{Y}_0) = 0$) is confirmed for only one value $\lambda = \lambda_0$, which corresponds to the the saddle point solution.

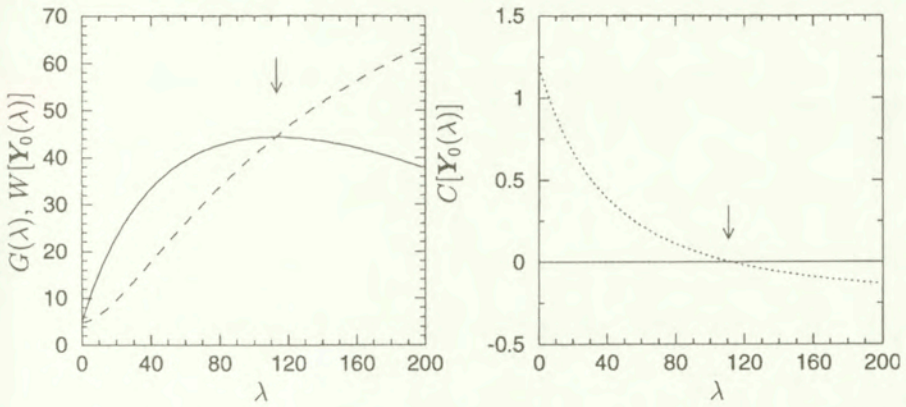


FIG. 1. Evolution of $G(\lambda) = L(\mathbf{Y}_0(\lambda), \lambda)$ (solid line), the energy dissipation $F[\mathbf{Y}_0(\lambda)]$ (dashed line) and the constraint $C[\mathbf{Y}_0(\lambda)]$ (dotted line) as a function of the Lagrange multiplier $\lambda$ for $\beta = 0.01$ and $r = 0.5$. The arrows show the value of $\lambda_0$ corresponding to the maximum of $G(\lambda)$ (i.e., the saddle point solution).

This value $\lambda_0$ depends on the grain anisotropy parameter $\beta$ and on the heterogeneity parameter $r$. Figure 2 shows the evolution of the calculated Lagrange multiplier $\lambda_0$ as a function of the heterogeneity parameter $r$. Theoretically, we

should get an infinite value for $\lambda_0$ when the heterogeneity parameter is zero (upper bound). Numerically, the convergence of the method is not achieved when the value of $r$ is lower than the precision expected on the constraint $C(\mathbf{Y}_0)$. On the other hand, with the adopted function (3.16), the lower bound can be calculated, even when $r > R$. Numerically, when $r > R$ the constraint becomes negative, but the Lagrange multiplier is very close to zero (of the order of $10^{-14}$).

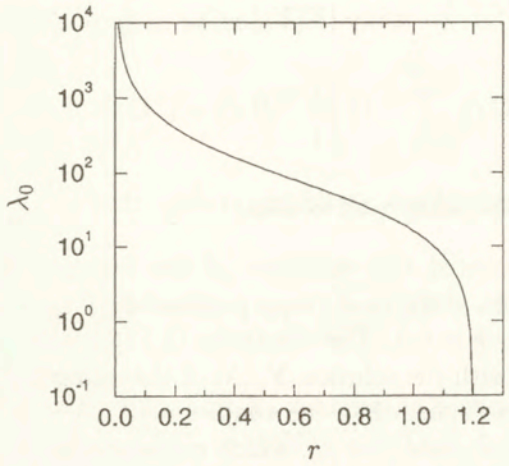


FIG. 2. Evolution of the Lagrange multiplier $\lambda_0$ corresponding to the saddle point solution as a function of the strain-rate heterogeneity parameter $r$ for $\beta = 0.01$.

Numerically, with a relative precision of about $10^{-7}$, it is found that the Lagrange multiplier verifies the relation

$$\lambda_0 = \frac{h((\mathbf{S}_0^k))}{h((\mathbf{D}_0^k))}, \tag{4.1}$$

where $(\mathbf{S}_0^k)$ and $(\mathbf{D}_0^k)$ are the microscopic stress and strain-rate distributions, respectively, corresponding to the solution of the optimization problem.

#### 4.2. Macroscopic behaviour of isotropic polycrystalline ice

In this section, the mechanical response of isotropic ice is analysed as a function of the strain-rate heterogeneity parameter $r$ and the grain anisotropy parameter $\beta$. The value of the viscosity parameter $\eta$ has no influence on the strain-rate distribution and merely acts as a scaling parameter on the stresses. Therefore, all the numerical results presented have been obtained for an applied macroscopic strain-rate such that $\eta \mathrm{tr}\mathbf{D}^2 = 1$. The polycrystal is made up of $N = 200$ randomly distributed grains and then the number of optimization variables is 995.

In Fig. 3a is presented the evolution of the calculated strain-rate and deviatoric stress heterogeneities as functions of the imposed heterogeneity parameter $r$. The calculated strain-rate heterogeneity $h$ is equal to the heterogeneity parameter $r$ until the maximum value of $h$, i.e. $R = 1.2$, is reached. As for the strain-rate heterogeneity, the stress heterogeneity evolution is linear, but it decreases from the maximum value 96.8 when $r = 0$ to zero when $r \geq R$. As expected, the stress heterogeneity function $h((\mathbf{S}^k)) = 0$ when $r \geq R$, which means that the (average) deviatoric stress is the same in all the constituents (static model).

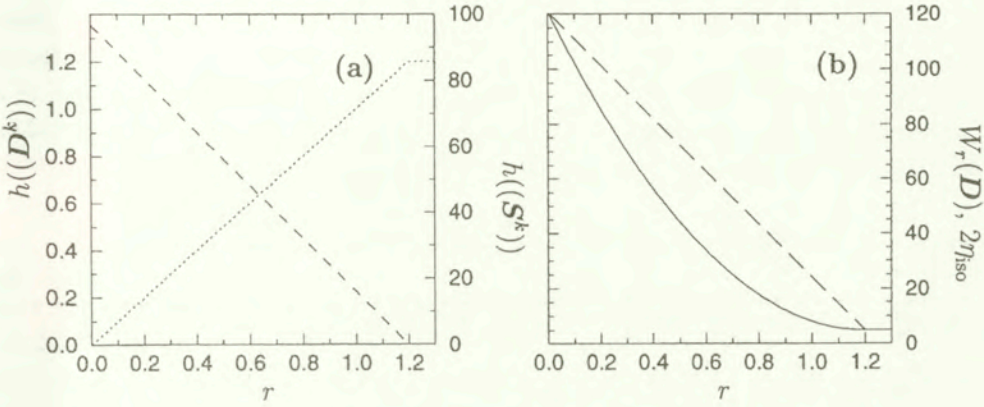


FIG. 3. Evolution of (a) the calculated strain-rate and stress heterogeneities, $h((\mathbf{D}^k))$ and $h((\mathbf{S}^k))$, (dotted and dashed lines, respectively) and (b) the average of the dissipation potential $W_r(\mathbf{D})$ (solid line) and the viscosity for isotropic ice $\eta_{\rm iso}$ (long dashed line) as a function of the imposewd heterogeneity parameter $r$ for $\beta = 0.01$.

By testing twenty different $\mathbf{D}$ tensors, we have found numerically that the stress response $\mathbf{S}$ is very nearly proportional to the strain-rate direction $\mathbf{D}$ and, moreover, the proportionality coefficient does not depend on the investigated $\mathbf{D}$ tensor. In other words, the macroscopic response of the isotropic polycrystal is numerically found to be of the form:

$$\mathbf{S} = 2\eta_{\rm iso}\mathbf{D}\,, \tag{4.2}$$

where $\eta_{\rm iso}$ is an effective viscosity of isotropic ice. The numerical departure from this exact equation is found to be smaller than 1%. This departure can be attributed to the randomly created texture, which is not *exactly* isotropic.

Figure 3b shows the evolution of the energy dissipation as a function of the heterogeneity parameter $r$. For $\beta = 0.01$, the analytical values of the upper and lower bounds (3.7) and (3.8) are $W_{\rm sup,iso} = 120.8$ and $W_{\rm inf,iso} = 4.92$. As shown in Fig. 3a, the calculated potential reaches these two values for $r = 0$ and $r \geq R = 1.2$, respectively. The upper bound was calculated for $r = 10^{-10}$

since for $r = 0$ the convergence is not achieved with the algorithm used here. Of course, the programming of the Taylor model is trivial and can be included, so as to take into account the case $r = 0$.

Because there are very few reliable experimental results on ice crystals and also because the constituent in a micro-macro model does not behave as a single isolated ice crystal, it is more convenient to determine the rheological values of the constituent (here the values of $\eta$ and $\beta$) by using experimental results on polycrystalline ice.

According to the experimental results of PIMIENTA *et al.* [31], a polycrystal with all its grain symmetry axes parallel, undergoing simple shear in a plane perpendicular to the grain symmetry $c-$axes, would deform $10 \pm 2$ times faster than an isotropic polycrystal. Since in a micro-macro model the response of a polycrystal in which all the constituents have the same orientation is equal to the response of a single constituent, this leads to the relation:

$$\frac{\eta_{\text{iso}}}{\eta} = 10 \pm 2\,. \tag{4.3}$$

As shown in Fig. 3b, $\eta_{\text{iso}}\text{tr}\mathbf{D}^2$ is numerically found to decrease linearly as a function of the heterogeneity parameter $r$, from the Taylor value to the static one. Taking benefit of this linearity (assumed exact), and using the analytical solutions (3.7) and (3.8) for the two bounds, one can easily derive the following analytical relation between the grain viscosity for shear in the plane perpendicular to the basal plane, $\eta$, and the effective viscosity for isotropic ice, $\eta_{\text{iso}}$:

$$\frac{\eta_{\text{iso}}}{\eta} = \frac{3+2\beta}{5\beta} - \frac{6(1-\beta)^2}{5\beta(2+3\beta)}\frac{r}{R}\,, \tag{4.4}$$

where $R$ can be approximated from numerical results by $R = \beta^2 - 2.23\beta + 1.23$.

The contours of the ratio $\eta_{\text{iso}}/\eta$ (??) from 4 to 20 by step of 2 are drawn in Fig. 4 as a function of the grain anisotropy parameter $\beta$ and the heterogeneity ratio $r/R$. If the grain anisotropy parameter $\beta$ decreases, then to get the same value of the ratio $\eta_{\text{iso}}/\eta$, the strain-rate heterogeneity has to increase. If the grain anisotropy parameter is between 0.001 and 0.01, which seems to be a reasonable range of values for ice [31], then the value $\eta_{\text{iso}}/\eta = 10$ corresponds to a range of heterogeneity parameter between $r = 0.87R$ and $r = 0.987R$, i.e. very close to the solution given by the static model ($r = R$). As shown in Fig. 4, the value $\eta_{\text{iso}}/\eta = 10$ can be obtained only if the grain anisotropy parameter $\beta$ is lower than 0.0625. Figure 4 should be used to select a pair ($\beta$,$r$) corresponding to the required macroscopic anisotropy.

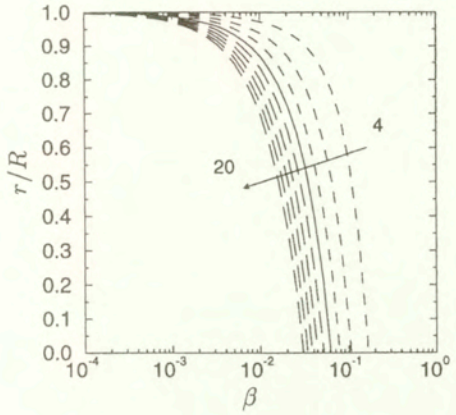


FIG. 4. Contours of the ratio $\eta_{\text{iso}}/\eta$ from 4 to 20 by step of 2 as a function of the grain anisotropy parameter $\beta$ and the heterogeneity ratio $r/R$ ($R$ is the heterogeneity obtained for the static solution).

#### 4.3. Deviation from the no-correlation condition

In this section, the deviation from the following *no-correlation condition*:

$$\langle \mathbf{D}^k \rangle . \langle \mathbf{S}^k \rangle = \langle \mathbf{D}^k . \mathbf{S}^k \rangle , \tag{4.5}$$

is studied as a function of the heterogeneity parameter $r$ and the grain anisotropy parameter $\beta$. To this goal, we compare the calculated macroscopic dissipation energy

$$\mathbf{D}.\mathbf{S} = \langle \mathbf{D}^k \rangle . \langle \mathbf{S}^k \rangle , \tag{4.6}$$

and the average of the dissipation energy (used previously for the minimization problem)

$$W^{\text{av}} = \langle W^k \rangle = \langle \mathbf{D}^k . \mathbf{S}^k \rangle . \tag{4.7}$$

When formulating the model used here [6, 7], it was assumed that condition (4.5) applies when $\mathbf{D}^k$ and $\mathbf{S}^k$ are the respective average values of the *actual* field of strain-rate, $\mathbf{d}$, and of the *actual* field of deviatoric stress, $\mathbf{s}$, in the volume occupied by constituent $(k)$:

$$\mathbf{D}^k_{\text{act}} = \int_{\Omega_k} \mathbf{d} dV/V(\Omega_k) \quad \text{and} \quad \mathbf{S}^k_{\text{act}} = \int_{\Omega_k} \mathbf{s} dV/V(\Omega_k) . \tag{4.8}$$

Furthermore, the model assumes that, for the relevant value $r_0$ of the heterogeneity parameter $r$, the strain-rate distribution $(\mathbf{D}^k)$ solution of the minimum problem (3.3) – (3.4) is equal to the actual distribution $(\mathbf{D}^k_{\text{act}})$. It is well known

that condition (4.5) applies trivially when the extreme models are used: either the upper bound model ($\mathbf{D}^k = \mathbf{D} \, \forall k$) or the lower bound model ($\mathbf{S}^k = \mathbf{S} \, \forall k$). Now it is apparent in Fig. 5 that, except for these extreme models (which corresponds respectively to $r = 0$ and $r = R$), the strain-rate distribution ($\mathbf{D}_r^k$) does not fulfil condition (4.5). Therefore, at least one among the following three possibilities is true:

(*i*) The actual distribution does not fulfil condition (4.5). This could be due to the strong heterogeneity of the polycrystal (due to the strong anisotropy of the crystals) and it would mean that using a one-point model is not well justified.

(*ii*) The proposed variational model does not predict correctly the actual strain-rate distribution when the polycrystal heterogeneity is too large. Again, this would mean that using a one-point model, such as the present model, is not wise for strong material heterogeneity.

(*iii*) One of the two extreme models (Static or Voigt-Taylor) corresponds to the actual solution. This possibility does not seem to be very realistic.

In any case, it should be emphasized that the no-correlation condition (4.5) is different from Hill's macrohomogeneity condition [32, 33]. The latter must be written in terms of the microscopic fields and their volume averages in the representative volume element $\Omega$ of the polycrystal ($\Omega$ is the union of the domains $\Omega_k, k = 1, .., N$):

$$\overline{\boldsymbol{\sigma} : \mathbf{d}} \equiv \frac{1}{V(\Omega)} \int_{\Omega} \boldsymbol{\sigma} : \mathbf{d} dV \tag{4.9}$$

$$= \overline{\boldsymbol{\sigma}} : \overline{\mathbf{d}} \equiv \left( \frac{1}{V(\Omega)} \int_{\Omega} \boldsymbol{\sigma} dV \right) : \left( \frac{1}{V(\Omega)} \int_{\Omega} \mathbf{d} dV \right) .$$

In fact, ARMINJON [6], as well as ARMINJON and IMBAULT [7] derive condition (4.5) from Hill's condition (4.9) and using an additional assumption (Eq. (4.5) in [7]).

As shown in Fig. 5, the ratio $\langle \mathbf{D}^k . \mathbf{S}^k \rangle / (\mathbf{D} . \mathbf{S})$ decreases as the grain anisotropy increases (i.e., as $\beta$ decreases) and the location of the maximum difference tends towards $r/R = 1$ with $\beta$.

MEYSSONNIER and PHILIP [12] have proposed a self-consistent "one-site" model (SC1) based on the same model for the grain behaviour, *i.e* linear transversely isotropic medium. In the SC1 model, the texture is described by the use of an ODF, and the linearity of the grain behaviour allows analytical developments of the strain-rate and stress fields as functions of the grain orientations.

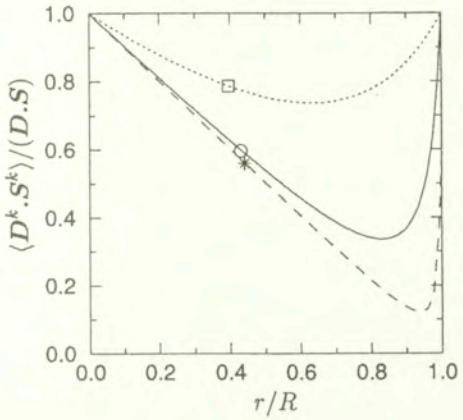


FIG. 5. Evolution of the ratio $\langle \mathbf{D}^k.\mathbf{S}^k\rangle/(\mathbf{D}.\mathbf{S})$ as a function of $r\{R\}$, for $\beta = 0.1$ (dotted line), $\beta = 0.01$ (solid line) and $\beta = 0.001$ (dashed line). In this figure is plotted the value find for the ratio $\langle \mathbf{D}^k.\mathbf{S}^k\rangle/(\mathbf{D}.\mathbf{S})$ by using the 1-site self-consistent model of [12] for $\beta = 0.1$ (square), $\beta = 0.01$ (circle) and $\beta = 0.001$ (star).

Since the SC1 model is based on the same model for the grain behaviour, it allows an objective comparison of both models. In Fig. 5, the value of the ratio $\langle \mathbf{D}^k.\mathbf{S}^k\rangle/(\mathbf{D}.\mathbf{S})$ obtained with the SC1 model is plotted for the corresponding calculated strain-rate heterogeneity (the latter is not imposed in the SC1 model). As shown in Fig. 5, for a given grain anisotropy, the solution obtained with the SC1 model corresponds exactly to one solution given by the present model. As shown in Fig. 6 for $\beta = 0.01$ and an applied compression $D_2 = 1$ and $D_1 = 0$, the strain-rate distribution given by the SC1 model is almost exactly the same as that given by the present model when the heterogeneity parameter $r$ imposed for the present model is equal to the value $h_{\mathrm{SC1}}$ of the strain-rate heterogeneity, calculated with the SC1 model ($h_{\mathrm{SC1}} = 0.52$). In other words, up to a negligible error, the strain-rate distribution predicted by the self-consistent model is (in this linear case) solution of the variational problem (3.3) – (3.4), for some particular value $r$. Howewer, that particular value $r = 0.52$ corresponds to $r/R \approx 0.42$ and gives an effective viscosity $\eta_{\mathrm{iso}} \approx 36\eta$, which seems to be inconsistent with the experimental data $\eta_{\mathrm{iso}}/\eta \approx 10$ of PIMIENTA *et al.* [31]. This latter value of the ratio is obtained with the SC1 model only for one value $\beta = 0.04$ [12]. The behaviour of polycrystalline ice is much closer to the static model than on would expect using the self-consistent model.

CASTELNAU *et al.* [34] found similar results with a 1-site self-consistent model but for a non-linear behaviour of the grains. By introducing an interaction coefficient $\alpha$, which is used to constrain the interaction between grains and the matrix (a zero value of $\alpha$ corresponds to the Taylor model and an infinite value to the static model), these authors showed that the maximum deviation from the

no-correlation condition (4.5) is obtained for the classical tangent formulation of the model ($\alpha = 1$). (It is recalled that, in the linear case studied here, there is only one self-consistent solution, i.e., there is no parameter like $\alpha$).

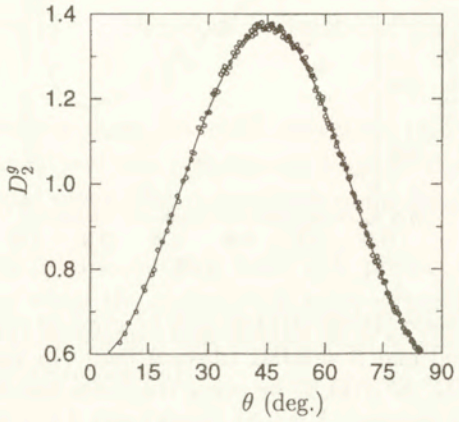


FIG. 6. Evolution of the strain-rate $D_2^g$ in the grains as a function of the grain orientation angle $\theta$, for $\beta = 0.01$, calculated with the present model for an imposed strain-rate heterogeneity parameter $r = 0.52$ (circle) and with the CS! model (solid line).

## 5. Conclusions and discussion

A variational micro-macro model has been numerically implemented to predict the strain-rate distribution in polycrystalline ice, when the behaviour of the constituent crystals is assumed linearly viscous (i.e., an anisotropic fluid). This convenient assumption is suggested by an analysis of data resulting from deep ice-cores [11]. The variational problem defining the model allows a continuous transition between the extreme (Taylor-Voigt and Reuss-static) models, depending on the value of the strain-rate heterogeneity parameter $r$. In this work, the numerical solution of this variational problem with constraints has been found by using a saddle point method. This has proved more accurate and even more efficient than the penalty method that was used previously, though it should be remembered that the linear behaviour, as envisaged here, leads to a simpler minimization problem.

From the strain-rate distribution, obtained as the solution of the minimization problem, it is easy to deduce the stress distribution and the effective behaviour. All three depend on: (*i*) the crystal behaviour, here characterized by the crystal viscosity $\eta$ and the crystal anisotropy parameter $\beta$, (*ii*) the heterogeneity parameter $r$ and (*iii*) the (current) texture or orientation distribution. In this work, a uniform texture has been considered, thus leading to an isotropic effective behaviour (for an application to non-uniform textures see [8]). The effective be-

haviour depends then only on $\eta$, $\beta$ and $r$, and is found to be an isotropic linearly viscous behaviour, involving an effective viscosity $\eta_{\rm iso}$. The ratio $\eta_{\rm iso}/\eta$ depends analytically on $\beta$ and $r$ (Eq. (4.4)). Since $\eta_{\rm iso}/\eta$ and $\beta$ can be constrained from experimental data, this leads to an evaluation of the heterogeneity parameter $r$, which is found to be high: $r/R \approx 0.9$, where $R$ is the strain-rate heterogeneity that corresponds to the static model. In contrast, the self-consistent model predicts $r/R \approx 0.4$, which seems incompatible with experimental data. Thus, the behaviour of polycrystalline ice seems to be much closer to the static model than is the self-consistent estimate. This is probably due to the strong material heterogeneity, which is likely to favour a behaviour close to the static model.

When using "one-point" (volume fractions) models like self-consistent models or that investigated here, one hopes that the discrete strain-rate and stress distributions calculated by the model are representative of the actual strain-rate and stress fields and, in particular, allow calculation of the macroscopic work-rate as the corresponding discrete average. This needs the no-correlation condition (4.5) to be fulfilled. However, it has been found that the distribution predicted by the model used here, and which depends on the heterogeneity parameter $r$, does not satisfy Eq. (4.5), except for the extreme models ($r = 0$ or $r = R$). The same is true for the self-consistent model (it has been found that the self-consistent model corresponds almost exactly to the model used here for a particular value of $r$). The analysis of this condition by ARMINJON [6] and by ARMINJON and IMBAULT [7], suggests that the use of a one-point model cannot be entirely satisfactory as the material heterogeneity (here the parameter $1/\beta$) is high. More precisely, it is less justified in that case to assume that the volume average of the stress field in a given constituent is related to the corresponding strain-rate average by a constitutive relation. If one keeps using a one-point model to get the effective behaviour, one should probably consider that the macroscopic work-rate is given by the left-hand side of Eq. (4,5), which is greater than the right-hand side. This would mean that some additional "accommodation work" is not included in the r.h.s. of Eq. (4.5), being due to the correlated heterogeneity of the microscopic fields $\mathbf{c}$ and $\mathbf{d}$ at the sub-constituent scale. There is also the possibility to use a model involving a description of the micro-geometry (see e.g. [29]), at the price of signficantly increasing the computation time.

## References

1. P. DUVAL, M. F. ASHBY, and I. ANDERMAN, *Rate-controlling processes in the creep of polycrystalline ice*, J. of Phys. Chem., **87**, 10, 4066–4074, 1983.

2. A. MANGENEY, F. CALIFANO, and O. CASTELNAU, *Isothermal flow of an anisotropic ice sheet in the vicinity of an ice divide*, J. Geophys. Res., **101**, 12, 28, 189–28,204, 1996.

3. A. MANGENEY, F. CALIFANO, and K. HUTTER, *A numerical study of anisotropic, low Reynolds number, free surface flow of ice sheet modeling*, J. Geophys. Res., **102**, B10, 22, 749–22,764, 1997.

4. O. GAGLIARDINI and J. MEYSSONNIER, *Plane flow of an ice sheet exhibiting strain-induced anisotropy*, K. HUTTER, Y. WANG, H. BEER [Eds.], Advances in Cold-Region Thermal Engineering and Sciences: technological, environmental and climatological Impact. Berlin, etc. Springer-Verlag, (Lecture Notes in Physics) **533**, 171–182, 1999.

5. O. CASTELNAU, P. DUVAL, R. A. LEBENSOHN, and G. CANOVA, *Viscoplastic modeling of texture development in polycrystalline ice with a self-consistent approach: Comparison with bound estimates*, J. Geophys. Res., **101**, 6, 13, 851–13,868, 1996.

6. M. ARMINJON, *Limit distributions of the states and homogenization in random media*, Acta Mech., **88**, 27–59, 1991.

7. M. ARMINJON and D. IMBAULT, *Variational micro-macro model and deformation textures predicted for steels*, Textures and Microstructures, **26-27**, 191–220, 1996.

8. O. GAGLIARDINI, M. ARMINJON and D. IMBAULT, *Predicting the macroscopic behaviour of anisotropic ice with a variational polycrystal model*, Proceedings of the 4th European Mechanics of Materials Conf., June 2000, Metz (E. GAUTIER, M. CLAVEL and F. DUNNE, [Eds.]), to appear.

9. M. ARMINJON and J. P. BOEHLER, *Comportement plastique et texture cristallographique des métaux anisotropes*, Comportement plastique des solides anisotropes (J. P. BOEHLER [Ed.]), Editions du CNRS, 133–155, Paris 1985.

10. PH. LEQUEU, P. GILORMINI, F. MONTHEILLET, B. BACROIX, and J. J. JONAS, *Yield surfaces for textured polycrystals –I. Crystallographic approach*, Acta Metall., **35**, 2, 439–451, 1987.

11. V. YA. LIPENKOV, A. N. SALAMATIN, and P. DUVAL, *Bubbly-ice densification in ice sheets: II. Applications*, J. Glaciol., **43**, 145, 397–407, 1997.

12. J. MEYSSONNIER and A. PHILIP, *A model for the tangent viscous behaviour of anisotropic polar ice*, Ann. Glaciol., **23**, 253–261, 1996.

13. O. GAGLIARDINI and J. MEYSSONNIER, *Analytical derivations for the behaviour and fabric evolution of a linear orthotropic ice polycrystal*, J. Geophys. Res., **104**, B8, 17 797–17 809, 1999.

14. R. STAROSZCZYK and O. GAGLIARDINI, *Two orthotropic models for strain-induced anisotropy of polar ice*, J. Glaciol., **45**, 151, 485 – 494, 1999.

15. A. V. HERSHEY, J. Appl. Mech., **21**, pp. 236 and 241, 1954.

16. E. KRÖNER, *Berechnung der elastischen Konstanten des Vielkristalls aus den Konstanten des Einkristalls*, Z. Phys., **151**, 504–518, 1958.

17. J. D. ESHELBY, Phil. Trans. A, **244**, p. 87, 1951.

18. J. D. ESHELBY, *The determination of the elastic field of an ellipsoidal inclusion, and related problems*, Proc. Roy. Soc. A, **241**, 376–396, 1957.

19. M. ARMINJON, *Macro-homogeneous strain fields with arbitrary local inhomogeneity*, Arch. Mech., **43**, 191–214, 1991.

20. E. KRÖNER, *Self-consistent scheme and graded disorder in polycrystal elasticity*, J. Phys. F: Metal Phys., **8**, 2261–2267, 1978.

21. E. KRÖNER, *Zur plastischen Verformung des Vielkristalls*, Acta Metall., **9**, 155–161, 1961.

22. P. GILORMINI, *A shortcoming of the classical non-linear extension of the self-consistent model*, C. R. Acad. Sci., **320**, Série IIb, 115–122, Paris 1995.

23. R. HILL, *Continuum micro-mechanics of elastoplastic polycrystals*, J. Mech. Phys. Solids, **13**, 89–101, 1965.

24. P. PONTE CASTAÑEDA, *The effective mechanical properties of nonlinear isotropic composites*, J. Mech. Phys. Solids, **39**, 45–71, 1991.

25. G. J. WENG, *Self-consistent determination of time-dependent behavior of metals*, J. Appl. Mech., **48**, 41–46, 1981.

26. A. MOLINARI, G. R. CANOVA and S. AHZI, *A self-consistent approach of the large deformation polycrystal viscoplasticity*, Acta Metall., **35**, 12, 2983–2994, 1987.

27. P. LIPINSKI, M. BERVEILLER and F. CORVASCE, *Statistical approach to elastoplastic behaviour of polycrystal at finite deformations*, Arch. Mech., **40**, 725–740, 1988.

28. G. J. DVORAK, *Micromechanics of inelastic composite materials: theory and experiment*, J. Engng. Mater. Technol., **115**, 327–338, 1993.

29. M. ARMINJON and B. GUESSAB, *A model with two micro-scales for the effects of geometrical distribution of material inhomogeneity*, Acta Mechanica, **134**, 61–79, 1999.

30. M. ARMINJON and D. IMBAULT, *On variational micro-macro models and their application to polycrystals*, Dynamical Plasticity and Structural Behaviors (SH. TANIMURA and A. S. KHAN [Eds.]), Gordon and Breach, 245–248, Luxembourg 1995.

31. P. PIMIENTA, P. DUVAL and V. Y. LIPENKOV, *Mechanical behaviour of anisotropic polar ice*, In International Association of Hydrological Sciences, Publication 170 (Symposium on The Physical Basis of Ice Sheet Modelling, Vancouver), 57–66, 1987.

32. J. F. W. BISHOP and R. HILL, *A theory of the plastic distortion of a polycrystalline aggregate under combined stresses*, Phil. Mag., **42**, 414–427, 1951.

33. R. HILL, *The essential structure of constitutive laws for metal composites and polycrystals*, J. Mech. Phys. Solids, **15**, 79–95, 1967.

34. O. CASTELNAU, G. R. CANOVA, R. A. LEBENSOHN and P. DUVAL, *Modelling viscoplastic behavior of anisotropic polycrystalline ice with a self-consistent approach*, Acta. Mater., **45**, 11, 4823–4834, 1997.

*Received June 21, 2000; revised version November 6, 2000.*

Arch. Mech., **53**, 1, pp. 23–43, Warszawa, 2001

# On quantum turbulence in superfluid $^4$He

Ł. LIPNIACKI

*Polish Academy of Sciences*
*Institute of Fundamental Technological Research*
*Świętokrzyska St. 21, 00–049 Warsaw, Poland*

THE ALTERNATIVE APPROACH to the homogeneous quantum turbulence is proposed in order to derive the evolution equation for vortex line-length density. Special attention is paid to reconnections of vortex lines. According to our previous paper, the summary line-length change $\Delta S$ of two vortex lines resulting from the reconnection (in the presence of counterflow $V_{ns}$) can be approximated by the expression: $\Delta S = -at^{1/2} + bV_{ns}^2 t^{3/2}$, with $a > 0$, $b \geq 0$. The dynamics of vortex lines in the tangle is considered as a sequence of reconnections followed by "free" evolutions. For the steady-state turbulence, the average line-length change $<\Delta S>$ between reconnections has to be zero. If, for a given value of the counterflow, the line density is smaller than the equilibrium one, the reconnections occur less frequently and $<\Delta S>$ becomes positive. As a result, the line density grows until the equilibrium is restored. On the other hand, when the line-density is too large, the reconnections are very frequent, so the lines shorten between reconnections and the line density becomes smaller. The time derivative of total line density is proportional to the reconnection frequency multiplied by the average line-length change due to a single reconnection. The evolution equation obtained in the proposed approach resembles the alternative Vinen equation.

**Key Words**: $^4$He, quantum turbulence, reconnection.

## 1. Introduction

THE VARIETY OF THE DYNAMIC phenomena exhibited by the superfluid $^4$He involves the appearance and motion of quantized vortices. Due to the existence of these singularities, the superfluid component is coupled dissipatively with the normal one. We recall that at low velocities, He II (superfluid $^4$He) flows in the frictionless, presumably laminar manner consistent with the ideal fluid description. When the counterflow (the relative velocity of the components) $V_{ns} = V_n - V_s$ becomes sufficiently large, the superfluid laminar flow develops into a superfluid turbulent flow in which the quantum vortices form a chaotic tangle.

The simplest way of generating a sizable $V_{ns}$ (SCHWARZ and ROZEN [11]) is to seal off one end of the channel and place a heater there. The normal fluid transporting the entropy flows out of the channel with average velocity

$V_n = \dot{Q}/A\rho ST$, where $\dot{Q}$ is the heat input, $A$ is the channel cross-sectional area, $\rho$ is the total fluid density, $S$ is the specific entropy, and $T$ is the temperature. The normal fluid moving away from the heater is replaced by the superfluid flowing in the opposite direction, the superfluid velocity being determined by the condition of zero net mass transport $\rho_n V_n + \rho_s V_s = 0$. Since the normal and superfluid densities $\rho_n$ and $\rho_s$ are known functions of temperature, $V_{ns}$ can the be varied in a controlled way, by simply adjusting the heater input $\dot{Q}$.

The pioneering studies of superfluid turbulence were conducted by VINEN [14, 15, 16, 17], who proposed the mechanisms of vortex generation and decay. He observed that in the presence of the counterflow velocity $V_{ns}$, the vortex ring can blow up, and that the line-line reconnections (predicted by Feynman) can give rise to new rings. These phenomenological considerations led him to the (Vinen) equation which described the evolution of line-length density $L$

$$\frac{\partial L}{\partial t} = \alpha_v V_{ns} L^{3/2} - \beta_v L^2 \ , \tag{1.1}$$

where $\alpha_v$ and $\beta_v$ are temperature-dependent coefficients which must be determined experimentally.

Since than, a considerable progress has been made and the new methodology based on careful analysis of the motion of quantized vortices using extensive numerical simulation has been developed.

SCHWARZ [10] simulated the evolution of a vortex tangle basing on an equation describing vortex motion in the localized induction approximation, and on the assumption that vortex lines reconnect when they get close enough. Schwarz defined some characteristic measures $I_l, c_2$ describing the vortex tangle, and in terms of these measures he interpreted the original Vinen coefficients $\alpha_v$ and $\beta_v$. He showed by scaling arguments that for the equilibrium turbulence, these measures do not depend on $L$, and evaluated them for various friction parameters $\alpha$. Later SCHWARZ and ROZEN [11] analyzing, by numerical simulations, large transients when the line-length density grows from very small to very large values, concluded that the coefficients $c_2$ and especially $I_l$ deviated substantially from their steady-state values. This means that despite the fact that Vinen equation can satisfactorily fit most of the experimental data, it is probably not proper, from a more theoretical point of view.

The more powerful computers allow now (NORE *et al.* [7], BARENGHI *et al.* [1]) the numerical simulations of quantum tangle basing on nonlinear Schrodinger equation (NLSE). NLSE describes the evolution of complex field $\Psi = \rho_s \exp(i\Theta)$, which is related to superfluid velocity ($V_s$ =grad $\Theta$) and density $\rho_s = |\Psi|$ via the Madelung transformation. The quantum vortices are traced by lines on which $\Psi = 0$.

In the present paper an alternative approach to the homogeneous quantum turbulence is proposed. The main aim is to derive the evolution equation for the vortex line-length density $L$ in which the coefficients may be determined with the help of relatively simple simulations of evolution of single vortex lines. The paper uses the analysis of motion of quantum vortices presented in two previous papers of the author (LIPNIACKI [4, 5]). The various aspects of the vortex three-dimensional dynamics like line-line and line-boundary reconnection, pinning and depinnig, can be found in the paper by SCHWARZ [9].

The dynamics of quantum vortices will be considered in the localized induction approximation (LIA) supplemented by the assumption that when two vortex lines cross each other, they undergo a reconnection. If the curve traced out by a vortex filament is specified in the parametric form $s(\xi, t)$, the instantaneous velocity of a given point of the filament can be approximated by the equation

$$\dot{s} = \beta s' \times s'' + V_s + \alpha s' \times (V_{ns} - \beta s' \times s'') - \alpha' s' \times [s' \times (V_{ns} - \beta s' \times s'')] , \tag{1.2}$$

where the dot and prime denote instantaneous derivatives with respect to time $t$ and arc length $\xi$, respectively, $\alpha$ and $\alpha'$ are the nondimensional friction coefficients, and

$$\beta = \frac{\kappa}{4\pi} \ln\left(\frac{c}{a_o <s''>}\right) \approx \kappa , \tag{1.3}$$

where $\kappa$ is the quantum of circulation, $c$ is a constant of order one, $<s''>$ is the average curvature of the vortices in the tangle, and $a_o \simeq 1.3 * 10^{-8}$ cm is the effective core radius of a quantized vortex.

The parameter $\alpha'$ is small and according to SCHWARZ [9] considerations confirmed by numerical analysis, the last term in Eq. (1.2) (proportional to $\alpha'$) can be neglected when the quantum tangle is considered. In the further analysis we also put $\alpha' = 0$.

The factor $\beta$ can be absorbed into the reduced time $\tau = \beta t$ and the velocity $v_n = V_n/\beta$, $v_s = V_s/\beta$, with $v_{ns} = v_n - v_s$. Hence in the superfluid reference frame Eq. (1.2) reduces to

$$\dot{s} = s' \times s'' + \alpha s'' + \alpha s' \times v_{ns} . \tag{1.4}$$

Moreover (SCHWARZ [11]), if one takes any solution of Eq. (1.4) and multiplies it by a scale factor $\lambda$, all the velocities by $\lambda^{-1}$, and the time (times) by $\lambda^2$, one obtains another solution of this equation. Any property $P(\mathbf{r}, v, \tau, ...)$ evaluated in any particular solution of Eq. (1.4), relates to the same property $P(\lambda \mathbf{r}, v/\lambda\, \lambda^2 \tau, ...)$, but evaluated on the scaled solution, according to

$$P(\lambda \mathbf{r}, v/\lambda, \lambda^2 \tau, ...) = f(\lambda) P(\mathbf{r}, v, \tau, ...) , \tag{1.5}$$

where the form of $f(\lambda)$ depends on the particular combination of distances and times represented by property $P$. For example, the evaluation of the line-length density at some point in the vortex tangle involves measuring the length of quantized vortex line contained in some sampling volume and dividing by the sampling volume. These scale as $\lambda$ and $\lambda^3$, respectively, so that $f(\lambda) = \lambda^{-2}$ for the line-length density $L$:

$$L(\lambda \mathbf{r}, v_{ns}/\lambda, \lambda^2 \tau) = \lambda^{-2} L(\mathbf{r}, v_{ns}, \tau) \ . \tag{1.6}$$

Hence for the steady-state turbulence, when the line density depends only on $v_{ns}$ one gets from Eq. (1.6)

$$L \sim v_{ns}^2 \ . \tag{1.7}$$

Let us note that the given line-length density determines the characteristic space scale $l_o$

$$l_o = L^{-1/2} \ . \tag{1.8}$$

The length $l_o$ plays an important role in the analysis of the turbulence. First, the quantities like average spacing between vortices or the characteristic radius of curvature $<|s''|>$ of lines in the tangle, scale as $L^{-1/2}$ and are of order $l_o$. The length $l_o$ gives also the minimal scale below which the macroscopic description of vortex tangle loses its sense.

If the motion of vortex filament fulfills Eq. (1.4), its line-length $l = \int d\xi$ satisfies the equation (SCHWARZ [9])

$$\frac{\partial l}{\partial \tau} = \int \Big( \alpha v_{ns} \cdot (s' \times s'') - \alpha |s''|^2 \Big) d\xi \ . \tag{1.9}$$

The first term of the above equation describes the influence of the counterflow velocity onto the line-length. This term can be positive or negative, depending on the angle between the binormal $(s' \times s'')$ and the counterflow. It is obvious that when the totally isotropic vortex tangle is considered, the first term has to average zero. This means that in the steady-state the vortex tangle cannot be totally isotropic since some directional anisotropy of the binormal is needed to balance the second term, which is always negative.

In the presented model, special attention will be paid to reconnections of vortex lines (Fig. 1). To see why the reconnections play the crucial role in the quantum turbulence, let us consider the evolution of a single circular vortex ring subject to the counterflow $v_{ns}$. Let $\Theta(t)$ be the relative angle between the counterflow $v_{ns}$ and the vortex binormal. It can be shown (LIPNIACKI [4]) that if initial ring radius $R_i$ and $\Theta_i = \Theta(0)$ satisfy the inequality

$$R_i > R_o(\Theta_i) = \frac{\Theta_i}{v_{ns} \sin \Theta_i} \ , \tag{1.10}$$

then the ring will blow up and die on the boundaries, and if $R_i < R_o(\Theta_i)$, the ring will contract to a point. The picture is not very different when instead of rings, one considers ovals. This simple example shows that to sustain turbulence, the reconnections are needed to produce new kinks which can develop into new loops.

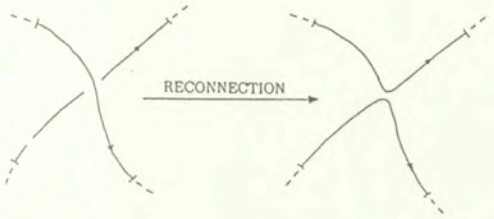


FIG. 1. Collision-reconnection of two vortex segments.

## 2. The model

Let us recall (LIPNIACKI [5]) some facts concerning the specific behavior of quantum vortices after reconnection. Immediately after each reconnection, both resulting lines have very big curvature (close to the reconnection point), the second term of Eq. (1.9) prevails and the lines shortens. Note also that just after the reconnection, close to the reconnection point, the two vortices have the binormals of opposite directions. During further evolution the characteristic curvatures get smaller, and also the two vortices turn so that the average value of $v_{ns} \cdot (s' \times s'')$ becomes positive. As a result, the total length of vortices starts growing. The anisotropy of the distribution of the binormal results from the "action" of the counterflow. In the idealized reconnection of two straight vortices, the summary line-length change $\Delta S(\tau)$ of two vortices resulting from the reconnection can be satisfactorily approximated in the following form:

$$\Delta S(\tau) = -a\,\tau^{1/2} + b\,\tau^{3/2} v_{ns}^2 \,, \tag{2.1}$$

where $a > 0$, $b \geq 0$ are the nondimesional coefficients dependent on friction coefficient $\alpha$ and the specific reconnection configuration (the relative angle between reconnecting lines and the counterflow velocity $v_{ns}$).

If the vortex tangle is considered as a whole, more important is the average line-length change $<\Delta S(\tau)>$ of lines resulting from reconnection. The function $<\Delta S(\tau)>$ has the same form as $\Delta S(\tau)$ and its parameters $<a>$, $<b>$ have been estimated (for isotropic tangle) in the previous paper (LIPNIACKI [5]); we will recall this result later. For steady-state turbulence, the average line-length change between reconnections has to be zero. If for the same value of the counterflow $v_{ns}$ the line density is smaller, the reconnections occur less frequently, and so, the

characteristic time between reconnections is longer and according to Eq. (2.1), the line-length change between reconnections becomes positive. As a result, the line density of vortex tangle grows until the equilibrium is restored. Inversely, when the line-length density is too large, the reconnections are more frequent so that the decaying term in Eq. (2.1) prevails and the line density gets smaller. The model of quantum turbulence we will construct below, bases on the presented mechanisms which explains how the equilibrium density of vortex tangle can be sustained and restored.

We concentrate on the quasi-isotropic turbulence (i.e. with net macroscopic superfluid vorticity equal to zero), derive the evolution equation for line-length density. Later, after some discussion and comparison of the obtained results with those of the Vinen-Schwarz theory, we signal how the model may be generalized in the case in which the considerable macroscopic vorticity is present.

In the quasi-isotropic case we assume (constructing the model) that directional distribution of vortex lines is uniform, i.e. we assume that the unit vector $s'$ is distributed uniformly over the unit sphere. Next we find that such assumption cannot be strictly valid; some directional anisotropy of vortex tangle results from the action of the counterflow $V_{ns}$. Moreover, the nonuniform distribution of the binormal is needed just to sustain the vortex tangle. The assumption of uniform directional distribution should be understood as the zero order approximation, while the anisotropy resulting from the model is the first order perturbation.

The plan of our considerations is the following; first we estimate the average velocity $v_o$ of vortex lines. This will be used to calculate the reconnections frequency $f_r$, and the characteristic time spacing $\tau_c$ between reconnections. Then the average line-length change due to a single reconnection will be found as $<\Delta S(\tau_c)>$. Having the reconnection frequency and length change due to single reconnection, we will obtain the time derivative of line-length density.

### 2.1. The average line velocity $v_o = <|\dot{s}|>$

Let us note that all three terms of Eq. (1.4) lie in the plane which is perpendicular to the local tangent $s'$ to the vortex line. Besides, the first two terms are perpendicular to each other, $|s'| = 1$, hence

$$v_{12} := |s' \times s'' + \alpha s''| = |s''|\sqrt{1+\alpha^2}\ . \tag{2.2}$$

The mean square value of the third term of Eq. (1.4) (under the assumption that the distribution of $s'$ is isotropic) is

$$<|s' \times v_{ns}|^2> = \frac{(\alpha v_{ns})^2}{4\pi} \int_0^{\pi} \int_0^{2\pi} \sin^3(\Theta_j)\, d\Theta_j\, d\phi_j = \frac{2}{3}(\alpha v_{ns})^2\ . \tag{2.3}$$

Hence $v_o^2$ reads:

$$v_i^2 = <|s''|^2> (1+\alpha^2) + \frac{2}{3}(\alpha v_{ns})^2 + <(s' \times s'' + \alpha s'')(\alpha s' \times v_{ns})> . \tag{2.4}$$

We assume (in the zero order approximation) that for given $s'$, both $s''$ and $-s''$ are equally probable i.e that the sign of curvature is not correlated with the tangent to the vortex. This means that the last term of Eq. (2.4) vanishes, and as a result

$$v_o = \sqrt{<|s''|^2> (1+\alpha^2) + \frac{2}{3}(\alpha v_{ns})^2} . \tag{2.5}$$

Assuming that $|s''| = 1/l_o = L^{1/2}$ we get finally the estimate of the mean square value of vortices velocity $v_o$ in the form

$$v_o = \sqrt{L(1+\alpha^2) + \frac{2}{3}(\alpha v_{ns})^2} . \tag{2.6}$$

**2.2. The total reconnection frequency (number of reconnections per time and unit volume)**

Let us divide the vortex lines into segments of length $l_o$ which is equal to average value of the radius of lines curvature, and characteristic spacing between vortex lines forming the tangle. Because the length $l_o$ is equal to spacing between the lines, we may expect that each segment moves (more or less) as a unity, but the motions of the neighboring segments are not strongly correlated. Moreover, because the length of segments are equal to the characteristic radius of curvature, when considering the collisions, the segments can be roughly treated as straight ones. We will assume that every collision of vortex segments leads to a reconnection; such assumption is well justified by numerical simulations (SCHWARZ [9]). For the sake of simplicity we assume that all the segments move with the same speed $v_o$.

Consider now the collision of two segments parallel to unit vectors $e^i$, $e^j$. Let us asign the reference frame to the first unit vector. Let $R_{i,j}$ be the rhombus with center placed in the center of the first segment, and sides (having length $l_o$) parallel to $e^i$, $e^j$.

When the center of the second segment goes through $R_{i,j}$, then the two segments come into collision (Fig. 2). The oriented area $\mathbf{S}_{i,j}$ of rhombus $R_{i,j}$, called from now on the "collision surface", is

$$\mathbf{S}_{i,j} = (l_o)^2 e^i \times e^j . \tag{2.7}$$

The collision frequency $f_{i,j}$ of the given segment parallel to $e^i$ and moving with velocty $v_i$, with other segments parallel to $e^j$ and moving with velocity $v_j$, is

$$f_{i,j} = n_j \mathbf{S}_{i,j} \cdot (v_i - v_j) , \tag{2.8}$$

where $n_j$ denotes the density of segments parallel to $e_j$ and moving with velocity $v_j$. Let $\Theta_i$, $\Theta_j$ denote the angles between normal to $\mathbf{S}_{i,j}$ and velocities $v_i$, $v_j$, respectively, then

$$f_{i,j} = n_j v_o l_o^2 |e^i \times e^j| |\cos(\Theta_i) - \cos(\Theta_j)| \,. \tag{2.9}$$

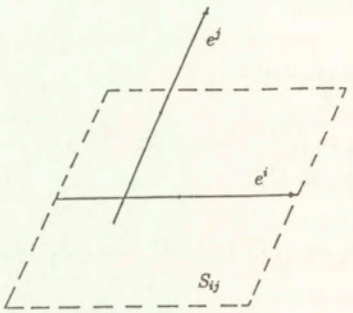


FIG. 2. Collision surface $\mathbf{S}_{i,j}$, corresponding to the collision of two vortex segments which have length $l_o$, and are parallel to $\mathbf{e}^i$, $\mathbf{e}^j$.

Hence the average collision frequency for a segment (of length $l_o$) is

$$f(l_o) = n v_o l_o^2 \, <|e^i \times e^j| |\cos(\Theta_i) - \cos(\Theta_j)|> \,, \tag{2.10}$$

where $<>$ means averaging over the directions $e^i, e^j$ and angles $\Theta_i \in (0, \pi)$, $\Theta_j \in (0, \pi)$, and $n = L/l_o$ is the total segment density. Let us note that because unit vectors $e^i$, $e^j$ are uncorrelated with $\Theta^i$, $\Theta^j$, one can average $|\mathbf{S}_{i,j}|$ and $|\cos(\Theta_i) - \cos(\Theta_j)|$ separately. Calculating the average collision surface $\sigma_o$ one can, without any loss of generality, assume that $e^i$ is parallel to the $\hat{z}$ axis. Then

$$\sigma_o = <|\mathbf{S}_{i,j}|> = \frac{(l_o)^2}{4\pi} \int_0^{\pi} \int_0^{2\pi} \sin(\Theta_j)^2 \, d\Theta_j \, d\phi_j = \frac{\pi}{4} l_o^2 \,, \tag{2.11}$$

while

$$<|\cos(\Theta_i) - \cos(\Theta_j)|> = \frac{1}{\pi^2} \int_0^{\pi} \int_0^{\pi} |\cos(\Theta_i) - \cos(\Theta_j)| \, d\Theta_i \, d\Theta_j = \frac{8}{\pi^2} \,. \tag{2.12}$$

Finally from Eq. (2.10)

$$f(l_o) = \sigma_o \, <|\cos(\Theta_i) - \cos(\Theta_j)|> n v_o = \frac{2}{\pi} l_o v_o L \tag{2.13}$$

since $n = L/l_o$.

In fact, such a calculated reconnection frequency is probably underestimated due to the following reasons.

(1) According to SCHWARZ [9] numerical considerations, the reconnection is initiated by nonlocal interactions when the spacing between lines is smaller than $\Delta \approx 2R/\ln(R/a_o)$, where $R$ is the radius of curvature and $a_o = 1.3\ 10^{-8}$ cm is the vortex core radius. The typical tangle density is $L \sim 10^4 \div 10^6/\mathrm{cm}^2$, what corresponds to $R \sim 10^{-2} \div 10^{-3}$cm, so $\Delta \approx R/5 \approx l_o/5$. This means that even if $\Theta_1 = \Theta_2$ or $S_{i,j} = 0$, the reconnection may take place if only the passing distance is smaller than $l_o/5$. Because of a very complicated nature of nonlocal interactions it is very difficult to analyze the effect of additional collisions quantitatively. For example, two antiparallel vortices reconnect when passing close enough, being parallel do not. Probably the best way to take into account those additional reconnections is to enlarge the collision surface by $l_o^2/5$ or just the reconnection frequency by $l_o v_o L/5$.

(2) The assumption that all the vortex segments move with the same speed reduce the average relative velocity of segments, and the reconnection frequency $f(l_o)$.

Taking into account points (1), (2) we have

$$f(l_o) = c l_o v_o L \ . \tag{2.14}$$

where $c$ is close to unity.

Hence, the total reconnection frequency (per unit volume) $f_r$ is equal to

$$f_r = \frac{n f(l_o)}{2} = \frac{c v_o L^2}{2} \ . \tag{2.15}$$

The factor $1/2$ results from the fact that in each reconnection two segments are involved.

The lines resulting from reconnection are sharply bent close to the reconnection point where the characteristic curvature is much greater than the average curvature of the vortex lines forming a tangle. In our considerations we neglect the lines curvature at the moment prior to reconnection and use the results of the previous paper (LIPNIACKI [5]), where the reconnection of straight vortex filaments has been analyzed. Such approximation seems reasonable until the characteristic curvature caused be the reconnection is greater than the average curvature in a vortex tangle, or (what in fact means the same) until the length of reconnection disturbance is smaller than $l_o$. Fortunately, the average time $\tau_c(l_o)$ after which the segment of length $l_o = L^{-1/2}$ will come into next collision is

$$\tau_c(l_o) = \frac{1}{f(l_o)} = \frac{1}{c L^{1/2} v_o} = \frac{l_o}{c v_o} \ , \tag{2.16}$$

while time $\tau_o(l_o)$ in which the disturbance caused by reconnection grows to the size of order $l_o$ is (LIPNIACKI [4])

$$\tau_o(l_o) = l_o^2 \,. \tag{2.17}$$

Because

$$v_o = \sqrt{(1+\alpha^2)L + \frac{2}{3}(\alpha v_{ns})^2} \approx L^{1/2} \approx l_o^{-1}, \tag{2.18}$$

these two times are roughly equal. This means that the evolution of line segment of length $l_o$ looks as follows: reconnection – evolution during which the reconnection disturbance grows (roughly) up to the size of the segment – next reconnection. Of course after each reconnection the segment loses its identity.

According to the above, the line-length change caused by each reconnection will be approximated by the line-length change of straight reconnecting lines $\Delta S(\tau_c)$, where

$$\tau_c(l_o) = \frac{1}{cL^{1/2}v_o} \,. \tag{2.19}$$

Hence the time derivative of line-length density $L$ reads

$$\frac{dL}{d\tau} = f_r \; <\Delta S(\tau_c)> \;, \tag{2.20}$$

where (recall) $f_r$ is the total reconnection frequency and $< \Delta S(\tau_c) >$ is the average line-length change due to the single reconnection. According to Eq. (2.1), the average line-length change reads:

$$<\Delta S(\tau_c)> = - <a(\alpha)> \; \tau^{1/2} + <b(\alpha)> \; \tau^{3/2} v_{ns}^2 \,, \tag{2.21}$$

where $< \; >$ denotes the averaging over all reconnection configurations (which are described by directional vectors of reconnecting lines in the direction of counterflow velocity $v_{ns}$).

Putting $< \Delta S(\tau_c) >$ from Eq. (2.21) with $\tau_c$ from Eq. (2.19) and $f_r$ from Eq. (2.15) into Eq. (2.20), we get finally

$$\frac{dL}{d\tau} = \frac{1}{2}\Big( - c^{1/2} <a(\alpha)> \; L^{7/4} \, v_o^{1/2} + c^{-1/2} <b(\alpha)> \; L^{5/4} \, v_o^{-1/2} \, v_{ns}^2 \Big) \,, \tag{2.22}$$

with

$$v_o = \sqrt{<|s''|^2> (1+\alpha^2) + \frac{2}{3}(\alpha v_{ns})^2} \,. \tag{2.23}$$

The nondimensional coefficients $<a(\alpha)>$, $<b(\alpha)>$ have been estimated in the previous paper (LIPNIACKI [5]) with the help of numerical simulations, and in the following section we will recall these results.

## 3. Numerical estimations

To determine the average line-length change $<\Delta S(\tau)>$ of lines $\Delta S(\tau)$ resulting from reconnection, one should average over all reconnection configurations with respect to the direction of counterflow. Numerically it is rather impossible, hence to estimate $<\Delta S(\tau)>$ it was assumed that all lines in the tangle are parallel or antiparallel to 3 directions: $\hat{x}, \hat{y}, \hat{z}$, while the direction of counterflow is $(1, 1, 0)$. Let us note that such assumption may be only adequate for quasi isotropic case. For anisotropic case other representation should be used. The accuracy of the above method may be augmented by taking more directions into account.

The numerical simulations for the equation

$$\dot{s} = s' \times s'' + \alpha s'' + \alpha s' \times v_{ns} \tag{3.1}$$

were carried for $\alpha = 0.1$. The best fit for $\Delta S_o =< \Delta S >$ in the form (discussed previously)

$$\Delta S_o = - <a(\alpha)> \tau^{1/2} + <b(\alpha)> \tau^{3/2} v_{ns}^2 \tag{3.2}$$

was found for $a = 0.710$ , $b = 0.0138$. The characteristic nondimensional time $\tau_o v_{ns}^2$ after which $\Delta S_o = 0$ is $\tau\, v_{ns}^2 = a/b = 51.2$. The time $\tau_o$ plays an important role in the analysis of turbulence, because in the equilibrium state $\tau_o$ and $\tau_c$ – characteristic times between reconnection should be equal.

To estimate the average line-length change for different $\alpha$, we note that neglecting the first term of Eq. (3.1) i.e. the self-induction and using the simplified dynamic equation in the form

$$\dot{s} = \alpha s'' + \alpha s' \times v_{ns} \ , \tag{3.3}$$

one gets roughly the same rate of line change, when averaging over representative sample of reconnection configurations. This is due to the fact (see LIPNIACKI [5] for more details) that the first term in Eq. (3.1) pushes the vortex along local binormal which does not change the vortex length. Indeed (for $\alpha = 0.1$) the characteristic time of zero line-length change obtained in the simulations without self-induction is 45.7, so it is only 12% smaller when calculated with the use of the full dynamic equation. The use of the simplified dynamic equation has such an advantage that now the coefficient $\alpha$ can be absorbed into time scale. Hence

Eq. (3.2) can be transformed into

$$\Delta S_o = - <a(\alpha)> \tau^{1/2} + <b(\alpha)> \tau^{3/2} v_{ns}^2 = -a_o(\alpha\tau)^{1/2} + b_o(\alpha\tau)^{3/2} v_{ns}^2 , \tag{3.4}$$

what implies

$$<a(\alpha)> = a_o \alpha^{1/2} , \quad <b(\alpha)> = b_o \alpha^{3/2}, \tag{3.5}$$

with numerically calculated $a_o = 2.34$, $b_o = 0.514$. Let $A = a_o/2 = 1.17$, $B = b_o/2 = 0.257$. Then from Eqs. (2.22), (3.5) one gets

$$\frac{dL}{d\tau} = -c^{1/2} A \alpha^{1/2} \, L^{7/4} \, v_o^{1/2} + c^{-1/2} B \alpha^{3/2} \, L^{5/4} \, v_o^{-1/2} \, v_{ns}^2 . \tag{3.6}$$

Now we set $c = 1$ to get estimated but concrete coefficients in final form of the evolution equation; in primary variables $t = \tau/\beta$ and $V_{ns} = \beta v_{ns}$, $V_o = \beta v_o$ we have

$$\frac{dL}{dt} = -A\beta^{1/2}\alpha^{1/2} \, L^{7/4} \, V_o^{1/2} + B\beta^{-1/2}\alpha^{3/2} \, L^{5/4} \, V_o^{-1/2} \, V_{ns}^2 , \tag{3.7}$$

with

$$V_o = \sqrt{\beta^2(1+\alpha^2)L + \frac{2}{3}(\alpha V_{ns})^2} . \tag{3.8}$$

The equilibrium vortex density $L_\infty$ is given by

$$L_\infty = \frac{V_{ns}^2}{\beta^2(1+\alpha^2)} \left( \sqrt{\frac{\alpha^4}{9} + (1+\alpha^2)\left(\frac{B\alpha}{A}\right)^2} - \frac{\alpha^2}{3} \right) = w(\alpha) \left(\frac{V_{ns}}{\beta}\right)^2 . \tag{3.9}$$

When $\alpha \ll 1$ and $\alpha V_{ns} \ll \beta L$, the particle velocity can be approximated by $\tilde{V}_o = \beta L^{1/2}$ and the evolution equation simplifies to

$$\frac{dL}{dt} = -A\beta\alpha^{1/2} \, L^2 + B\beta^{-1}\alpha^{3/2} \, L \, V_{ns}^2 . \tag{3.10}$$

## 4. Results

### 4.1. Critical remarks

The time derivative of line-length density (Eq. (2.20))

$$\frac{dL}{d\tau} = f_r \; <\Delta S(\tau_c)> \; , \tag{4.1}$$

is expressed as a product of reconnection frequency and average line-length change due to a single reconnection. Such approach includes of course some

idealization. In real turbulence one may expect that there are line segments (of length $l_o$) for which the time of "free" evolution is significantly shorter or longer than the average $\tau_c(l_o)$ used to calculate $\Delta S$. Expression (4.1) cannot be valid when considering the line density changes in times shorter than the average time spacing between reconnections $\tau_c(l_o)$ (Eq. (2.16)). This can be important when considering sharp transitions in which the value of $V_{ns}$ grows significantly. Besides, both the reconnection frequency $f_r$ and the average line-length change $\Delta S(\tau)$ are estimated with some errors.

1) The coefficient $c$ appearing in the expression for reconnection frequency

$$f_r = \frac{cv_oL^2}{2} \tag{4.2}$$

has been finally replaced by unity. Fortunately, in evolution equation (3.6) coefficient $c$ appears only as $c^{1/2}$ and $c^{-1/2}$. This means that possible input error is roughly two times smaller than the error made by replacing $c$ by unity, and probably is not greater than 10%.

2) The possible errors in estimation of the average line-length change $<\Delta S(\tau)>$

i) The initial curvature of reconnecting lines has been neglected.

ii) The relatively small sample of reconnecting lines has been considered to calculate the average value of $\Delta S(\tau)$. The possible error is of the order of $10 \div 20\%$ (see discussion in LIPNIACKI [5]).

iii) To calculate $\Delta S(\tau)$ for $\alpha \neq 0.1$, the simplified dynamical equation has been applied; the expected error is also of the order of $10 \div 20\%$.

Keeping in mind the above remarks one cannot expect that the numerical accuracy of Eq. (3.7) will be better than 50%; what is not so bad when comparing with the experimental data which varies significantly from experiment to experiment.

#### 4.2. The obtained evolution equation versus Schwarz and Rozen simulation and experiments

Equations (3.7), (3.10) should be confronted with other two equations describing the evolution of vortex line density, namely:

1) The classical Vinen (-Schwarz) equation

$$\frac{dL}{dt} = -\beta\alpha{c_2}^2\ L^2 + \alpha I_l\ L^{3/2}|V_{ns}|\ , \tag{4.3}$$

with nondimensional coefficients $c_2(\alpha)$ and $I_l(\alpha)$:

$$c_2^2 = \frac{1}{\Omega L^2}\int (s'')^2 d\xi\ , \tag{4.4}$$

$$I_l \hat{V}_{ns} = \frac{1}{\Omega L^{3/2}} \int s' \times s'' d\xi \ , \tag{4.5}$$

where $\hat{V}_{ns}$ is the unit vector in the direction of $V_{ns}$ and $\Omega$ is the element of volume. This equation, originally devised by VINEN [16] in phenomenological considerations, was later developed by SCHWARZ [10]. Schwarz expressed original Vinen coefficients by $c_2(\alpha)$ and $I_l(\alpha)$, which describe the microscopic state of quantum tangle. He showed also by dynamical scaling that in the case of steady-state turbulence, these coefficients do not depend on $L$ or $V_{ns}$.

2) Alternative Vinen equation (VINEN [16])

$$\frac{dL}{dt} = -\beta_{alt} \ L^2 + \alpha_{alt} L \ V_{ns}^2 \ , \tag{4.6}$$

where $\beta_{alt}$ and $\alpha_{alt}$ are some new parameters.

First, we should note that the simplified Eq. (3.10) obtained in the proposed model strictly corresponds to the alternative Vinen equation. The generation term is proportional to $LV_{ns}^2$ what is closer to the phenomenological theory of classical turbulence (LANDAU, LIFSHITZ 1980). Indeed, (NIEMIROWSKI, FISZDON [6]) by assuming that turbulence can be characterized by a parameter, say, $L$, and that its time derivative $dL/dt$ is an analytic function of $L$, the alternative form of Vinen equation can be interpreted as the first two terms of the series expansion. Furthermore, as the generation term is the scalar function of vector argument $V_{ns}$, it is reasonable that the series expansion starts with this argument squared. The last comment concerns also the complete form of the evolution equation obtained in the model, i.e. Eq. (3.7) where the counterflow velocity $V_{ns}$ is also everywhere squared. The presence of absolute value of $V_{ns}$ in the classical Vinen equation is rather strange.

Now we concentrate on the steady state turbulence and compare the equilibrium line-length densities $L_\infty$ obtained in the model (Eq. (3.9)), in numerical simulations done by Schwarz (with the use of Vinen-Schwarz theory) and in real experiments. The equilibrium density obtained in our model is given by:

$$L_\infty = w(\alpha) \left( \frac{V_{ns}}{\beta} \right)^2 \ , \tag{4.7}$$

while in the Vinen-Schwarz theory

$$L_\infty = \left( \frac{I_l}{c_2^2} \right)^2 \left( \frac{V_{ns}}{\beta} \right)^2 = c_L^2 \left( \frac{V_{ns}}{\beta} \right)^2 \ . \tag{4.8}$$

As the dependence on $V_{ns}$ is the same (as we noted in the introduction $L_\infty$ must be proportional to $V_{ns}$), we have only to compare our function $w(\alpha)$ with

Schwarz's $c_L^2(\alpha) = \left(I_l/c_2^2\right)^2$, and with experimental results. Because the line-length density is measured indirectly by measuring the mutual friction force, we have to remind some facts. The normal fluid component exerts a force on the quantized vortices of the vortex tangle, and on the other hand, superfluid interacts with vortices by the Magnus force. In the result the vortices give rise to the friction force $F_{ns}$ between the two components

$$F_{ns} = \rho_s \kappa \alpha I_m L V_{ns} \,, \tag{4.9}$$

where $I_m(\alpha)$ is another anisotropy coefficient, characterizing the vortex tangle. When the tangle is isotropic $I_m = 2/3$, but usually it varies between $2/3$ and 1. Schwarz found that it can be expressed as $I_m = I_{||} - c_L I_l$, where

$$I_{||} = \frac{1}{\Omega L} \int (1 - (s' \cdot \hat{V}_{ns})^2) d\xi \tag{4.10}$$

is the other directional anisotropy coefficient, and calculated it in his simulations. Because we cannot simply calculate $I_{||}$ in our model, to compare the results we take $I_m$ from the Schwarz simulation.

Putting $L$ from Eq. (4.8) or from Eq. (4.7) to Eq. (4.8), one gets:

$$F_{ns} = \frac{\rho_s \kappa \alpha}{\beta^2} f_\alpha V_{ns}^3 \,, \tag{4.11}$$

where the coefficient $f_\alpha = c_L^2 I_m$ in the Vinen-Schwarz theory or $f_\alpha = w I_m$ in the proposed model. The force $F_{ns}$ can be determined in the counterflow experiments by measuring the temperature gradient

$$F_{ns} = \rho S \nabla T \,, \tag{4.12}$$

where $S$ is the entropy per unit mass.

The coefficient $f_\alpha$ was used by SCHWARZ[10] and later by SCHWARZ and ROZEN [11] to compare the numerical results with experiments. In Fig. 3 we compare our results with Schwarz predictions and some experimental results chosen by Schwarz. Besides in Table 1 we present some coefficients characterizing quantum turbulence. From Fig. 3 one can see that the experimental results vary significantly from one experiment to another. For the same $\alpha$ the coefficient $f_\alpha^{1/3}$ vary by $20 - 40\%$, when considering various experiments; this gives the uncertainty of L of the order of 2. This is because the experiments are still not a good test for the model proposed here, or for the Schwarz theory. We may notice however, that our theoretical curve fits relatively better the recent SCHWARZ and ROZEN [11] experiment than the Schwarz theoretical curve.

Now we concentrate on non-equilibrium turbulence. Because even the measurements of steady state turbulence give very different results, comparing our

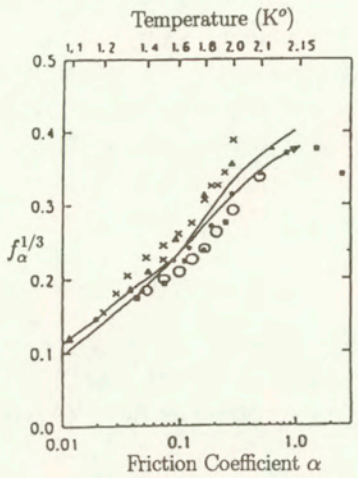


FIG. 3. The $\alpha$ dependence of the friction coefficient $(f_\alpha)^{1/3}$. The line ending with arrows – model predictions (3.9), second line – SCHWARZ [10] predictions basing on numerical simulations. Crosses represent pure superflow in 0.0057 cm by 0.057 cm channel (OPATOWSKI and TOUGH [8]), dots represent counterflow in 0.0366 cm capillary (BREWER and EDWARDS [2]), triangles are counterflow in a 0.240 by 0.645 cm channel (VINEN [14, 15, 17, 17]) squares represent counterflow in a 1.0 by 1.0 cm channel (SWANSON [12], SWANSON and DONNELLY [13]), and open circles are counterflow in 1.00 by 2.32 cm channel (SCHWARZ and ROZEN [11]).

evolution equation with experiments seems to be not useful. SCHWARZ and ROZEN found that the Vinen equation can fit satisfactorily their experimental curves, however the fitted coefficients $I_l$ and $c_L$ differ substantially from the calculated ones. In Fig. 4 we fit our evolution equation to Vinen evolution equation (with coefficients used by SCHWARZ and ROZEN to fit their experiments). Those two curves lie so close to each other that until we have no better experiments, we can not judge from them which form of evolution equation is better.

**Table 1. Values of dimensionless parameters characterizing quantum turbulence. S – Schwarz simulation, M – proposed model.**

| Temp | 1.07 | 1.26 | 1.62 | 2.01 | 2.15 |
|---|---|---|---|---|---|
| $\rho_n/\rho$ | 0.013 | 0.039 | 0.174 | 0.576 | 0.886 |
| $\alpha$ | 0.010 | 0.030 | 0.100 | 0.300 | 1.00 |
| $I_{\|\|} - c_L I_I$ | 0.70 | 0.72 | 0.71 | 0.77 | 0.85 |
| $w_\alpha$ [M] | 0.0022 | 0.0070 | 0.019 | 0.041 | 0.061 |
| $c_L \sim w_\alpha$ [S] | 0.0013 | 0.0053 | 0.019 | 0.0484 | 0.076 |
| $\overline{f}_\alpha^{1/3}$ [M] | 0.115 | 0.171 | 0.238 | 0.317 | 0.374 |
| $f_\alpha^{1/3}$ [S] | 0.097 | 0.156 | 0.238 | 0.334 | 0.401 |

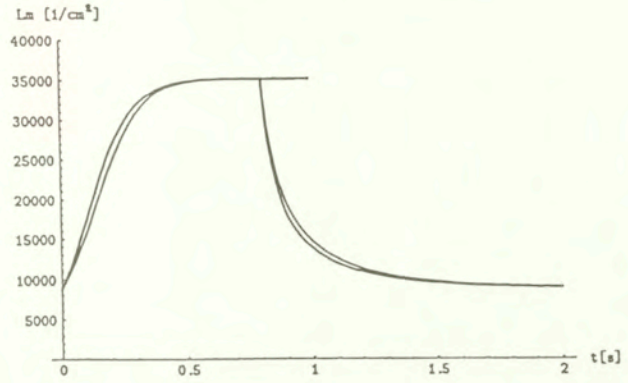


FIG. 4. The evolution of line-length density during the growth and decasy transient. At $t = 0$ the counterflow velocity is switched from $V_{ns} = 1$ cm/s to 2 cm/s, than at $t = 0.8$ s it is switched again to 1 cm/s. The "inner" line is a prediction of the Vinen equation with coefficients $c_{lm} = 0.0937$ and $I_{lm} = 0.65$ used by Schwarz to fit his experiments with Rozen. The "outer" line is the solution of our Eq. (3.7) with $A = 0.86$, $B = 0.137$.

Instead of comparing the theoretical predictions of our model with experiments, we propose to compare them with SCHWARZ [10] and SCHWARZ and ROZEN [11] simulations. In the paper [10] SCHWARZ assumed that the coefficient $I_l$ and $c_2$ depend neither on $L$ nor on $V_{ns}$ and calculated them in the numerical simulations for equilibrium turbulence. Later, in the paper [11] SCHWARZ and ROZEN analyzed, by numerical simulations, large transients when the line-length density grows from very small to very large value, and concluded that $I_l = I_l(tL_\infty, L_i/L_\infty)$ and $c_2 = c_2(tL_\infty, L_i/L_\infty)$ where $L_i$ is the initial value of line-length density. That conclusion written in a rather curious form (curious because it can not be simply applied e.g. to the case when $V_{ns}$ varies harmonically) means in fact that $I_l$ and $c_2$ depend on $L$ and $V_{ns}$. This means that the classical Vinen equation is improper. Especially, as they found, the coefficient $I_l$ which measured the anisotropy of the distribution of the binormal to the tangle varied significantly. In the simulations with $T = 1.6$ K i.e. $\alpha = 0.1$, the sudden change of counterflow $V_{ns}$ by factor 3 causes a sharp change of $I_l$ by roughly 50% (see Fig. 5). This phenomenon can be interpreted in our model; as we noted, the anisotropy results from the action of the counterflow between two subsequent reconnections, so it is clear that for the same line-length density the anisotropy will be larger for larger $V_{ns}$. Moreover we can calculate the anisotropy coefficient $I_l$ from our model, by comparing the growth term of our evolution equation with the Vinen one. As the result we get:

$$\tilde{I}_l = B\alpha^{1/2}\,\beta^{-1/2}\,|V_{ns}|\,L^{-1/4}\,V_o^{-1/2}\,. \tag{4.13}$$

First, we notice that for steady-state turbulence ($L = L_\infty$)

$$\tilde{I}_{l\infty} = B\alpha^{1/2} \left( w_\alpha \left( (1+\alpha^2) w_\alpha + \frac{2}{3}\alpha^2 \right) \right)^{-1/4} . \tag{4.14}$$

For $\alpha = 0.1$ we get $\tilde{I}_{l\infty} = 0.55$, while Schwarz obtained $I_{l\infty} = 0.45$ as asymptotic value for steady state turbulence. During the transition $I_l$ varies. To conpare the dependence of $I_l$ on scaled time $t_{sc} = \beta t L_\infty$ with Schwarz numerical results, we multiply our $I_l$ by 0.45/0.55 to have the same asymptotic value; such difference of order 20% in asymptotic values is rather meaningless. The result is shown in Fig. 5. The coefficient $\tilde{c}_2^2$ corresponding to $c_2^2$ can be calculated by comparing the decaying terms in both equations:

$$\tilde{c}_2^2 = A\alpha^{-1/2}\, \beta^{-1/2}\, L^{-1/4}\, V_o^{1/2}; \tag{4.15}$$

its asymptotic value (for $L = L_\infty$) $c_{2\infty}^2$ is

$$\tilde{c}_{2\infty}^2 = A\alpha^{-1/2} \left( 1 + \alpha^2 + \frac{2\alpha^2}{3w_\alpha} \right)^{1/4} . \tag{4.16}$$

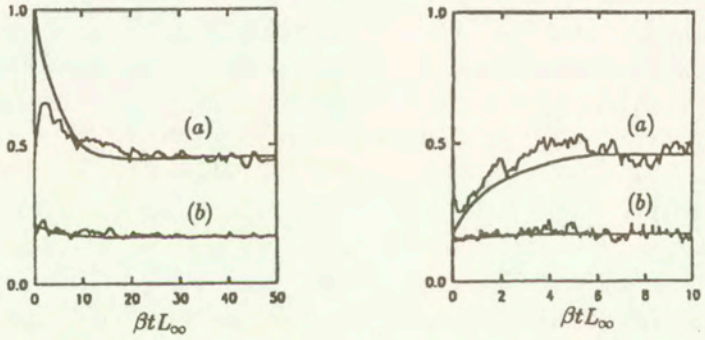


FIG. 5. The evolution of coefficients (a) – $I_l$ and (b) – $c_2^2/20$ and the corresponding coefficient $\bar{I}_l$ and $\bar{c}_2^2/20$ during the growth (left) and the decay (right) transient. The smooth lines are the coefficients $\bar{I}_l$ and $\bar{c}_2^2/20$. In the growth transient the counterflow velocity $V_{ns}$ is suddenly increased from $V_o$ to $3V_o$, while in the decay transient it is decreased from $V_o$ to $V_o/3$.

For $\alpha = 0.1$ we get $\tilde{c}_{\infty 2}^2 = 4.00$ while the Schwarz numerical value is $c_2^2 = 3.31$. Again, to compare our result with those of Schwarz, we rescaled our $\tilde{c}_2^2$ to have the same asymptotic value. From Fig. 5 we see the time dependence of our coefficient $\tilde{I}_l$ and $\tilde{c}_2^2$ corresponds somehow to the time dependence of Schwarz coeficients $I_l$ and $c_2^2$. This means that our dynamic equation corresponds better to Schwarz simulations than to Vinen equation with constant coefficients. Our coefficients

$\tilde{I}_l$ , $\tilde{c}_2^2$ depend only on $L$ and $V_{ns}$, but in reality, some time after $V_{ns}$ is switched, it is needed to change them. The reaction time in which the coefficients change is roughly equal to the characteristic time between the reconnections (Eq. (2.17))

$$t_c = \frac{1}{(\beta L)^{1/2} V_o} \,. \tag{4.17}$$

For the steady state turbulence for $\alpha = 0.1$ one gets $t_c = 0.86/\beta L$. This corresponds to the scaled time $t_{sc} = \beta t L_\infty$; $t_{sc} = 8$ in the beginning of growth transient, $t_{sc} = 0.1$ in the beginning of decay transient. This roughly agrees with the reaction time which can be deduced from Fig. 5. During the reaction time, the coefficients $\tilde{I}_l$ and $\tilde{c}_2^2$ cannot agree with those measured in the simulations. To determine the behavior of $\tilde{I}_l$ and $\tilde{c}_2^2$ during the reaction time, the separate equations are needed to supplement the evolution equation for line-length density.

## 5. Conclusions and perspectives

The main result of this work is the construction of the simple model in which the microscopic analysis of quantum tangle leads to macroscopic evolution equation for line-length density. The numerical simulations needed to estimate coefficients $A, B$ in Eq. (3.7) are relatively simple and not time-consuming, when compared with the simulations of Schwarz. The main advantage of the presented approach is the possibility of generalizing it to anisotropic flows with significant macroscopic superfluid vorticity. Such flows are expected in such phenomena as spin-up or boundary layer forming. The viscous forces in a cylinder, which start spinning from the rest, acting on normal component, may give rise to the counterflow, large enough to cause the quantum turbulence which may significantly influence the dynamics of both components. In this way the angular momentum can be transferred from the cylinder via the normal component to the superfluid component. One may expect the following scenario: due to viscous forces, the normal component starts spinning, and this implies counterflow which generates quantum turbulence. The mutual friction forces couple the two components ($V_{ns} \to 0$) and in the end, the quantum vortices polarize to form a pattern of straight parallel lines and both fluids spin together. However, because of the large normal fluid velocity gradients, even in first stages of spin-up process the arising quantum turbulence is highly anisotropic; the tangle of quantized vortices is polarized to carry considerable macroscopic superfluid vorticity. This is probably why the description of spin-up process in terms of the Vinen model was found to be inconsistent (LIPNIACKI [3]). The line-length density calculated from Vinen equation was smaller then the line density calculated from superfluid velocity profiles. The origin of these vortices cannot be explained within the Vinen model.

To analyze the superfluid turbulent flows with net vorticity, the generalization of the model for an anisotropic turbulence is needed.

Macroscopic vorticity introduces into quantum turbulence an additional anisotropy parameter $q$.

$$q = \frac{\omega_s}{\kappa L} = \frac{L_{\|}}{L} = \frac{\int s' \cdot \hat{z} d\xi}{\int d\xi} , \tag{5.1}$$

where $L_{\|} = \omega_s/\kappa$ is the minimal vortex line-density needed to generate superfluid vorticity $\omega_s$, $\hat{z}$ is unit vector parallel to the $z$ axis, and $s'$ (recall) is the unit vector tangent to vortex line $s(\xi, \tau)$. The parameter $q \in [0, 1]$; $q = 0$ corresponds to the isotropic case, while $q = 1$ corresponds to the system of straight parallel vortex lines.

The anisotropy influences significantly the evolution of the tangle, and at least three aspects must be taken in to account:

1) The non-zero macroscopic superfluid vorticity $\omega_s$ influences the superfluid flow. Hence to calculate the counterflow $V_{ns}$ the superfluid macroscopic velocity $V_s$ must be calculated from macroscopic $\omega_s$ by the Biot-Savart law. Another way will be to calculate the superfluid vortex velocities directly from the Biot-Savart law basing on positions of all vortices (see BARENGHI *et al.* [1]) but this method is numerically very expensive and can be applied only to relatively rarefied vortex tangle.

2) For $q > 0$ the vortex lines prefer to lie along one direction, so the average relative angle between vortex lines is smaller than in the isotropic case. This implies that average collision surface $\sigma(q)$ and reconnection frequency $f_{rq}$ are smaller than $\sigma_o$ and $f_r$, respectively. Because the reconnection frequency is proportional to the collision surface (Eq. (2.13), (2.15)), we may express $f_{rq}$ as follows:

$$f_{qr} = \frac{\sigma(q)}{\sigma_o} f_r = \frac{\sigma(q)}{\sigma_o} \, l_o \, v_o \, L , \tag{5.2}$$

where $\sigma_o = \pi/4$ and $f_r = l_o \, v_o \, L$ correspond to the isotropic case, and $\sigma(q)$ has to be calculated.

3) The average relative angle between reconnecting lines will be smaller, hence the average line-length change $\Delta S_o(q)$ due to each reconnection will be different. $\Delta S_o(q)$ may be expressed in the same form as in Eq. (3.4)

$$\Delta S_o(q, \tau) = -a(q) \, (\alpha\tau)^{1/2} + b(q) \, (\alpha\tau)^{3/2} v_{ns}^2 , \tag{5.3}$$

but with coefficients $a(q)$, $b(q)$ instead $a_o$, $b_o$.

## Acknowledgments

The author is grateful to Professor Peradzyński for stimulating discussion and comments. This work was supported by the KBN grant 7T07A 01817.

## References

1. C. F. BARENGHI, G. H. BAUER, R. J. DONNELLY, D. C. SAMUELS, *Superfluid vortex lines in a model of turbulent flow*, Phys. Fluids, **9**, 9, 2631–2643, 1997.
2. B. F. BREWER, D. O. EDWARDS, *Heat Conduction by liquid helium II in capillary tubes III mutual friction*, Philos. Mag., **7**, 721–735, 1962.
3. T. LIPNIACKI, *Dynamics of superfluid Helium – limits of the Vinen model*, Arch. Mech., **49**, 4, 615–633, 1997.
4. T. LIPNIACKI, *Dynamics of quantum vortices in superfluid $^4$He*, Arch. Mech., **50**, 3, 467–482, 1998.
5. T. LIPNIACKI, *Evolution of quantum vortices following reconnection*, Eur. J. Mech., B/Fluids, **19**, 361–378, 2000.
6. S. K. NEMIROWSKI, W. FISZDON, *Chaotic quantized vortices and hydrodynamic processes in superfluid helium*, Rev. Mod. Phys., **67**, 1, 37–84, 1995.
7. C. NORE, M. ABID, M. E. BRACHET, *Decaying Kolmogorov turbulence in a model of superflow*, Phys. Fluids, **9**, 9, 2644–2669, 1997.
8. L. B. OPATOWSKY, J. T. TOUGH, *Homogeneity of turbulence in pure superflow*, Phys. Rev., **B 24**, 5420–5421, 1981.
9. K. W. SCHWARZ, *Three-dimensional vortex dynamics in superfluid $^4$He: Line-line and line-boundary interactions*, Phys. Rev., **B 31**, 5782–5804, 1984.
10. K. W. SCHWARZ, *Three-dimensional vortex dynamics in superfluid $^4$He: Homogenous superfluid turbulence*, Phys. Rev., **B 38**, 2398–2417, 1988.
11. K. W. SCHWARZ, J. R. ROSEN, *Transient behavior of superfluid turbulence in a large channel*, Phys. Rev., **B 44**, 7563–7577, 1991.
12. C. E. SWANSON, *A study of vortex dynamics in counterflowing helium II*, Ph. D. thesis, University of Oregon, 1985.
13. C. E. SWANSON, R. J. DONNELLY, *Vortex dynamics in turbulent counterflowing helium II*, J. Low Temp. Phys., **61**, 363–399, 1985.
14. W. F. VINEN, *Mutual friction in heat current in liquid helium II, I, Experiments on Steady Currents*, Proc. R. Soc. London, Ser. A **240**, 114–127, 1957a.
15. W. F. VINEN, *Mutual friction in heat current in liquid helium II, II, Experiments on transient effects*, Proc. R. Soc. London, Ser. A **240**, 128–143, 1957b.
16. W. F. VINEN, *Mutual friction in heat current in liquid helium II, III. Theory of the mutual friction*, Proc. R. Soc. London, Ser. A **242**, 493–515, 1957c.
17. W. F. VINEN, *Mutual friction in heat current in liquid helium II, IV. Critical heat currents in wide channels*, Proc. R. Soc. London, Ser. A **243**, 400–413, 1958.

*Received August 30, 2000; revised version November 27, 2000.*

Arch. Mech., 53, 1, pp. 45–63, Warszawa 2001

# A qualitative approach to Hooke's tensors. Part II

J. RYCHLEWSKI

*Polish Academy of Sciences*
*Institute of Fundamental Technological Research*
*Świętokrzyska 21, 00-049 Warszawa, Poland*

*University of Warmia and Mazury in Olsztyn*

A STRAIGHTFORWARD AND COMPLETE DESCRIPTION of all possible invariant linear decompositions of the space of Hooke's tensors has been given in Part I, [1]. In this Part II we demonstrate various eleborations and consequences of these decompositions. This gives a qualitative decription of the anisotropy of Hooke's tensors. In particular, we demonstrate examples A through G, not only important but also astonishing. When reference is made to the formulae in [1], we shall add "Part I" to the number. The notions and notations are the same (see Appendices 1, 2 in [1]).

## 1. Introduction

THIS PART IS A DIRECT CONTINUATION of [1], but it has a different character. The purpose now is to investigate the qualitative consequences of the invariant decompositions presented in the previous part. The main and most interesting results are grouped in seven examples A-G, Sec. 7. We intend to demonstrate on these examples that materials of totally different structure can, under certain types of action, react quite similarly or even identically. We hope that these examples will contribute to a novel kind of thinking on the isotropy of properties of condensed matter.

## 2. Energy decompositions of Hooke's tensors

**2.1.** Let us decompose the quadratic form (energy, work, stress intensity and so on)

$$\upsilon \cdot \mathbf{H} \cdot \omega = \omega_{\mathcal{P}} \cdot \mathbf{H} \cdot \omega_{\mathcal{P}} + 2\omega_{\mathcal{D}} \cdot \mathbf{H} \cdot \omega_{\mathcal{P}} + \omega_{\mathcal{D}} \cdot \mathbf{H} \cdot \omega_{\mathcal{D}}, \tag{2.1}$$

where $\omega_{\mathcal{P}} \equiv \mathbb{I}_{\mathcal{P}} \cdot \omega$, $\omega_{\mathcal{D}} \equiv \mathbb{I}_{\mathcal{D}} \cdot \omega$.

EXAMPLE 1. Let $\mathbf{C}$ be a compliance tensor of an elastic material, and $\sigma$ an acting stress. Then (see (1.4), Part I):

• $\sigma_{\mathcal{P}} \cdot \mathbf{C} \cdot \sigma_{\mathcal{P}} = \sigma_{\mathcal{P}} \cdot (\mathbf{C} \cdot \sigma_{\mathcal{P}})_{\mathcal{P}}$ is doubled work of the hydrostatic part of stress $\sigma_{\mathcal{P}}$ on the resultant deformation,

• $\sigma_{\mathcal{P}} \cdot \mathbf{C} \cdot \sigma_{\mathcal{D}} = \sigma_{\mathcal{P}} \cdot (\mathbf{C} \cdot \sigma_{\mathcal{D}})_{\mathcal{P}}$ is doubled work of the hydrostatic part on the deformation caused by the deviatoric part of stress and *vice versa*,

• $\sigma_{\mathcal{D}} \cdot \mathbf{C} \cdot \sigma_{\mathcal{D}} = \sigma_{\mathcal{D}} \cdot (\mathbf{C} \cdot \sigma_{\mathcal{D}})_{\mathcal{D}}$ is doubled work of the deviatoric part on the resultant deformation.

Quite similarly, we can decompose energy of deformation $\varepsilon \cdot \mathbf{S} \cdot \varepsilon$. Let us note that, for example, $\varepsilon_{\mathcal{P}} \cdot \mathbf{S} \cdot \varepsilon_{\mathcal{P}} \neq \sigma_{\mathcal{P}} \cdot \mathbf{C} \cdot \sigma_{\mathcal{P}}$.

**2.2.** There is a correspondence between the used decomposition of quadratic form (2.1) and the unique decomposition of its Hooke's tensor

$$\mathbf{H} = \mathbf{H}^{\mathcal{P}} + \mathbf{H}^{\mathcal{PD}} + \mathbf{H}^{\mathcal{D}}, \tag{2.2}$$

where

$$\mathbf{H}^{\mathcal{P}} \equiv \mathbb{I}_{\mathcal{P}} \circ \mathbf{H} \circ \mathbf{I}_{\mathcal{P}}, \tag{2.3}$$

$$\mathbf{H}^{\mathcal{PD}} \equiv \mathbb{I}_{\mathcal{P}} \circ \mathbf{H} \circ \mathbb{I}_{\mathcal{D}} + \mathbb{I}_{\mathcal{D}} \circ \mathbf{H} \circ \mathbb{I}_{\mathcal{P}}, \tag{2.4}$$

$$\mathbf{H}^{\mathcal{D}} \equiv \mathbb{I}_{\mathcal{D}} \circ \mathbf{H} \circ \mathbb{I}_{\mathcal{D}}. \tag{2.5}$$

This is an immediate result of two identities: $\mathbf{H} = \mathbb{I}_{\mathcal{S}} \circ \mathbf{H} \circ \mathbb{I}_{\mathcal{S}}$ and $\mathbb{I}_{\mathcal{S}} = \mathbb{I}_{\mathcal{P}} + \mathbb{I}_{\mathcal{D}}$ (see (4.15), Part I).

Clearly, linear operators on the space $\mathcal{H}$

$$\mathbf{H} \to \mathbf{H}^{\mathcal{L}}, \qquad \mathcal{L} = \mathcal{P}, \mathcal{PD}, \mathcal{D} \tag{2.6}$$

are invariant orthogonal projectors, i.e.

$$(\mathbf{R} * \mathbf{H}^{\mathcal{L}}) = (\mathbf{R} * \mathbf{H})^{\mathcal{L}}, \qquad (\mathbf{H}^{\mathcal{L}})^{\mathcal{L}} = \mathbf{H}^{\mathcal{L}}, \qquad \mathbf{R} \in \mathcal{O}.$$

They are mutually orthogonal, i.e.

$$\mathbf{H}^{\mathcal{P}} \cdot \mathbf{H}^{\mathcal{PD}} = \mathbf{H}^{\mathcal{P}} \cdot \mathbf{H}^{\mathcal{D}} = \mathbf{H}^{\mathcal{D}} \cdot \mathbf{H}^{\mathcal{PD}} = 0$$

and their sum is an identity operator.

We have obtained a new *invariant orthogonal decomposition of the space of Hooke's tensors*

$$\mathcal{H} = \mathcal{H}^{\mathcal{P}} \dot{+} \mathcal{H}^{\mathcal{PD}} \dot{+} \mathcal{H}^{\mathcal{D}}, \qquad 21 = 1 + 5 + 15 \tag{2.7}$$

which we will call *energy decomposition*. The dimensions will become evident soon.

**2.3.** It is not difficult to obtain this decomposition in an explicit form. It is simplest to begin with non-orthogonal decomposition (see (7.15), Part I).

$$\mathbf{H} = \mathbf{h}_{\mathcal{P}}\mathbb{I}_{\mathcal{P}} + \mathbf{h}_{\mathcal{D}}\mathbb{I}_{\mathcal{D}} + (\mathbf{1}\otimes\omega + \omega\otimes\mathbf{1}) + \mathfrak{c}\times(\mathbf{1}\otimes\varrho + \varrho\otimes\mathbf{1}) + \mathbf{D}. \tag{2.8}$$

Only the decomposition of the part

$$\mathbf{L} \equiv \mathfrak{c}\times(\mathbf{1}\otimes\varrho + \varrho\otimes\mathbf{1}) \tag{2.9}$$

is not immediately clear. But $\mathbf{1}\cdot\mathbf{L}\cdot\mathbf{1} = \mathbf{0}$ and taking $\mathbb{I}_{\mathcal{D}} = \mathbb{I}_{\mathcal{S}} - \mathbb{I}_{\mathcal{D}}$, we have

$$\begin{aligned} \mathbb{I}_{\mathcal{P}}\circ\mathbf{L}\circ\mathbb{I}_{\mathcal{P}} &= \mathbf{0}, \\ \mathbb{I}_{\mathcal{P}}\circ\mathbf{L}\circ\mathbb{I}_{\mathcal{D}} + \mathbb{I}_{\mathcal{D}}\circ\mathbf{L}\circ\mathbb{I}_{\mathcal{P}} &= \mathbb{I}_{\mathcal{P}}\circ\mathbf{L} + \mathbf{L}\circ\mathbb{I}_{\mathcal{P}} = \frac{2}{3}(\mathbf{1}\otimes\varrho + \varrho\otimes\mathbf{1}), \\ \mathbb{I}_{\mathcal{D}}\circ\mathbf{L}\circ\mathbb{I}_{\mathcal{D}} &= \mathbf{L} - \frac{2}{3}(\mathbf{1}\otimes\varrho + \varrho\otimes\mathbf{1}). \end{aligned} \tag{2.10}$$

Finally, a *complete energy decomposition of Hooke's tensor* has the following unique explicit form:

$$\begin{aligned} \mathbf{H} = h_{\mathcal{P}}\mathbb{I}_{\mathcal{P}} &+ (\mathbf{1}\otimes\varphi + \varphi\otimes\mathbf{1}) \\ &+ \left[h_{\mathcal{D}}\mathbb{I}_{\mathcal{D}} + \left(\mathfrak{c} - \frac{2}{3}\mathfrak{i}\right)\times(\mathbf{1}\otimes\psi + \psi\otimes\mathbf{1}) + \mathbf{D}\right], \end{aligned} \tag{2.11}$$

where

$$\varphi = \frac{1}{3}(3\omega + 2\varrho) = \frac{1}{7}(7\alpha + 2\beta), \qquad \psi = \varrho = \frac{2}{3}(\alpha - \beta). \tag{2.12}$$

This is an orthogonal decomposition. The orthogonality of the second and fourth part follows from ((5.14), Part I). Deviators $\varphi, \psi$ are expressed by Novozhilov's deviators ((7.12), Part I) as follows:

$$\varphi = \frac{1}{3}\mu_{\mathcal{D}}, \qquad \psi = \varrho = \frac{2}{7}(3\nu_{\mathcal{D}} - 2\mu_{\mathcal{D}}). \tag{2.13}$$

**2.4.** *The complete energy decomposition of the space of Hooke's tensor* which corresponds to (2.11) has the form

$$\mathcal{H} = \mathcal{J}_{\mathcal{P}} \dot{+} \mathfrak{D}_i \dot{+} (\mathcal{J}_{\mathcal{D}} \dot{+} \mathfrak{D}_{\mathfrak{n}} \dot{+} \mathsf{D}), \qquad 21 = 1 + 5 + (1 + 5 + 9), \tag{2.14}$$

where $\mathfrak{n} = \mathfrak{c} - \frac{2}{3}\mathfrak{i}$. This decomposition is unique.

The quadratic form (2.1) we started with takes the form

$$\omega \cdot \mathbf{H} \cdot \omega = h_{\mathcal{P}} |\omega_{\mathcal{P}}|^2 + 2\mathrm{tr}\,\omega\,(\varphi \cdot \omega_{\mathcal{D}}) + h_{\mathcal{D}} |\omega_{\mathcal{D}}|^2 + 2\psi\,(\omega_{\mathcal{D}})^2 + \omega_{\mathcal{D}} \cdot \mathbf{D} \cdot \omega_{\mathcal{D}}. \tag{2.15}$$

EXAMPLE 2. There is an important class of elastic anisotropic materials, in which the deviatoric and spherical parts of stress and deformation are *energy orthogonal* in the sense [2] of, i.e. such as

$$\mathbf{C}^{\mathcal{PD}} = \mathbf{0} \quad \Leftrightarrow \quad \mathbf{S}^{\mathcal{PD}} = \mathbf{0}. \tag{2.16}$$

According to (2.11), (2.13) we have

$$\mathbf{C}^{\mathcal{PD}} = \frac{1}{3}\,(\mathbf{1} \otimes \mu_{\mathcal{D}} + \mu_{\mathcal{D}} \otimes \mathbf{1}), \tag{2.17}$$

so $\mu_{\mathcal{D}} = 0$. By the definition,

$$\mathbf{C} \cdot \mathbf{1} = c_{\mathcal{P}}\mathbf{1} \quad , \quad \mathbf{S} \cdot \mathbf{1} = s_{\mathcal{P}}\mathbf{1} \quad , \quad c_{\mathcal{P}} s_{\mathcal{P}} = 1. \tag{2.18}$$

Thus, the hydrostatic stress causes a change in volume without any deviatoric deformation, whereas deviatoric stress causes only deviatoric deformation without change in volume. Such materials we called in [3, 4] *volume isotropic*. Their spectral decomposition ((1.9), Part I) takes the form

$$\mathbf{S} = s_{\mathcal{P}}\mathbb{I}_{\mathcal{P}} + \mu_1 \delta_1 \otimes \delta_1 + \cdots + \mu_5 \delta_5 \otimes \delta_5, \tag{2.19}$$

where $\delta_1, \cdots, \delta_5$ are proper deviators, and 6 Kelvin moduli are the bulk modulus $s$ and 5 deviatoric moduli $\mu_1, \cdots, \mu_5$.

## 3. On true Hooke's tensors

**3.1.** A non-zero Hooke's tensor $\mathbf{H}$ will be called *a true Hooke's tensor* when its quadratic form is non-negative definite:

$$\omega \cdot \mathbf{H} \cdot \omega \geqslant 0 \qquad \text{for every} \qquad \omega \in \mathcal{S}. \tag{3.1}$$

The true character of a Hooke's tensor can be easily determined when spectral decomposition ((1.9), Part I) is used: Kelvin moduli $h_1 \geqslant \mathbf{0}, \cdots, h_6 \geqslant \mathbf{0}$ are to be non-negative. It would be more difficult, however, to satisfy the necessary and sufficient conditions imposed on the systems $(h_{\mathcal{P}}, h_{\mathcal{D}}, \boldsymbol{\alpha}, \boldsymbol{\beta}, \mathbf{D})$ or on equivalent systems[1] (see (7.4), Part I).

[1] Of course, one can use the classical Sylvester criterion, when $\mathbf{H}$ is taken in a matrix form, but this does not lead to easy formulation.

**3.2.** The invariant parts of a true Hooke's tensor *do not have to be* true Hooke's tensors. This is, however, the case for the most important part. For basic decomposition

$$\mathbf{H} = \mathbf{H}^{is} \dot{+} \mathbf{H}^{an}\,, \qquad 21 = 2 + 19 \tag{3.2}$$

we have the following, not at all obvious, theorem.

THEOREM 1. The isotropic part $\mathbf{H}^{is}$ of every true Hooke's tensor $\mathbf{H}$ is a true Hooke's tensor. This means that for (3.1) the following inequalities are the case:

$$h_{\mathcal{P}} \equiv \frac{1}{3}\,\mathbf{1}\cdot\mathbf{H}\cdot\mathbf{1} \geqslant \mathbf{0}, \tag{3.3}$$

$$h_{\mathcal{D}} \equiv \frac{1}{5}\,(\mathrm{Tr}\,\mathbf{H} - h_{\mathcal{P}}) \geqslant \mathbf{0}, \tag{3.4}$$

with one of them being sharp. If the tensor $\mathbf{H}$ is not isotropic, i.e. $\mathbf{H}^{an} \neq \mathbf{0}$, then

$$h_{\mathcal{P}} \geqslant 0\,, \qquad h_{\mathcal{D}} > 0. \tag{3.5}$$

P r o o f. If tensor $\mathbf{H}$ is isotropic, $\mathbf{H}^{an} = \mathbf{0}$, then

$$\omega\cdot\mathbf{H}\cdot\omega = h_{\mathcal{P}}\,|\omega_{\mathcal{P}}|^2 + h_{\mathcal{D}}\,|\omega_{\mathcal{D}}|^2 \tag{3.6}$$

and condition (3.1) means exactly (3.3) and (3.4).

Let us take a true Hooke's tensor which is not isotropic, i.e. $\mathbf{H}^{an} \neq \mathbf{0}$. For spherical action $\omega = \omega_{\mathcal{P}} = p\,\mathbf{1}$ we have

$$\omega\cdot\mathbf{H}\cdot\omega = h_{\mathcal{P}}\,p^2 \geqslant \mathbf{0} \Longrightarrow h_{\mathcal{P}} \geqslant \mathbf{0}. \tag{3.7}$$

Let us take any deviatoric action $\omega = \omega_{\mathcal{D}} = \delta \in \mathcal{D}$. We have

$$\omega\cdot\mathbf{H}\cdot\omega = \delta\cdot\mathbf{H}\cdot\delta = \delta\cdot\mathbf{H}^{\mathcal{D}}\cdot\delta = \delta\cdot(h_{\mathcal{D}}\mathbb{I}_{\mathcal{D}} + \mathbf{K})\cdot\delta \geqslant \mathbf{0}, \tag{3.8}$$

where

$$\mathbf{K} \equiv (\mathbf{H}^{an})^{\mathcal{D}} = \mathbb{I}_{\mathcal{D}}\circ\mathbf{H}^{an}\circ\mathbb{I}_{\mathcal{D}}\,. \tag{3.9}$$

The operator $\delta \to \mathbf{K}\cdot\delta$ is a symmetric linear operator which transforms the 5-dimensional space of deviators $\mathcal{D}$, with scalar product $\delta_1\cdot\delta_2$, into itself. Thus we have its spectral decomposition

$$\mathbf{K} = k_1\varkappa_1\otimes\varkappa_1 + \cdots + k_5\varkappa_5\otimes\varkappa_5, \tag{3.10}$$

where proper deviators constitute the orthonormal basis in $\mathcal{D}$, $\varkappa_i\cdot\varkappa_j = \delta_{ij}$.

Since $\mathbb{I}_{\mathcal{D}}$ is the unity operator on $\mathcal{D}$, $\mathbb{I}_{\mathcal{D}} \cdot \delta \equiv \delta$, then every deviator is its proper element corresponding to eigenvalue 1, so

$$\mathbb{I}_{\mathcal{D}} = \varkappa_1 \otimes \varkappa_1 + \cdots + \varkappa_5 \otimes \varkappa_5 . \tag{3.11}$$

Operator $h_{\mathcal{D}}\mathbb{I}_{\mathcal{D}} + \mathbf{K}$ is non-negative definite, so all its eigenvalues are non-negative

$$h_{\mathcal{D}} + k_1 \geqslant 0, \ldots, h_{\mathcal{D}} + k_5 \geqslant 0 . \tag{3.12}$$

But

$$k_1 + \cdots + k_5 = \operatorname{Tr}\mathbf{K} \equiv K_{pqpq} = \mathbb{I}_{\mathcal{D}\,pqab} H^{an}_{abcd} \mathbb{I}_{cdpq} = H^{an}_{abcd} \mathbb{I}_{\mathcal{D}\,abcd} = \mathbf{H}^{an} \cdot \mathbb{I}_{\mathcal{D}} \tag{3.13}$$

because of $\mathbb{I}_{\mathcal{D}} \circ \mathbb{I}_{\mathcal{D}} = \mathbb{I}_{\mathcal{D}}$. Since the anisotropic part $\mathbf{H}^{\mathrm{an}}$ is orthogonal to any isotropic Hooke's tensor, then

$$k_1 + \cdots + k_5 = 0. \tag{3.14}$$

As tensor $\mathbf{H}$ is not isotropic, then $\mathbf{K} \neq \mathbf{0}$, hence its smallest eigenvalue $k_{\min}$ must be negative. We have therefore

$$h_{\mathcal{D}} \geqslant |k_{\min}| > 0. \tag{3.15}$$

COROLLARY 1. A true Hooke's tensor without an isotropic part does not exist. Indeed, for $\mathbf{H} = \mathbf{H}^{an}$, one can always find such a deviator $\delta$ that

$$\delta \cdot \mathbf{H} \cdot \delta = \delta \cdot \mathbf{K} \cdot \delta = k_{\min} |\delta|^2 < 0.$$

COROLLARY 2. The isotropic part of a true Hooke's tensor is its closest true Hooke's tensor (in the sense of distance $|\mathbf{A} - \mathbf{B}|$). Indeed, it is an orthogonal projection of $\mathbf{H}$ on $\mathcal{H}^{is}$.

REMARK. The norm of the isotropic part $|\mathbf{H}^{is}|$ can differ substantially from the norm of the entire Hooke's tensor

$$|\mathbf{H}|^2 = |\mathbf{H}^{is}|^2 + |\mathbf{H}^{an}|^2 . \tag{3.16}$$

Similarly, the values of quadratic forms $\omega \cdot \mathbf{H}^{is} \cdot \omega$ (e.g. energy) can substantially differ from one another. The problem of choosing a 'good' isotropic approximation of Hooke's tensor, for example choosing an isotropic elastic material to approximate an anisotropic elastic material, is a problem *per se* (see e.g. [5, 6]). Everything here depends on the purpose of the approximation.

## 4. Spatial symmetry and invariant decompositions

**4.1.** The relation between spatial symmetry of Hooke's tensors and their spectral decompositions was examined in detail (see [3, 7, 8] and review [4]). Here we

shall only deal with the relation between this symmetry and the **invariant linear** decompositions obtained in Part I.

THEOREM 2. A group of spatial symmetry of Hooke's tensor is the intersection of symmetry groups of its anisotropy deviators, e.g.

$$\mathcal{O}(\mathbf{H}) = \mathcal{O}(\boldsymbol{\alpha}) \cap \mathcal{O}(\boldsymbol{\beta}) \cap \mathcal{O}(\mathbf{D}). \tag{4.1}$$

P r o o f. obvious (see also [9]). Clearly, the pair $(\boldsymbol{\alpha}, \boldsymbol{\beta})$ can be replaced by any other pair $(\boldsymbol{\xi}_1, \boldsymbol{\xi}_2)$ described in ((7.3), Part I).

Therefore, all the possible types of symmetry of Hooke's tensors are types of symmetry of triples: two second-order deviators $(\boldsymbol{\alpha}, \boldsymbol{\beta})$ and a fourth-order deviator $\mathbf{D}$. An analysis of the resultant possibilities would lead us in a new way to eight classical groups of symmetry of linear elasticity (see also [9]). We will not do so.

IMPORTANT REMARK. In a general situation, the triple $(\boldsymbol{\alpha}, \boldsymbol{\beta}, \mathbf{D})$ loses the common elements of symmetry very quickly. In other words, most anisotropic materials do not have any axes or planes of elastic symmetry

**4.2.** We shall demonstrate how, in the language of anisotropy deviators, appear the axes of symmetry of Hooke's tensors.

Let $\mathbf{R}_{\mathbf{k}}(\varphi)$ be a rotation of our basic Euclidean space by the angle $\varphi$ around the axis directed by a unit vector $\mathbf{k}$. The straight line will be called a *total symmetry axis* of the tensor $\mathbf{A}$ when

$$\mathbf{R}_{\mathbf{k}}(\varphi) * \mathbf{A} = \mathbf{A} \qquad \text{for every angle } \varphi, \tag{4.2}$$

and its *n-fold symmetry axis* when it is not its axis of total symmetry, but

$$\mathbf{R}_{\mathbf{k}}(\varphi) * \mathbf{A} = \mathbf{A} \qquad \text{for } \varphi = \frac{2\pi}{n}, \tag{4.3}$$

where $n$ is the minimal integer $\geqslant 2$ of such integers for which this equation is satisfied. As the tensor $\mathbf{A}$ we can here take any Euclidean tensor.

It can be demonstrated that the space of second-order deviators can be decomposed with respect to any fixed axis into an orthogonal direct sum

$$\mathcal{D} = \overset{\circ}{\mathcal{D}}_{\mathbf{k}} + \overset{1}{\mathcal{D}}_{\mathbf{k}} + \overset{2}{\mathcal{D}}_{\mathbf{k}}, \qquad 5 = 1 + 2 + 2 \tag{4.4}$$

such that any rotation $\mathbf{R}_{\mathbf{k}}(\varphi)$

– preserves every deviator on the straight line $\overset{\circ}{\mathcal{D}}_{\mathbf{k}}$,

– rotates every deviator in plane $\overset{l}{\mathcal{D}}_{\mathbf{k}}$, $l = 1, 2$, by the angle $l\varphi$[2].

Clearly, every deviator on the straight line $\overset{\circ}{\mathcal{D}}_{\mathbf{k}}$ has the form

$$\omega = a\,(\mathbf{1} - 3\mathbf{k} \otimes \mathbf{k})\,. \tag{4.5}$$

Similarly, an orthogonal decomposition of the space of fourth-order deviators

$$\begin{gathered} \mathsf{D} = \overset{0}{\mathsf{D}}_{\mathbf{k}} + \overset{1}{\mathsf{D}}_{\mathbf{k}} + \overset{2}{\mathsf{D}}_{\mathbf{k}} + \overset{3}{\mathsf{D}}_{\mathbf{k}} + \overset{4}{\mathsf{D}}_{\mathbf{k}} \\ 9 = 1 + 2 + 2 + 2 + 2, \end{gathered} \tag{4.6}$$

takes place. In this case, every rotation $\mathbf{R}_{\mathbf{k}}(\varphi)$

– preserves every deviator on the straight line $\overset{0}{\mathsf{D}}_{\mathbf{k}}$,

– rotates every deviator in plane $\overset{l}{\mathsf{D}}_{\mathbf{k}}$, $l = 1, 2, 3, 4$, by the angle $l\varphi$.

Therefore, higher symmetry axes (i.e. 3-fold and 4-fold) of a Hooke's tensor are caused only by the presence of the invariant term $\mathbf{D}$ in its decomposition. Strictly speaking, the following theorem is the case.

THEOREM 3. A Hooke's tensor $\mathbf{H}$ has a higher symmetry axis $\mathbf{k}$ only if its anisotropy deviators have the form

$$\alpha = a\,(\mathbf{1} - 3\mathbf{k} \otimes \mathbf{k})\,, \qquad \beta = b\,(\mathbf{1} - 3\mathbf{k} \otimes \mathbf{k})\,, \qquad \mathbf{D} \neq \mathbf{0}. \tag{4.7}$$

It has more than one higher symmetry axis only if

$$\alpha = \mathbf{0}\,, \qquad \beta = \mathbf{0}\,, \qquad \mathbf{D} \neq \mathbf{0}. \tag{4.8}$$

P r o o f. Let $\mathbf{k}$ be a higher symmetry axis of $\mathbf{H}$. Rotations around $\mathbf{k}$ by the angles $2\pi/3$ or $2\pi/4$ preserve second-order deviator $\omega$ only if $\mathbf{k}$ is its total symmetry axis, so if $\omega \in \overset{0}{\mathsf{D}}_{\mathbf{k}}$. If $\mathbf{D} = \mathbf{0}$ then $\mathbf{k}$ would be a total symmetry axis of $\mathbf{H}$, which we dismissed. Let $\mathbf{k}, \mathbf{l}$ be two different higher symmetry axes of $\mathbf{H}$. Then the formulae (4.7) would have to be the case both for $\mathbf{k}$ and for $\mathbf{l}$, which is only possible when $a = b = 0$.

Let us examine only one, but important example.

EXAMPLE 3. Elasticity tensor $\mathbf{S}$ of a *cubic crystal*. The symmetry group $\mathcal{O}(\mathbf{S})$ is a symmetry group of a cube. We have here three 4-fold axes and four 3-fold axes. This is more than needed, according to the theorem and decomposition

[2] All the elements $\overset{1}{\mathcal{D}}_k, \overset{2}{\mathcal{D}}_k$ are pure shears (see [8]).

(7.3), Part I, for tensor $\mathbf{S}$ to belong to the following important class of Hooke's tensors

$$\mathbf{S} = \mathbf{S}^{is} + \mathbf{D}, \qquad \boldsymbol{\alpha} = \boldsymbol{\beta} = \mathbf{0}. \tag{4.9}$$

The deviator $\mathbf{D}$ is easy to be explicitly define. By denoting by $\mathbf{k}, \mathbf{l}, \mathbf{m}$ the directions of the edges of the cube, we see that tensor

$$\mathbf{D} \backsim 3\mathbb{I}_5 - 5\mathbf{K} = 3iI_{\mathcal{P}} + 2\mathbb{I}_{\mathcal{S}} - 5\mathbf{K}, \tag{4.10}$$

where

$$\mathbf{K} \equiv \mathbf{k}\otimes\mathbf{k}\otimes\mathbf{k}\otimes\mathbf{k} + \mathbf{l}\otimes\mathbf{l}\otimes\mathbf{l}\otimes\mathbf{l} + \mathbf{m}\otimes\mathbf{m}\otimes\mathbf{m}\otimes\mathbf{m}, \tag{4.11}$$

is a deviator with the required symmetry of a cube.

A complete invariant decomposition of elasticity tensor of the cubic crystal has, therefore, the form

$$\mathbf{S} = \lambda_{\mathcal{P}}\mathbb{I}_{\mathcal{P}} + \lambda_{\mathcal{D}}\mathbb{I}_{\mathcal{D}} + \delta\mathbf{D}. \tag{4.12}$$

The relation with the given spectral decomposition (1.10), Part I, is obvious

$$\begin{aligned} \mathbb{I}_{\mathcal{P}} &= \mathbf{P_1}, & \lambda_{\mathcal{P}} &= h_1, \\ \mathbb{I}_{\mathcal{D}} &= \mathbf{P_2} + \mathbf{P_3}, & \lambda_{\mathcal{D}} &= \frac{1}{5}(2h_2 + 3h_3), \\ \mathbf{D} &= -3\mathbf{P_2} + 2\mathbf{P_3}, & \delta &= \frac{1}{5}(h_3 - h_2). \end{aligned} \tag{4.13}$$

The projectors onto proper subspaces defined by (1.12), Part I, are therefore

$$\mathbf{P_1} = \mathbb{I}_{\mathcal{P}}, \quad \mathbf{P_2} = \mathbf{K} - \mathbb{I}_{\mathcal{P}}, \quad \mathbf{P_3} = \mathbb{I}_{\mathcal{S}} - \mathbf{K} \tag{4.14}$$

which can be demonstrated by direct projecting: $\boldsymbol{\omega} \to \mathbf{P}_i \cdot \boldsymbol{\omega}$, $i = 1, 2, 3$.

## 5. Invariant decompositions of plane Hooke's tensors (see also [10])

**5.1.** Plane tensors of any order $q$ are generated by the Euclidean plane $\mathcal{E}$, $\dim \bigotimes^q \mathcal{E} = 2^q$. Still

$$\mathcal{S} = \operatorname{sym} \mathcal{E}\bigotimes\mathcal{E}, \qquad \mathcal{H} = \operatorname{sym} \mathcal{S}\bigotimes\mathcal{S}, \tag{5.1}$$

but now the situation is far simpler since

$$\dim \mathcal{S} = 3, \qquad \dim \mathcal{H} = 6. \tag{5.2}$$

**5.2.** The counterpart of decompositions ((4.12), (4.13), Part I), is

$$\mathcal{S} = \mathcal{P} \dot{+} \mathcal{D}, \quad 3 = 1 + 2,$$

(5.3)

$$\omega = \omega_{\mathcal{P}} + \omega_{\mathcal{D}}, \quad \begin{pmatrix} a & c \\ c & b \end{pmatrix} = \begin{pmatrix} x & 0 \\ 0 & x \end{pmatrix} + \begin{pmatrix} u & v \\ v & -u \end{pmatrix}.$$

The plane deviator $\omega_{\mathcal{D}}$ is always, in the sense of mechanics, a *pure shear* $\tau$ in plane $\mathcal{E}$, (see any textbook of solid mechanics or [8]). We have

$$\omega_{\mathcal{P}} = \tau, \qquad \tau = t(\mathbf{m} \otimes \mathbf{n} + \mathbf{n} \otimes \mathbf{m}), \qquad t^2 \equiv \frac{1}{2}\tau \cdot \tau \tag{5.4}$$

where mutually orthogonal unit vectors $(\mathbf{m}, \mathbf{n})$ are the *shear directions*.

**5.3.** The nonlinear invariant spectral decompositions of the plane Hooke's tensor have the form

$$\mathbf{H} = h_1 \omega_1 \otimes \omega_1 + h_2 \omega_2 \otimes \omega_2 + h_3 \omega_3 \otimes \omega_3 \tag{5.5}$$

where $\omega_k \cdot \omega_l = \delta_{kl}$. These decompositions are presented simply and in enough detail in [4].

**5.4.** The action of permutation operators remains exactly the same as that described in Part I, but its results are far simpler. *The first basic decomposition of the space $\mathcal{H}$, with respect to internal symmetry* has the form

$$\mathcal{H} = \mathcal{H}_{\mathfrak{s}} \dot{+} \mathcal{H}_{\mathfrak{t}}, \qquad 6 = 5 + 1. \tag{5.6}$$

The dimension of $\mathcal{H}_{\mathfrak{s}}$ follows from the fact that the condition of total symmetry $\mathfrak{s} \times \mathbf{H} = \mathbf{H}$ imposes on the six free components $H_{1111}$, $H_{2222}$, $H_{1122}, H_{1212}, H_{1112}, H_{2212}$, only one constraint $H_{1122} = H_{1212}$.

**5.5.** *The second basic decomposition of $\mathcal{H}$, according to the symmetry with respect to the group of rotations and mirror reflections in plane $\mathcal{E}$, has the form*

$$\mathcal{H} = \mathcal{H}^{is} \dot{+} \mathcal{H}^{an}, \qquad 6 = 2 + 4. \tag{5.7}$$

The description of the plane $\mathcal{H}^{is}$ of plane isotropic Hooke's tensors differs from the former one only by the change of coefficient $3^{-1}$ into $2^{-1}$ in formulae (4.10), (4.11), Part I

$$\begin{aligned} \mathbb{I}_{\mathcal{S}} &= \mathfrak{c} \times (\mathbf{1} \otimes \mathbf{1}), & \mathbb{I}_{\mathcal{S}} \cdot \mathbb{I}_{\mathcal{S}} &= \dim \mathcal{S} = 3, \\ \mathbb{I}_{\mathcal{D}} &= \left(\mathfrak{c} - \frac{1}{2}\mathfrak{i}\right) \times (\mathbf{1} \otimes \mathbf{1}), & \mathbb{I}_{\mathcal{D}} \cdot \mathbb{I}_{\mathcal{D}} &= \dim \mathcal{D} = 2, \\ \mathbb{I}_{\mathcal{P}} &= \frac{1}{2}(\mathbf{1} \otimes \mathbf{1}), & \mathbb{I}_{\mathcal{P}} \cdot \mathbb{I}_{\mathcal{P}} &= \dim \mathcal{P} = 1. \end{aligned} \tag{5.8}$$

Here and henceforth, the symbol $\mathbf{1}$ denotes now the *plane* unit $\mathbf{1} \backsim \begin{pmatrix} 1 & 0 \\ 0 & 1 \end{pmatrix}$.

**5.6.** Let us consider the counterparts of two anisotropic parts of the canonical decomposition (6.4), Part I. There are two simple albeit not self-evident facts.

LEMMA 1. Every plane tensor of the form

$$\mathbf{1} \otimes \boldsymbol{\tau} + \boldsymbol{\tau} \otimes \mathbf{1}, \tag{5.9}$$

where $\boldsymbol{\tau}$ is any plane deviator (so any pure shear), is totally symmetric with respect to permutations.

P r o o f. Taking proper directions of $\boldsymbol{\tau}, \mathbf{a} = (\mathbf{m} + \mathbf{n})/\sqrt{2}\,, \mathbf{b} = (\mathbf{n} - \mathbf{m})/\sqrt{2}$, we have

$$\boldsymbol{\tau} = t\,(\mathbf{a} \otimes \mathbf{a} - \mathbf{b} \otimes \mathbf{b}) \sim t \begin{pmatrix} 1 & 0 \\ 0 & -1 \end{pmatrix}. \tag{5.10}$$

At the same time, of course,

$$\mathbf{1} = \mathbf{a} \otimes \mathbf{a} + \mathbf{b} \otimes \mathbf{b} \sim \begin{pmatrix} 1 & 0 \\ 0 & 1 \end{pmatrix}. \tag{5.11}$$

Hence

$$\mathbf{1} \otimes \boldsymbol{\tau} + \boldsymbol{\tau} \otimes \mathbf{1} = t\,(\mathbf{a} \otimes \mathbf{a} \otimes \mathbf{a} \otimes \mathbf{a} - \mathbf{b} \otimes \mathbf{b} \otimes \mathbf{b} \otimes \mathbf{b}) \tag{5.12}$$

and the right-hand side does not react to permutations.

**5.7.** Therefore, the plane counterpart of the 10-dimensional invariant space $\mathfrak{D}$ will be the plane $\mathfrak{D}$ consisting of all plane tensors of the form (5.9). As $\dim \mathcal{H}_5 = 5$, then the plane counterpart of q-dimensional complement $\mathsf{D}$ will be the plane of fourth-order plane deviators $\mathsf{D}$.

COROLLARY. The anisotropic part $\mathbf{H}^{an}$ of plane Hooke's tensor is totally symmetric

$$\mathbf{H}_5 = h_5 \mathbb{I}_5 + \mathbf{H}^{an}, \qquad \mathbf{H}_1 = h_1 \mathbb{I}_1. \tag{5.13}$$

LEMMA 2. For every non-zero plane fourth-order deviator $\mathbf{D}$, there exists a pure shear $\boldsymbol{\gamma}$ such that

$$\mathsf{D} = \boldsymbol{\gamma} \otimes \boldsymbol{\gamma} - \boldsymbol{\gamma}^{\perp} \otimes \boldsymbol{\gamma}^{\perp} = 2\boldsymbol{\gamma} \otimes \boldsymbol{\gamma} - |\boldsymbol{\gamma}|^2 \mathbb{I}_{\mathcal{D}} \tag{5.14}$$

where the complementary pure shear $\boldsymbol{\gamma}^{\perp}$ is defined by $\boldsymbol{\gamma}$ through formulae $\boldsymbol{\gamma}^{\perp} \cdot \boldsymbol{\gamma} = \mathbf{0}$, $|\boldsymbol{\gamma}^{\perp}| = |\boldsymbol{\gamma}|$.

P r o o f. Let us apply a spectral decomposition (5.5)

$$\mathbf{D} = d_1\,\boldsymbol{\omega}_1 \otimes \boldsymbol{\omega}_1 + d_2\boldsymbol{\omega}_2 \otimes \boldsymbol{\omega}_2 + d_3\boldsymbol{\omega}_3 \otimes \boldsymbol{\omega}_3. \tag{5.15}$$

From conditions of orthogonality to $\mathcal{H}^{is}$ we have $\mathbf{1}\cdot\mathbf{D} = 0$, $\operatorname{Tr}\mathbf{D} = 0$ which gives

$$d_1\,\mathbf{tr}\boldsymbol{\omega}_1 = d_2\,\mathbf{tr}\boldsymbol{\omega}_2 = d_3\,\mathbf{tr}\boldsymbol{\omega}_3 = 0\,, \qquad d_1 + d_2 + d_3 = 0\,. \tag{5.16}$$

The only non-zero solution $\mathbf{D}$ ordered in such a manner that $d_1 < d_2 < d_3$, is

$$d_3 = -d_1\,, \qquad d_2 = 0\,, \qquad \mathbf{tr}\boldsymbol{\omega}_1 = \mathbf{tr}\boldsymbol{\omega}_2 = 0 \tag{5.17}$$

which gives the first formula (5.14). The second formula follows from the equation

$$\mathbb{I}_{\mathfrak{D}} = \boldsymbol{\tau}_1 \otimes \boldsymbol{\tau}_1 + \boldsymbol{\tau}_2 \otimes \boldsymbol{\tau}_2 \tag{5.18}$$

valid for every orthonormal basis in $\mathfrak{D}, \boldsymbol{\tau}_i \cdot \boldsymbol{\tau}_k = \delta_{ik}$.

**5.8.** Summing up: *The canonical decomposition of the space of plane Hooke's tensors has the form*

$$\mathcal{H} = \mathcal{H}^{is} \dotplus \mathfrak{D} \dotplus \mathsf{D}, \qquad 6 = 2 + 2 + 2, \tag{5.19}$$

*while every complete invariant decomposition has the form*

$$\mathcal{H} = (\mathcal{J}_{\mathfrak{n}_1} + \mathcal{J}_{\mathfrak{n}_2}) \dotplus \mathfrak{D} \dotplus \mathsf{D}\,, \qquad 6 = (1 + 1) + 2 + 2. \tag{5.20}$$

*In other words, every plane Hooke's tensor has the form*

$$\mathbf{H} = h_1\mathbb{I}_{\mathfrak{n}_1} + h_2\mathbb{I}_{\mathfrak{n}_2} + (\mathbf{1} \otimes \boldsymbol{\tau} + \boldsymbol{\tau} \otimes \mathbf{1}) + \mathbf{D}. \tag{5.21}$$

*Pure shear* $\boldsymbol{\tau}$ *and fourth-order deviator* $\mathbf{D}$ (5.14) *are uniquely defined, whereas invariants* $h_1, h_2$ *depend on the choice of permutation operators* $\mathfrak{n}_1, \mathfrak{n}_2$.

Explicit formulae for $(h_1, h_2, \boldsymbol{\tau}, \mathbf{D})$ are easy to obtain.

**5.9.** *Energy decomposition* of plane Hooke's tensor

$$\mathbf{H} = \mathbf{H}^{\mathcal{P}} + \mathbf{H}^{\mathcal{PD}} + \mathbf{H}^{\mathcal{D}} \tag{5.22}$$

is unique,

$$\mathbf{H} = h_{\mathcal{P}}\mathbb{I}_{\mathcal{P}} + (\mathbf{1} \otimes \boldsymbol{\tau} + \boldsymbol{\tau} \otimes \mathbf{1}) + (h_{\mathcal{D}}\mathbb{I}_{\mathcal{D}} + \mathbf{D})\,, \tag{5.23}$$

and the quadratic form corresponding to $\mathbf{H}$ can be written in the form

$$\boldsymbol{\omega}\cdot\mathbf{H}\cdot\boldsymbol{\omega} = h_{\mathcal{P}}\,|\boldsymbol{\omega}_{\mathcal{P}}|^2 + 2\operatorname{tr}\boldsymbol{\omega}\,(\boldsymbol{\tau}\cdot\boldsymbol{\omega}_{\mathcal{D}})^2 + \left(h_{\mathcal{D}} - |\boldsymbol{\gamma}|^2\right)|\boldsymbol{\omega}_{\mathcal{D}}|^2 + \mathbf{2}\,(\boldsymbol{\gamma}\cdot\boldsymbol{\omega}_{\mathcal{D}})^2\,. \tag{5.24}$$

**5.10.** The rotation $\mathbf{R}$ of plane $\mathcal{E}$ by the angle $\varphi$ rotates the 3-dimensional space $\mathcal{S}$ around the axis $\mathcal{P}$ by the angle $2\varphi$ as it immediately follows from formula (5.4).

Thus the orthogonal basis of pure shears $(\boldsymbol{\gamma}, \boldsymbol{\gamma}^{\perp})$ rotates in the usual manner

$$\mathbf{R} * \boldsymbol{\gamma} = \cos 2\varphi \boldsymbol{\gamma} + \sin 2\varphi \boldsymbol{\gamma}^{\perp}, \qquad \mathbf{R} * \boldsymbol{\gamma}^{\perp} = -\sin 2\varphi \boldsymbol{\gamma} + \cos 2\varphi \boldsymbol{\gamma}^{\perp}; \tag{5.25}$$

hence, by taking $\mathbf{D} = \boldsymbol{\gamma} \otimes \boldsymbol{\gamma} - \boldsymbol{\gamma}^{\perp} \otimes \boldsymbol{\gamma}^{\perp}$ we obtain

$$(\mathbf{R} * \mathbf{D}) \cdot \mathbf{D} = |\mathbf{D}|^2 \cos 4\varphi. \tag{5.26}$$

So, every fourth-order deviator $\mathbf{D}$ rotates, as it should, by the angle $4\varphi$. Therefore the plane Hooke's tensor $\mathbf{H}$ can have three well-known kinds of symmetry:

1. Symmetry of circle (isotropy), if $\boldsymbol{\tau} = \mathbf{0}$, $\mathbf{D} = 0$,
2. Symmetry of square (tetragonal), if $\boldsymbol{\tau} = \mathbf{0}$, $\mathbf{D} \neq 0$,
3. Symmetry of rectangle (ortothropy), if $\boldsymbol{\tau} \neq \mathbf{0}$, $\mathbf{D} \neq 0$,

(see also [10] where it was also pointed out that the plane elastic continuum without any symmetry has orientation 'left' or 'right').

**5.11.** To every 3-dimensional Hooke's tensor we can assign an infinite number of plane Hooke's tensors that correspond to it.

Let us take, in 3-dimensional space $\mathcal{E}$, a plane $\mathcal{K}$ defined by its unit normal vector $\mathbf{k}$. The orthogonal projection of the vectors $\mathbf{x} \in \mathcal{E}$ onto the plane $\mathcal{K}$ is an operation defined by projector $\mathbf{P}(\mathbf{k})$,

$$\mathbf{P}(\mathbf{k}) = \mathbf{1} - \mathbf{k} \otimes \mathbf{k}, \qquad \mathbf{x} \to \mathbf{P}\mathbf{x} = \mathbf{x} - (\mathbf{k}\mathbf{x})\,\mathbf{k}. \tag{5.27}$$

To this corresponds the linear operation of orthogonal projecting of 3-dimensional tensors onto the plane $\bigotimes^q \mathcal{E} \ni \mathbf{A} \to \mathbf{P} * \mathbf{A} \in \bigotimes^q \mathcal{K}$, defined for simple tensors by the formula

$$\mathbf{P} * (\mathbf{a}_1 \otimes \cdots \otimes \mathbf{a}_q) \equiv \mathbf{P}\mathbf{a}_1 \otimes \cdots \otimes \mathbf{P}\mathbf{a}_q. \tag{5.28}$$

The orthogonal plane projection of the 3-dimensional tensor of $q$-order

$$\mathbf{A} = \mathbf{A}_{i\ldots j}\mathbf{n}_i \otimes \cdots \otimes \mathbf{n}_j \tag{5.29}$$

onto the plane will therefore be the plane tensor of $q$-order

$$\mathbf{P}(\mathbf{k}) * \mathbf{A} = \mathbf{A}_{i\ldots j}\,\mathbf{P}(\mathbf{k})\,\mathbf{n}_i \otimes \cdots \otimes \mathbf{P}(\mathbf{k})\,\mathbf{n}_j. \tag{5.30}$$

The relations between the tensor $\mathbf{A}$ and its plane projections $\mathbf{P}(\mathbf{k}) * \mathbf{A}$ are in many situations quite essential.

EXAMPLE 4. Let us take an elastic sample with the compliance tensor $\mathbf{C}$. Let us cut out from this sample a thin plate with the normal vector $\mathbf{k}$. The plane

part of the plate's deformation under the plane state of stress is defined by the plane compliance tensor of the plate, being nothing else but a plane projection $\mathbf{P}(\mathbf{k}) * \mathbf{C}$.

## 6. On description, qualification and design of elastic materials

**6.1.** Let us begin with remarks on the qualitative description and qualification of elastic materials.

The issue of symmetry is purposefully left out. It is so extensively discussed that one gets a false impression that the main differences in the behavior of elastic materials consist in the differences in their symmetry. *This is not so.* The fascination with the symmetry of physical properties is quite well justified in the physics of crystals, and also due to the simple and economical production technologies of composites, imposing the symmetry of their structure, e.g. ortothropy. Yet the contemporary technologies offer more and more sophisticated opportunities for shaping of the materials with pre-selected properties. But complicated structure leads to a prompt loss of symmetry. It suffices, for instance, to put into a composite three different kinds of fibres, mutually non-orthogonal, and there is no trace of symmetry. More importantly, materials of totally different symmetry can, in certain conditions, behave similarly or even identically.

It is therefore necessary to find manners of description, not connected with symmetry (ortothropy, etc.), and as a consequence, designing of the properties of materials, which would be deeper and more universal than those now used. One can remain particulalrly hopeful about the *invariant descriptions: non-linear of type ((1.9), Part I) and linear of type ((7.3), Part I). As decision variables* of designing of the properties of a material at the point under cosideration can serve here, in particular, spectral variables $(h_1, ..., h_6; \omega_1, ..., \omega_6)$ or the invariant parts of tensors like $(h_{\mathcal{P}}, h_{\mathcal{D}}, \boldsymbol{\alpha}, \boldsymbol{\beta}, \mathbf{D})$. This, however, calls for a deeper insight into the sense of these quantities.

**6.2.** Even at the stage of formulation of invariant decompositions, we gave introductory examples, pointing out their qualitative sense and possible applications. While illustrating the first basic decomposition (2.12), Part I, we made reference in Example 1 to the classical discussion on the number of parts of an elasticity tensor. While recalling the second basic decomposition (3.1), Part I, we demonstrated, in Theorem 1, the sense of the isotropic part of the elasticity tensor as an independent elasticity tensor. In Theorem 3 we showed the independent meaning of the deviatoric part $\mathbf{D}$ of Hooke's tensor as a true source of the presence of the axis of elastic symmetry of the third or/and fourth order. By introducing the energy decomposition (1.7) we made an immediate reference, in Example 2, to

an important class of elastic materials, in which hydrostatic pressure and stress deviator are separated in terms of energy.

## 7. Some surprising applications: astonishing elastic materials

**7.1.** Let us now quote **quite different** examples. By using the technique of invariant linear decompositions, we shall point out some *novel types of elastic anisotropy*. The very fact of their existence was, at least for me, quite surprising. I shall therefore use a manner of presentation slightly different from the standards of applied mathematics. I shall posit a series of questions, deliberately provocative. Yet each will have an unambiguous answer, proven in the papers quoted below. We shall limit our presentation to examples of linear elastic materials.

**7.2.** EXAMPLE A. Let us begin with acoustics. The great practical and theoretical role of longitudinal elastic waves is widely known (see, e.g. [6, 11]). An isotropic elastic material is capable of conducting a longitudinal wave in *each* direction and with the same speed. Many courses of the theory of elasticity and acoustics consider this property to be almost synonymous with elastic isotropy. Moreover, proving this is recommended as its experimental verification. The following question should be inportant:

> *Are there any anisotropic materials with the stiffness tensor* $\mathbf{S} = \mathbf{S}^{is} + \mathbf{S}^{an}, \mathbf{S}^{an} \neq 0$ *, capable of conducting a longitudinal acoustic signal in each direction?*

The answer is not less surprising than the question: YES, there are. In paper [12] I proved that these were the materials with the stiffness

$$\mathbf{S} = \mathbf{S}^{is} + \mathrm{t} \times (\mathbf{1} \otimes \boldsymbol{\beta} + \boldsymbol{\beta} \otimes \mathbf{1}) \tag{7.1}$$

and only these. The proof follows from the invariant decomposition (7.4), Part I. Let us note that the anisotropy of these materials is completely *undetectable* (so to speak, invisible) in experiments with longitudinal waves.

**7.3.** EXAMPLE B. Let us realize, in an elastic body with compliance $\mathbf{C}$, a stress state of *pure shear* $\sigma = \tau = t\,(\mathbf{m} \otimes \mathbf{n} + \mathbf{n} \otimes \mathbf{m})$. This is one of the favorite ways of loading a sample (often realized on thin metal plates or twisted pipes). The size of the change of the originally right angle between shear directions $(\mathbf{m}, \mathbf{n})$, $\mathbf{mn} = 0$, is decided by the parameter

$$G\,(\mathbf{m}, \mathbf{n}) \equiv [4\,(\mathbf{m} \otimes \mathbf{n}) \cdot \mathbf{C} \cdot (\mathbf{m} \otimes \mathbf{n})]^{-1} \tag{7.2}$$

usually called *shear modulus for directions* $(\mathbf{m}, \mathbf{n})$ (see, e.g. [13]). As an isotropic material does not have any pre-distinguished direction, the shear modulus $\mathbf{G}(\mathbf{m}, \mathbf{n})$ will be identical for each pair $(\mathbf{m}, \mathbf{n})$, so it will be an invariant of the stiffness tensor $\mathbf{C}$, called *the Kirchhoff modulus*. Our next off-beat problem is:

*Are there any* **anisotropic** *elastic materials, for which* $G(\mathbf{m}, \mathbf{n})$ *does not depend on the shear directions ?*

In [14] we showed that there was an infinite number of such materials and that they were defined by the formula

$$\mathbf{C} = \mathbf{C}^{is} + (\mathbf{1} \otimes \boldsymbol{\omega} + \boldsymbol{\omega} \otimes \mathbf{1}) \tag{7.3}$$

(cf. the invariant decomposition (7.15), Part I, in which we need to take $\boldsymbol{\rho} = \mathbf{0}$, $\mathbf{D} = \mathbf{0}$).

**7.4.** EXAMPLE C. In Example 4 we have demonstrated that the plane part of deformation of a thin plate, cut out from a material with compliance $\mathbf{C}$ and under plane load $\boldsymbol{\sigma}$, is defined by plane Hooke's tensor, being an orthogonal projection of the tensor $\mathbf{C}$ onto the plane of this plate. We formulate another off-beat qualitative question:

*Is there any such anisotropic material* $\mathbf{C} = \mathbf{C}^{is} + \mathbf{C}^{an}$, $\mathbf{C}^{an} \neq \mathbf{0}$, *that each thin plate cut out from it will be isotropic, i.e.*

$$\mathbf{P}(\mathbf{k}) * \mathbf{C} \in \mathcal{H}^{is}(\mathbf{k}) \quad \textit{for each direction } \mathbf{k} \,? \tag{7.4}$$

Here $\mathcal{H}^{is}(\mathbf{k})$ is a set of plane isotropic Hooke's tensors.

The answer is surprising, again: YES. In [15] I have demonstrated that all such materials are defined by the formula

$$\mathbf{C} = \mathbf{C}^{is} + \mathrm{t} \times (\mathbf{1} \otimes \boldsymbol{\beta} + \boldsymbol{\beta} \otimes \mathbf{1}) \tag{7.5}$$

(see the invariant decomposition (7.4), Part I, where $\boldsymbol{\alpha} = \mathbf{0}$, $\mathbf{D} = \mathbf{0}$).

**7.5.** EXAMPLE D. In an isotropic material the Hooke's stress tensor $\boldsymbol{\sigma}$ and the corresponding tensor of small deformations $\boldsymbol{\varepsilon}$ are coaxial, i.e. they take the diagonal form in a common basis, or they are commutative $\boldsymbol{\sigma\varepsilon} = \boldsymbol{\varepsilon\sigma}$. Is this property equivalent to isotropy? Or, in other words:

*Are there any linear elastic* **anisotropic** *materials which preserve the coaxiality of stress and deformation?*

I was relieved to establish that the answer is NO, at least when there is lack of internal stresses. The proof is given in [16].

**7.6.** EXAMPLE E. In a similar manner I have proved that only isotropic materials have an invariant elasticity constant $\nu$ called *Poisson's ratio*, [16]. Both proofs follow from the invariant decompositions of Hooke's tensors presented in Part I.

**7.7.** EXAMPLE F. Let us take an example that looks a bit more sophisticated. Let us introduce the main tensor of the theory of elastic waves – *Christoffel's tensor* $\Lambda(\mathbf{n})$

$$\rho\Lambda(\mathbf{n}) \equiv \mathbf{nSn}, \qquad \rho\Lambda_{ij} = S_{pijq}n_p n_q . \tag{7.6}$$

It defines the triple of plane elastic waves that can propagate in the direction $\mathbf{n}$, $\mathbf{n}\cdot\mathbf{n} = 1$. The displacement vectors accompanying these waves are mutually orthogonal, while the phase velocities are $v_1, v_2, v_3$. It is not difficult to demonstrate that

$$\operatorname{tr}\Lambda(\mathbf{n}) = v_1^2 + v_2^2 + v_3^2 . \tag{7.7}$$

Neighbours [17] have demonstrated a long time ago that in cubic crystals, as in an isotropic body, the sum of squares of phase velocities does not depend on the direction of propagation $\mathbf{n}$ (this directly follows, after all, from the formulae in Examples 3) Question:

*Is this property the case for other materials?*

YES. By using the invariant decomposition (7.3), Part I, one can demonstrate that $v_1^2 + v_2^2 + v_3^2 = \text{const}$ for all materials with the stiffness

$$\mathbf{S} = \mathbf{S}^{is} + \mathfrak{m} \times (\mathbf{1}\otimes\boldsymbol{\gamma} + \boldsymbol{\gamma}\otimes\mathbf{1}) + \mathbf{D}, \tag{7.8}$$

where $\mathfrak{m} = 5 - 4\mathfrak{c}$.

**7.8.** EXAMPLE G. Let us finish with a neat example. As regards the first and simplest property of a solid body, taught at secondary schools (at least in Europe, as to my knowledge), is the elasticity modulus. At the more advanced stages of education this is called the *Young modulus in direction* $\mathbf{n}$ defined by the formula

$$E(\mathbf{n}) = [(\mathbf{n}\otimes\mathbf{n})\cdot\mathbf{C}\cdot(\mathbf{n}\otimes\mathbf{n})]^{-1} . \tag{7.9}$$

It determines the stiffness of a thin fibre (thin bar), cut out from an elastic body, with compliance $\mathbf{C}$, in direction $\mathbf{n}$, under tension $\boldsymbol{\sigma} = s\,\mathbf{n}\otimes\mathbf{n}$.

For an isotropic body $E(\mathbf{n})$ is independent of the direction $\mathbf{n}$, hence $E$ is an invariant – a true elasticity constant, called simply the *Young modulus* of the isotropic material in question. For an anisotropic body one should rather not expect that such a constant exists. More interesting becomes our next off-beat question:

> *Are there any* **anisotropic** *bodies,* $\mathbf{C}^{an} \neq 0$, *having yet the invariant Young modulus, i.e. the bodies with fibres of equal stiffness,*

$$E(\mathbf{n}) = E = \text{const} \qquad \text{for all} \quad \mathbf{n}? \tag{7.10}$$

A closer look at the invariant decomposition (7.4), Part I, and formula (7.9) demonstrarte that the answer is YES! Indeed, the tensor $\mathbf{n}\otimes\mathbf{n}\otimes\mathbf{n}\otimes\mathbf{n}$ is orthogonal to the part $\mathrm{t} \times (\mathbf{1}\otimes\boldsymbol{\beta} + \boldsymbol{\beta}\otimes\mathbf{1})$ of the tensor $\mathbf{C}$. Thus, for $E(\mathbf{n}) = \text{const}$ it is sufficient that

$$\mathbf{C} = \mathbf{C}^{is} + \mathrm{t} \times (\mathbf{1}\otimes\boldsymbol{\beta} + \boldsymbol{\beta}\otimes\mathbf{1}) \,. \tag{7.11}$$

A proof of the necessity of this form and a detailed description of this type of anisotropy can be found in [15].

**7.9.** By using the technique of invariant decompositions of Hooke's tensors we have demonstrated that there are broad classes of **anisotropic** materials of any marked anisotropy, which, in certain conditions, behave just as if they were **isotropic** ones.

This was a deliberate intellectual provocation. Were these thoughts to be elaborated on, a different broader problem could be formulated. This would be *the issue of distinguishability and indistinguishability of the classes of anisotropy in fixed classes of actions.* This immediately leads to another problem of the *choice of anisotropy type* adapted to the prevailing mode of the predicted work of the material being designed. Another group of problems follows from the choice of strategy of experimental *identification* of a Hooke's tensor when there is no preliminary, given *a priori*, information, e.g. information on the structure of the material in question. Finally, as a matter of course, there come several natural ideas of transposing the ideas developed herein onto non-linear elasticity and non-elasticity. Each of these subjects calls for a separate study.

## References

1. J. RYCHLEWSKI, *A qualitative approach to Hooke's tensors. Part I*, Arch. Mech., **52**, 4–5, 737–759, 2000.

2. J. RYCHLEWSKI, *Elastic energy decomposition and the limit criteria*, Uspekhy Mekh. (Advances in Mechanics), **7**, 3, 51–80, 1984.

3. J. RYCHLEWSKI, *On Hooke's law*, PMM, **48**, 420–433, 1984, (English translation Prikl. Matem. Mekhan., **48**, 303–314, 1984).

4. J. RYCHLEWSKI, *Unconventional approach to linear elasticity*, Arch. Mech., **47**, 2, 149–171, 1995.

5. J. RYCHLEWSKI, *Zur Abschätzung der Anisotropie*, ZAMM, **65**, 256–258.

6. F. I. FEDOROV, *Theory of elastic waves in crystals*, Nauka, Moscow 1965, (English ed. Plenum Press, New York 1968).

7. S. SUTCLIFFE, *Spectral decomposition of the elasticity tensor*, Trans. ASME J. Appl. Mech., **59**, 762–773, 1992.

8. A. BLINOWSKI, J. RYCHLEWSKI, *Pure shears in the mechanics of materials*, Mat. Mech. of Solids, **4**, 471–503, 1998.

9. S. FORTE, M. VIANELLO, *Symmetry classes for elasticity tensors*, J. of Elasticity, **43**, 81–108, 1996.

10. A. BLINOWSKI, J. OSTROWSKA-MACIEJEWSKA, J. RYCHLEWSKI, *Two-dimensional Hooke's tensors isotropic decomposition, effective symmetry criteria*, **48**, 2, 325–345, 1996.

11. G. BACKUS, *A geometrical picture of anisotropic elastic tensors*, Reviews of Geophysics and Space Physics, **8**, 633–671, 1970.

12. J. RYCHLEWSKI, *Elastic waves under unusual anisotropy*, J. Mech. Phys. Solids, (in print).

13. YU. I. SIROTIN, M. P. SHASKOLSKAYA, *Foundations of Crystal Physics*, Nauka, Moscow 1979 (2d ed.).

14. J. RYCHLEWSKI, *Anisotropic materials with invariant Kirchhoff shear modulus* (in print).

15. J. RYCHLEWSKI, *Anisotropic materials with invariant Young modulus* (in print).

16. J. RYCHLEWSKI, *Immanent properties of elastic isotropy* (in print).

17. J. R. NEIGIBOURS, *An approximation method for determining the elastic constants of single crystals*, J. Acoust. Soc. Am., **26**, 865–869, 1954.

*Received September 11, 2000.*

Arch. Mech., **53**, 1, pp. 65–85, 2001

# An orthotropic constitutive model for secondary creep of ice

R. STAROSZCZYK

*Polish Academy of Sciences*
*Institute of Hydroengineering*
*ul. Waryńskiego 17, 71–310 Szczecin, Poland*
*e-mail: rstar@hydros.ibwpan.szczecin.pl*

As POLYCRYSTALLINE ICE undergoes creep deformation over long time-periods, it develops a fabric (oriented structure) and associated, strain-induced anisotropy. In the paper, a frame-indifferent orthotropic constitutive model for secondary creep of ice is formulated, in which the strain-rate is expressed in terms of the deviatoric stress, strain, and three structure tensors based on the principal deformation axes. As an illustration, the model is used to determine the evolution of the creep response of ice to continued uniaxial compression and simple shearing.

**Key Words**: ice, creep, induced anisotropy, orthotropy, constitutive law.

## Notations

| | |
|---|---|
| $\mathbf{B}$ | left Cauchy-Green deformation tensor |
| $b_r$ $(r = 1, 2, 3)$ | principal values of the deformation tensor $\mathbf{B}$ |
| $\mathbf{D}$ | strain-rate tensor |
| $E_a$ | axial enhancement factor |
| $E_s$ | shear enhancement factor |
| $\mathbf{e}^{(r)}$ $(r = 1, 2, 3)$ | unit vectors of the principal stretch axes |
| $\mathbf{F}$ | material deformation gradient tensor |
| $h$ | material response function |
| $\mathbf{I}$ | unit tensor |
| $J_k$ $(k = 1, \ldots, 21)$ | invariants of second-order tensors |
| $K$ | trace of the deformation tensor $\mathbf{B}$ |
| $\mathbf{M}^{(r)}$ $(r = 1, 2, 3)$ | structure tensors |
| $Q, q$ | material response functions |
| $\mathbf{R}$ | rotation tensor |
| $\mathbf{S}$ | deviatoric Cauchy stress tensor |
| $\mathbf{V}$ | left stretch tensor |
| $\mathbf{v}$ | velocity vector |
| $x_i$ $(i = 1, 2, 3)$ | spatial rectangular Cartesian co-ordinates |
| $X_i$ $(i = 1, 2, 3)$ | material rectangular Cartesian co-ordinates |
| $\eta_0$ | isotropic ice fluidity |
| $\eta_a$ | axial fluidity |
| $\eta_s$ | shear fluidity |
| $\kappa$ | shear strain |
| $\lambda_r$ $(r = 1, 2, 3)$ | principal stretches |

| | |
|---|---|
| $\mu_0$ | isotropic ice viscosity |
| $\sigma$ | Cauchy stress tensor |
| $\phi_j \ (j,\ldots,12)$ | material response functions |

## 1. Introduction

ICE CAPS COVER approximately 15 million square kilometres of Earth's land in Antarctica and Greenland and, subject to seasonal variations, about 18 to 23 million square kilometres of Arctic and Antarctic waters. The presence of such huge masses of ice affects the thermodynamics of both the atmosphere and ocean and has a considerable impact on the global climate. In order to properly describe the processes taking place in polar regions, e.g. for predicting the climate changes in the future, it is necessary to understand the mechanical behaviour of ice and, in particular, to formulate adequate constitutive relations that are capable of capturing the observed behaviour of ice, both on large and small scales.

Ice is a complex material. In natural conditions it usually exists at high homologous temperatures (that is close to the melting point on the absolute temperature scale), therefore its behaviour resembles very much the behaviour of many metals and rocks prior to melting. Ice displays a wide range of mechanical responses that include: pure elasticity, nonlinear viscoelasticity (decelerating primary creep, also referred to as transient creep or delayed elasticity), and irreversible secondary ("steady-state") and tertiary (accelerating) creeps. The latter two types of creep, characteristic for the ductile behaviour of ice, occur at relatively low stress levels. At high stresses and strain-rates, the ice changes considerably its behaviour and becomes a very brittle material (more brittle than, for instance, glass).

In this paper we concentrate on secondary creep of ice, as this deformation mechanism dominates the flow of polar ice masses, and is also important in sea ice applications (since usually during this stage of deformation, a floating ice cover sustains maximum stresses, and hence for these stresses engineering structures are to be designed). An important process associated with the irreversible creep of ice is the formation and subsequent evolution of anisotropy in an initially isotropic material when it is subjected to changing stress and deformation. Such a phenomenon, known as induced anisotropy, is of crucial importance in the case of polar ice. As ice cores drilled at different sites in Antarctica and Greenland have shown (GOW and WILLIAMSON [7], RUSSELL-HEAD and BUDD [15], THORSTEINSSON *et al.* [21]), polar ice reveals strong fabrics, shown by significant alignment of individual ice crystal $c$-axes along some preferential directions, developing as ice descends from the free surface to depth in an ice sheet. The anisotropy of the medium affects considerably the flow of polar ice masses, what has been proved by the results of numerical simulations carried

out by MANGENEY *et al.* [10], MANGENEY *et al.* [11], and STAROSZCZYK and MORLAND [19]. In the case of sea ice, due to relatively short time-scales (years compared with thousands of years for polar ice), the process of fabric evolution plays a negligible role. Nonetheless, the constitutive relations developed for anisotropic polar ice can still be used for describing sea ice behaviour, since this type of ice is usually anisotropic (most often transversely isotropic) from the very moment of its origin. The macroscopic anisotropy of ice is due to underlying processes occurring in the material on the micro-scale of individual ice crystals, as the latter are very strongly anisotropic: shear stresses applied in planes normal to the crystal basal plane give strain-rates up to two orders of magnitude higher than the strain-rates resulting from shearing performed in planes parallel to the basal plane (PATERSON [14]). The main microscopic processes involved in the creation and evolution of the anisotropic fabric in ice are: (1) the rotation of crystal $c$-axes towards principal axes of compression and away from principal axes of extension, and (2) the process of rotation recrystallisation (or polygonisation), in which new ice grains with orientations similar to old grains are created (LLIBOUTRY and DUVAL [9]).

In order to construct macroscopic constitutive equations for polycrystalline ice, three different methods can be applied. The first method is to derive an average response of an ice aggregate from the properties of individual grains and assumptions on crystal interactions (AZUMA [1], VAN der VEEN and WHILLANS [22], CASTELNAU *et al.* [4]). Since this method, which can be called a discrete-grain approach, requires that the behaviour of several hundred grains at a given material point is followed to yield the macroscopic response, the constitutive theories of this type can be hardly implemented in current large-scale ice sheet numerical models.

Therefore, in order to significantly reduce the number of variables involved in the description of ice fabric, a group of micro-macroscopic models have been developed (LLIBOUTRY [8], SVENDSEN and HUTTER [20], MEYSSONNIER and PHILIP [12], GÖDERT and HUTTER [6], GAGLIARDINI and MEYSSONNIER [5]). In these models the polycrystalline aggregate is treated as a continuum, whose directional properties are described in terms of a so-called orientation distribution function (ODF), defining continuous weightings to the grain $c$-axes orientations in space. Unlike the discrete-grain models, in which the behaviour of each grain has to be considered, in the micro-macroscopic approach the evolution of only a few functions has to be followed at each node of an ice sheet model.

The third method is to assume that the macroscopic response of ice can be described in terms of the fabric induced entirely by macroscopic deformation, and to ignore all microscopic processes taking place at the crystal level. This leads to a phenomenological model formulated by MORLAND and STAROSZCZYK [13] and further extended by STAROSZCZYK and MORLAND [18]. The adopted assumption

that the induced anisotropy of ice depends only on the current macroscopic strain and does not depend on the deformation history is a significant simplification, since, in general, the fabric evolution is a path-dependent process. Nevertheless, the model allows a good agreement with observations and its predictions correlate well with the results given by the discrete-grain and micro-macroscopic models (STAROSZCZYK and GAGLIARDINI [17]). It is also believed that such an approximation provides the simplest approach to an evolving anisotropic flow law which can be tractable in large-scale ice sheet dynamics, since it requires that only current deformation gradients are calculated in addition to the velocity and stress fields.

The orthotropic constitutive law formulated by STAROSZCZYK and MORLAND [18] expresses the deviatoric stress in terms of the strain-rate, strain, and three structure tensors defined by the outer products of three orthogonal vectors along the current principal stretch axes. In the present work we formulate an inverse orthotropic flow law, in which the strain-rate is expressed in terms of the stress and deformation. Such a form of the flow law is a conventional glaciology form, despite the fact that it is less useful in applications, as it is more convenient to use with the momentum balance equations the stress – strain-rate form of the constitutive relation. However, it is possible that the inverse form will reveal different features which can improve correlations with experimental data.

The proposed law is derived from a general, frame-indifferent, orthotropic tensor representation given by BOEHLER [2]. The general law is subsequently reduced by retaining only those tensor generators which contribute to viscous responses that can be detected by simple shearing performed in different directions on different planes. Apart from three structure tensors, needed to describe the orthotropic symmetries in the material, the model involves two material response functions with dependence on the principal stretches and an invariant measure of total deformation. These functions are constructed by correlating the predicted model response with the observed limit behaviour of ice at large strains. The constitutive theory is then used to illustrate the evolution of the creep response of an initially isotropic sample of ice during indefinite uniaxial compression and simple shearing.

## 2. General orthotropic constitutive law

Newly formed compacted polar ice is assumed to be macroscopically isotropic due to the random distribution of individual crystals in the material. As the polycrystalline aggregate starts to deform, all crystal glide planes move in such a way that the crystal $c$-axes (the axes which are orthogonal to the grain basal planes) are rotated towards principal compression axes and away from principal exten-

sion axes. This movement of glide planes leads to the formation of an orthotropic fabric in the material, with orthotropic symmetry axes coinciding with the initial principal stretch axes. It is supposed that, due to the symmetric distribution of all glide planes about the principal directions of strain, the reflexional symmetries with respect to the three orthogonal principal stretch planes are maintained throughout the whole process of deformation, even though the orientations of the principal stretch axes change as the material creeps. Since the ice crystal basal planes are those planes over which the material can shear most easily, this implies that macroscopic shearing on the principal stretch planes should have ease of shearing, with fluidities (reciprocal viscosities) ordered by the respective magnitudes of normal compressions (the inverse stretches). Furthermore, the relative magnitudes of such fluidities should depend on, at least, the principal stretches. Therefore, the constitutive flow law should include the dependence on at least the principal stretches as arguments of the response functions, or more generally, on the deformation. The most simple approach which captures an evolving orthotropic fabric is then to relate the strain-rate to the Cauchy deviatoric stress and strain. As a deformation measure we adopt here the left Cauchy-Green deformation tensor which, like the Cauchy stress tensor and the strain-rate tensor, is a frame-indifferent quantity and as such can be used in an objective constitutive equation.

Let $Ox_i$ $(i = 1, 2, 3)$ be the spatial rectangular Cartesian co-ordinates, $OX_i$ $(i = 1, 2, 3)$ particle reference co-ordinates, and $v_i$ – the components of the velocity vector $\mathbf{v}$. Then the material deformation gradient $\mathbf{F}$ and strain-rate $\mathbf{D}$ have the components

$$F_{ij} = \frac{\partial x_i}{\partial X_j}, \qquad D_{ij} = \frac{1}{2}\left(\frac{\partial v_i}{\partial x_j} + \frac{\partial v_j}{\partial x_i}\right). \tag{2.1}$$

By the polar decomposition theorem (SPENCER [16]), the deformation gradient tensor $\mathbf{F}$ can be expressed in the form

$$\mathbf{F} = \mathbf{VR}, \tag{2.2}$$

where $\mathbf{R}$ is the rotation tensor and $\mathbf{V}$ is the left stretch tensor. The principal stretches $\lambda_r$ $(r = 1, 2, 3)$ along the principal stretch axes defined by the unit vectors $\mathbf{e}^{(r)}$ $(r = 1, 2, 3)$ are given by

$$\mathbf{V}\mathbf{e}^{(r)} = \lambda_r \mathbf{e}^{(r)}, \qquad \det(\mathbf{V} - \lambda_r \mathbf{I}) = 0, \tag{2.3}$$

where $\mathbf{I}$ is the unit tensor. The left Cauchy-Green deformation tensor $\mathbf{B}$ and its principal values $b_r$, equal to the squares of the principal stretches $\lambda_r$, are defined by

$$\mathbf{B} = \mathbf{V}^2 = \mathbf{F}\mathbf{F}^T, \quad \mathbf{B}\mathbf{e}^{(r)} = b_r \mathbf{e}^{(r)}, \quad \det(\mathbf{B} - b_r \mathbf{I}) = 0, \quad b_r = \lambda_r^2. \tag{2.4}$$

The three structure tensors, needed to describe the orthotropy of the material, are defined by the outer products of the principal stretch unit vectors by

$$\mathbf{M}^{(r)} = \mathbf{e}^{(r)} \otimes \mathbf{e}^{(r)}, \quad (r = 1,2,3), \quad \mathbf{M}^{(1)} + \mathbf{M}^{(2)} + \mathbf{M}^{(3)} = \mathbf{I}. \tag{2.5}$$

By ice incompressibility, a common glaciology approximation, we have

$$\mathrm{div}\mathbf{v} = 0, \quad \det \mathbf{F} = \lambda_1\lambda_2\lambda_3 = \det \mathbf{B} = b_1 b_2 b_3 = 1, \tag{2.6}$$

with $\lambda_1 = \lambda_2 = \lambda_3 = 1$ and $b_1 = b_2 = b_3 = 1$ in an undeformed isotropic state $\mathbf{F} = \mathbf{I}$ or in a rigid rotation motion $\mathbf{F} = \mathbf{R}$. The deviatoric Cauchy stress $\mathbf{S}$ is defined in terms of the Cauchy stress $\boldsymbol{\sigma}$ and the mean pressure $p$ by

$$\mathbf{S} = \sigma + p\mathbf{I}, \qquad p = -\frac{1}{3}\mathrm{tr}\sigma, \quad \mathrm{tr}\mathbf{S} = 0, \tag{2.7}$$

where $\mathrm{tr}\sigma$ denotes the trace of $\sigma$. Due to ice incompressibility, $p$ is a workless constraint not given by a constitutive law, but determined by the momentum balance and boundary conditions.

Any constitutive relation should satisfy the principle of frame-indifference, or objectivity, to ensure that material properties are independent of the observer. Here we are concerned with a frame-indifferent law that relates one symmetric tensor (strain-rate $\mathbf{D}$) to other two symmetric tensors (the deviatoric stress $\mathbf{S}$ and the deformation $\mathbf{B}$). For such a constitutive law the general orthotropic representation, given by BOEHLER [2], is

$$\begin{aligned}\mathbf{D} = \sum_{r=1}^{3} [\phi_r \mathbf{M}^{(r)} + \phi_{r+3}(\mathbf{M}^{(r)}\mathbf{S} + \mathbf{S}\mathbf{M}^{(r)}) + \phi_{r+6}(\mathbf{M}^{(r)}\mathbf{B} + \mathbf{B}\mathbf{M}^{(r)})] \\ + \phi_{10}\mathbf{S}^2 + \phi_{11}\mathbf{B}^2 + \phi_{12}(\mathbf{B}\mathbf{S} + \mathbf{S}\mathbf{B}),\end{aligned} \tag{2.8}$$

where the 12 response coefficients $\phi_i$ $(i = 1, \ldots, 12)$ are the functions of the 19 invariants formed from the tensors $\mathbf{M}^{(r)}$, $\mathbf{S}$ and $\mathbf{B}$:

$$\begin{aligned} J_r &= \mathrm{tr}\mathbf{M}^{(r)}\mathbf{S}, \qquad J_{r+3} = \mathrm{tr}\mathbf{M}^{(r)}\mathbf{B}, \quad J_{r+6} = \mathrm{tr}\mathbf{M}^{(r)}\mathbf{S}^2, \\ J_{r+9} &= \mathrm{tr}\mathbf{M}^{(r)}\mathbf{B}^2, \quad J_{r+12} = \mathrm{tr}\mathbf{M}^{(r)}\mathbf{S}\mathbf{B} \quad (r = 1,2,3), \\ J_{16} &= \mathrm{tr}\mathbf{B}\mathbf{S}^2, \qquad J_{17} = \mathrm{tr}\mathbf{B}^2\mathbf{S}, \quad J_{18} = \det \mathbf{S}, \quad J_{19} = \det \mathbf{B}. \end{aligned} \tag{2.9}$$

Due to the constraints that the strain-rate tensor $\mathbf{D}$ has zero trace and the material is incompressible, only 11 coefficients $\phi_i$ are independent, and only 18 invariants are nontrivial, as $J_{19} = \det \mathbf{B} = 1$. Since we suppose that in any state the strain-rate $\mathbf{D}$ vanishes when the deviatoric stress $\mathbf{S}$ vanishes, we require that the coefficients $\phi_1$, $\phi_2$, $\phi_3$, $\phi_7$, $\phi_8$, $\phi_9$, $\phi_{11}$ vanish when $\mathbf{S}$ vanishes; that is, when the invariants $J_1$, $J_2$, $J_3$, $J_7$, $J_8$, $J_9$, $J_{13}$, $J_{14}$, $J_{15}$, $J_{16}$, $J_{17}$, $J_{18}$ vanish.

The general constitutive model defined by equation (2.8), with 11 independent response functions and 18 invariants as their possible arguments, is far beyond the theory that can be correlated with available experimental data. Therefore, the relation (2.8) has to be significantly simplified by reducing the number of the functions $\phi_i$ and the invariants $J_k$. This needs to be done in such a way that the main features of the observed creep response of ice are still captured by a reduced model, and all the model coefficients can be determined from a limited number of simple laboratory tests, most commonly uniaxial compression and simple shearing. In order to simplify the general orthotropic relation (2.8) we follow here a method proposed by MORLAND and STAROSZCZYK [13, 18], based on the concept of so-called instantaneous directional viscosities that can be measured in a series of simple shear tests carried out on different co-ordinate planes.

Consider distinct axial stretches $\lambda_1, \lambda_2, \lambda_3$ along the fixed co-ordinate axes $x_1$, $x_2$, $x_3$, corresponding to the deformation

$$x_1 = \lambda_1 X_1, \quad x_2 = \lambda_2 X_2, \quad x_3 = \lambda_3 X_3, \quad \lambda_1\lambda_2\lambda_3 = 1, \tag{2.10}$$

where $X_1, X_2, X_3$ are particle co-ordinates in the initial isotropic reference state. The left stretch tensor $\mathbf{V}$, deformation gradient $\mathbf{F}$, rotation tensor $\mathbf{R}$ and the left Cauchy-Green deformation tensor $\mathbf{B}$ are given by

$$\mathbf{V} = \mathbf{F} = \begin{pmatrix} \lambda_1 & 0 & 0 \\ 0 & \lambda_2 & 0 \\ 0 & 0 & \lambda_3 \end{pmatrix}, \quad \mathbf{R} = \mathbf{I}, \quad \mathbf{B} = \begin{pmatrix} \lambda_1^2 & 0 & 0 \\ 0 & \lambda_2^2 & 0 \\ 0 & 0 & \lambda_3^2 \end{pmatrix}. \tag{2.11}$$

The principal stretch axes $\mathbf{e}^{(r)}$ coincide now with the co-ordinate axes, therefore the structure tensors $\mathbf{M}^{(r)}$ $(r = 1, 2, 3)$ are the single diagonal element matrices

$$\mathbf{M}^{(1)} = \begin{pmatrix} 1 & 0 & 0 \\ 0 & 0 & 0 \\ 0 & 0 & 0 \end{pmatrix}, \quad \mathbf{M}^{(2)} = \begin{pmatrix} 0 & 0 & 0 \\ 0 & 1 & 0 \\ 0 & 0 & 0 \end{pmatrix}, \quad \mathbf{M}^{(3)} = \begin{pmatrix} 0 & 0 & 0 \\ 0 & 0 & 0 \\ 0 & 0 & 1 \end{pmatrix}. \tag{2.12}$$

Now remove the stress and strain-rate, so the fabric defined by the current stretches $\lambda_1, \lambda_2, \lambda_3$ is frozen, and consider instantaneous responses to shearings performed in different directions on different co-ordinate planes. For simple shear in the $x_i$ direction on a glide plane normal to the $x_j$ direction $(i \neq j)$, with no summation implied by a repeated suffix, the new deformation field is defined by

$$x_i = \lambda_i X_i + \kappa_{ij} X_j, \quad x_j = \lambda_j X_j, \quad x_k = \lambda_k X_k, \tag{2.13}$$

where $i, j, k$ are distinct permutations of $1, 2, 3$, and $\kappa_{ij}$ is a shear strain. For the shearing occurring in the plane $Ox_ix_j$, all the components of the deviatoric stress

tensor are zero except the symmetric entries $S_{ij}$. Such a stress configuration induces a viscous response, described by (2.8), in which the strain-rate tensor has, in general, three nonzero diagonal components and two nonzero off-diagonal symmetric components $D_{ij}$. Instantaneously, at the frozen values of $\lambda_1$, $\lambda_2$, $\lambda_3$, the tensors $\mathbf{B}$ and $\mathbf{M}^{(r)}$ $(r = 1, 2, 3)$ are given by the diagonal tensors (2.11) and (2.12). The symmetric tensor generators in (2.8) have for $i \neq j$ the following instantaneous $(ij)$ components, equal to the $(ji)$ components:

$$(\mathbf{M}^{(r)}\mathbf{S} + \mathbf{S}\mathbf{M}^{(r)})_{ij} = \begin{cases} S_{ij} & (r = i \text{ or } r = j) \\ 0 & (r \neq i \text{ and } r \neq j) \end{cases}, \tag{2.14}$$

$$(\mathbf{M}^{(r)}\mathbf{B} + \mathbf{B}\mathbf{M}^{(r)})_{ij} = 0, \quad (\mathbf{S}^2)_{ij} = 0, \quad (\mathbf{B}^2)_{ij} = 0, \tag{2.15}$$

$$(\mathbf{B}\mathbf{S} + \mathbf{S}\mathbf{B})_{ij} = (b_i + b_j)S_{ij}\,. \tag{2.16}$$

There are also nonzero diagonal components of the instantaneous strain-rate $\mathbf{D}$, other than those defined above, these are however of no interest at this point, since they cannot be detected in the shearing tests.

The $(ij)$ component $(i \neq j)$ of the constitutive law (2.8) is therefore given by the following relation

$$D_{ij} = [\phi_{i+3} + \phi_{j+3} + (b_i + b_j)\phi_{12}]S_{ij}\,, \tag{2.17}$$

defining an instantaneous fluidity $\eta_{ij}$ (reciprocal viscosity) for shear in the $x_i$ direction on a glide plane normal to the $x_j$ direction by

$$\eta_{ij} = \frac{2D_{ij}}{S_{ij}} = 2[\phi_{i+3} + \phi_{j+3} + (b_i + b_j)\phi_{12}], \tag{2.18}$$

which depends for each $(ij)$ only on the response functions $\phi_{i+3}$, $\phi_{j+3}$ $(i, j = 1, 2, 3)$, and $\phi_{12}$; the other terms in the general law (2.8) do not contribute to the directional fluidities. In view of (2.18), the ratios of the instantaneous directional fluidities are defined by

$$\frac{\eta_{13}}{\eta_{23}} = \frac{\phi_4 + \phi_6 + (b_1 + b_3)\phi_{12}}{\phi_5 + \phi_6 + (b_2 + b_3)\phi_{12}}, \quad \frac{\eta_{12}}{\eta_{13}} = \frac{\phi_4 + \phi_5 + (b_1 + b_2)\phi_{12}}{\phi_4 + \phi_6 + (b_1 + b_3)\phi_{12}}. \tag{2.19}$$

If the values of $b_1$ and $b_2$ are interchanged in the first ratio, for any $b_3$, then that ratio must become $\eta_{23}/\eta_{13}$ with the original values, and, similarly, interchanging the values of $b_2$ and $b_3$ for any $b_1$ in the second ratio, must yield $\eta_{13}/\eta_{12}$ with the original values. Thus $\phi_{12}$ must not change when $b_1$, $b_2$, $b_3$ are permuted, the values of $\phi_4$ and $\phi_5$ are interchanged when $b_1$ and $b_2$ are interchanged, the values of $\phi_5$ and $\phi_6$ are interchanged when $b_2$ and $b_3$ are interchanged, and those of $\phi_4$

and $\phi_6$ when $b_1$ and $b_3$ are interchanged. Therefore, the function $\phi_{12}$ can depend in the frozen fabric only on the combinations of two invariants

$$J_{20} = \sum_{r=1}^{3} J_{r+3} = \mathrm{tr}\mathbf{B}, \quad J_{21} = \sum_{r=1}^{3} J_{r+9} = \mathrm{tr}\mathbf{B}^2, \tag{2.20}$$

while the functions $\phi_4$, $\phi_5$ and $\phi_6$ can have common dependence on $J_{20}$ and $J_{21}$ and common dependence on $J_4 = b_1$, $J_5 = b_2$ and $J_6 = b_3$, respectively.

## 3. Reduced model

Following STAROSZCZYK and MORLAND [18] we consider only those terms in the general constitutive relation (2.8) which contribute to the instantaneous directional fluidities (2.18), that is we retain only the terms with the fabric response functions $\phi_4$, $\phi_5$, $\phi_6$ and $\phi_{12}$. We further assume that the response functions depend on only two invariants of the deformation tensor $\mathbf{B}$, namely $J_{r+3} = b_r$ and $J_{20} = \mathrm{tr}\mathbf{B}$, which constitute a minimum set of invariants the model has to incorporate in order to satisfy the directional fluidity ratios (2.19). Accordingly, we express the response functions by

$$\phi_{r+3}(J_{r+3}, J_{20}, J_{21}) = \frac{\eta_0}{4}\, h(b_r), \quad \phi_{12}(J_{20}, J_{21}) = \frac{\eta_0}{4}\, q(K), \tag{3.1}$$

where $h(b_r)$ and $q(K)$ are single-argument response functions, $K = \mathrm{tr}\mathbf{B} = b_1 + b_2 + b_3 \geq 3$, and $\eta_0 = \eta_0(\mathrm{tr}\mathbf{S}^2, T)$ is the fluidity of isotropic ice, a function of the second invariant of the deviatoric stress $\mathbf{S}$ and temperature $T$. With the definitions (3.1), the reduced orthotropic constitutive model takes the following form:

$$\mathbf{D} = \frac{\eta_0}{4}\Big\{ \sum_{r=1}^{3} h(b_r)[\mathbf{M}^{(r)}\mathbf{S} + \mathbf{S}\mathbf{M}^{(r)} - \frac{2}{3}\mathrm{tr}(\mathbf{M}^{(r)}\mathbf{S})\mathbf{I}] + q(K)[\mathbf{B}\mathbf{S} + \mathbf{S}\mathbf{B} - \frac{2}{3}\mathrm{tr}(\mathbf{B}\mathbf{S})\mathbf{I}]\Big\}, \tag{3.2}$$

where the terms with isotropic tensors are introduced to recover zero trace, noting that the included scalar $(\mathbf{M}^{(r)}\mathbf{S}) = J_r$, and the scalar $\mathrm{tr}(\mathbf{B}\mathbf{S})$ is the sum of $J_{r+12}$. We require that when $\mathbf{B} = \mathbf{I}$, that is when $K = 3$, the relation (3.2) reduces to the isotropic fluid flow law $\mathbf{S} = 2\mu_0\mathbf{D}$, where $\mu_0 = 1/\eta_0$ is the viscosity of isotropic ice; thus

$$h(1) + q(3) = 1. \tag{3.3}$$

By Eq. (3.2), the instantaneous directional fluidity (2.18) becomes

$$\eta_{ij} = \frac{\eta_0}{2}[h(b_i) + h(b_j) + (b_i + b_j)q(K)], \tag{3.4}$$

and since this must remain bounded for any axial stretch $b_r$ increasing indefinitely, we rewrite $q$ and the normalisation (3.3) as

$$q(K) = K^{-1}Q(K), \quad h(1) + \frac{1}{3}Q(3) = 1. \tag{3.5}$$

We now employ the orthotropic constitutive relation (3.2) to simulate the behaviour of ice in simple configurations corresponding to those applied in typical creep tests, and in particular we predict the evolution of axial and shear fluidities during the uniaxial compression and simple shear experiments. In the first test, unconfined compression of an initially isotropic ice sample along, say, the $x_3$ axis, there are equal lateral stretches $\lambda_1 = \lambda_2 > 1$, and, due to the incompressibility condition (2.6), the axial stretch (a compression) is $\lambda_3 = \lambda_1^{-2} < 1$. The deformation field for this configuration is defined by the relations (2.10), and the corresponding deformation tensor $\mathbf{B}$ and the structure tensors $\mathbf{M}^{(r)}$ $(r = 1, 2, 3)$ are given by (2.11) and (2.12), respectively. The deviatoric stress tensor has only diagonal components

$$\mathbf{S} = \begin{pmatrix} S_{11} & 0 & 0 \\ 0 & S_{11} & 0 \\ 0 & 0 & -2S_{11} \end{pmatrix}, \tag{3.6}$$

and the invariants entering (3.2) are

$$\operatorname{tr}(\mathbf{M}^{(1)}\mathbf{S}) = \operatorname{tr}(\mathbf{M}^{(2)}\mathbf{S}) = S_{11}, \quad \operatorname{tr}(\mathbf{M}^{(3)}\mathbf{S}) = -2S_{11}, \tag{3.7}$$

$$\operatorname{tr}(\mathbf{BS}) = 2S_{11}(b_1 - b_1^{-2}),$$

and $K = \operatorname{tr}\mathbf{B} = 2b_1 + b_1^{-2}$. With the above definitions, the constitutive law (3.2) yields the following viscous response of ice in uniaxial compression:

$$\frac{2\mu_0 D_{11}}{S_{11}} = \frac{2\mu_0 D_{33}}{S_{33}} = \frac{1}{3}h(b_1) + \frac{2}{3}h(b_1^{-2}) + \frac{Q(K)}{3K}(b_1 + 2b_1^{-2}) = \frac{\eta_a}{\eta_0}, \tag{3.8}$$

where $\eta_a/\eta_0$ defines the ratio of the fabric induced axial fluidity to isotropic fluidity. BUDD and JACKA [3] have determined experimentally the limit value of this ratio for indefinite axial compression, together with an analogous limit ratio for indefinite shearing in a plane deformation. These limit ratios, commonly described in glaciology as enhancement factors, are used here to determine the limit values of the response functions $h$ and $Q$. Hence, as $b_1 \to \infty$, then $K \sim 2b_1$, and from (3.8) we obtain

$$\frac{\eta_a}{\eta_0} \to \frac{2}{3}h(0) + \frac{1}{3}h(\infty) + \frac{1}{6}Q(\infty) = E_a, \tag{3.9}$$

where $E_a$ is the axial enhancement factor.

Next consider a simple shear test on ice. For more generality, assume that the material is not isotropic at the beginning of shear deformation, that is it has already developed a fabric in a plane creep, the strength of which is described by the principal stretches $\lambda_3 = \lambda_1^{-1}$, $\lambda_2 = 1$. Now let us start shearing in the plane $Ox_1x_3$, driven by a shear stress $S_{13}$. The deformation field is described by

$$x_1 = \lambda_1 X_1 + \kappa X_3, \quad x_2 = X_2, \quad x_3 = \lambda_1^{-1} X_3, \tag{3.10}$$

where $\kappa$ is a shear strain in the plane $Ox_1x_3$. The deformation, deviatoric stress, and strain-rate tensors are now given by

$$\mathbf{B} = \begin{pmatrix} \lambda_1^2 + \kappa^2 & 0 & \lambda_1^{-1}\kappa \\ 0 & 1 & 0 \\ \lambda_1^{-1}\kappa & 0 & \lambda_1^{-2} \end{pmatrix}, \quad \mathbf{S} = \begin{pmatrix} S_{11} & 0 & S_{13} \\ 0 & S_{22} & 0 \\ S_{13} & 0 & S_{33} \end{pmatrix}, \tag{3.11}$$

$$\mathbf{D} = \begin{pmatrix} 0 & 0 & \frac{1}{2}\dot{\gamma} \\ 0 & 0 & 0 \\ \frac{1}{2}\dot{\gamma} & 0 & 0 \end{pmatrix},$$

with $S_{11} + S_{22} + S_{33} = 0$ and $\dot{\gamma} = \lambda_1 \dot{\kappa}$. The principal stretch squares $b_i$, $(i = 1, 2, 3)$, the eigenvalues of $\mathbf{B}$, are

$$b_2 = 1, \quad b_3 = b_1^{-1}, \quad 2b_1 = \lambda_1^2 + \lambda_1^{-2} + \kappa^2 + \sqrt{(\lambda_1^2 + \lambda_1^{-2} + \kappa^2)^2 - 4}\,, \tag{3.12}$$

and the associated principal unit vectors $\mathbf{e}^{(r)}$ are defined by

$$\mathbf{e}^{(2)} = (0, 1, 0), \quad e_2^{(s)} = 0, \quad \lambda_1^{-1}\kappa\, e_1^{(s)} + (\lambda_1^{-2} - b_s)\, e_3^{(s)} = 0, \tag{3.13}$$

$$[e_1^{(s)}]^2 + [e_3^{(s)}]^2 = 1 \quad (s = 1, 3).$$

The structure tensors are given by

$$\mathbf{M}^{(2)} = \begin{pmatrix} 0 & 0 & 0 \\ 0 & 1 & 0 \\ 0 & 0 & 0 \end{pmatrix}, \quad \mathbf{M}^{(s)} = \begin{pmatrix} e_1^{(s)} e_1^{(s)} & 0 & e_1^{(s)} e_3^{(s)} \\ 0 & 0 & 0 \\ e_1^{(s)} e_3^{(s)} & 0 & e_3^{(s)} e_3^{(s)} \end{pmatrix} \quad (s = 1, 3), \tag{3.14}$$

and the invariants are

$$\operatorname{tr}(\mathbf{M}^{(2)}\mathbf{S}) = S_{22}, \quad \operatorname{tr}(\mathbf{M}^{(s)}\mathbf{S}) = S_{11} e_1^{(s)} e_1^{(s)} + S_{22}\, e_3^{(s)} e_3^{(s)} + 2S_{13}\, e_1^{(s)} e_3^{(s)}, \tag{3.15}$$

$$(s = 1, 3), \qquad \operatorname{tr}(\mathbf{BS}) = S_{11}(\lambda_1^2 + \kappa^2 - 1) + S_{33}(\lambda_1^{-2} - 1) + 2S_{13}\lambda_1^{-1}\kappa,$$

$$K = \operatorname{tr}\mathbf{B} = b_1 + 1 + b_1^{-1} = \lambda_1^2 + \lambda_1^{-2} + \kappa^2 + 1.$$

The tensor combinations appearing in (3.2) are defined by

$$\mathbf{M}^{(2)}\mathbf{S}+\mathbf{S}\mathbf{M}^{(2)}-\frac{2}{3}\mathrm{tr}(\mathbf{M}^{(2)}\mathbf{S})\mathbf{I}=\frac{2}{3}\begin{pmatrix}-S_{22}&0&0\\0&2S_{22}&0\\0&0&-S_{22}\end{pmatrix}, \tag{3.16}$$

$$\mathbf{M}^{(s)}\mathbf{S}+\mathbf{S}\mathbf{M}^{(s)}-\frac{2}{3}\mathrm{tr}(\mathbf{M}^{(s)}\mathbf{S})\mathbf{I}=\begin{pmatrix}A_{11}^{(s)}&0&A_{13}^{(s)}\\0&A_{22}^{(s)}&0\\A_{13}^{(s)}&0&A_{33}^{(s)}\end{pmatrix}\quad(s=1,3), \tag{3.17}$$

where

$$A_{11}^{(s)}=\frac{2}{3}\left(2S_{11}e_1^{(s)}e_1^{(s)}-S_{33}e_3^{(s)}e_3^{(s)}+S_{13}e_1^{(s)}e_3^{(s)}\right), \tag{3.18}$$

$$A_{22}^{(s)}=-\frac{2}{3}\left(S_{11}e_1^{(s)}e_1^{(s)}+S_{33}e_3^{(s)}e_3^{(s)}+2S_{13}e_1^{(s)}e_3^{(s)}\right), \tag{3.19}$$

$$A_{33}^{(s)}=\frac{2}{3}\left(-S_{11}e_1^{(s)}e_1^{(s)}+2S_{33}e_3^{(s)}e_3^{(s)}+S_{13}e_1^{(s)}e_3^{(s)}\right), \tag{3.20}$$

$$A_{13}^{(s)}=(S_{11}+S_{33})\,e_1^{(s)}e_3^{(s)}+S_{13}, \tag{3.21}$$

and

$$\mathbf{B}\mathbf{S}+\mathbf{S}\mathbf{B}-\frac{2}{3}\mathrm{tr}(\mathbf{B}\mathbf{S})\mathbf{I}=\begin{pmatrix}C_{11}&0&C_{13}\\0&C_{22}&0\\C_{13}&0&C_{33}\end{pmatrix}\quad(s=1,3), \tag{3.22}$$

with

$$C_{11}=\frac{2}{3}[S_{11}\,(2\lambda_1^2+2\kappa^2+1)-S_{33}\,(\lambda_1^{-2}-1)+S_{13}\,\lambda_1^{-1}\kappa], \tag{3.23}$$

$$C_{22}=-\frac{2}{3}[S_{11}\,(\lambda_1^2+\kappa^2+2)+S_{33}\,(\lambda_1^{-2}+2)+2S_{13}\,\lambda_1^{-1}\kappa], \tag{3.24}$$

$$C_{33}=\frac{2}{3}[-S_{11}\,(\lambda_1^2+\kappa^2-1)+S_{33}\,(2\lambda_1^{-2}+1)+S_{13}\,\lambda_1^{-1}\kappa], \tag{3.25}$$

$$C_{13}=(S_{11}+S_{33})\,\lambda_1^{-1}\kappa+S_{13}\,(\lambda_1^2+\lambda_1^{-2}+\kappa^2). \tag{3.26}$$

In wiev of (3.16), (3.17) and (3.22), the constitutive law (3.2) gives for the shear strain-rate $D_{13}$ the following relation:

$$\begin{aligned}2\mu_0 D_{13}=\frac{1}{2}\,(S_{11}+S_{33})\left[h(b_1)e_1^{(1)}e_3^{(1)}+h(b_1^{-1})e_1^{(3)}e_3^{(3)}+\frac{Q(K)}{K}\,\lambda^{-1}\kappa\right]\\+\frac{1}{2}S_{13}\left[h(b_1)+h(b_1^{-1})+\frac{Q(K)}{K}(\lambda_1^2+\lambda_1^{-2}+\kappa^2)\right],\end{aligned} \tag{3.27}$$

which involves three stress tensor components, $S_{11}$, $S_{33}$, and $S_{13}$. In order to express the shear strain-rate in terms of the shear stress alone, two more equations relating the three stress components are required. These two equations are obtained from (3.2) by determining two axial strain-rate components, say $D_{11}$ and $D_{33}$, and then setting them to zero, since in the simple shear test all the axial strain-rates are zero due to lateral constraints imposed on a sample. Hence, for the axial components, Eq. (3.2) yields

$$
\begin{aligned}
(3.28)\quad 2\mu_0 D_{11} = \frac{1}{3}S_{11}\Big[2h(b_1)e_1^{(1)}e_1^{(1)} + h(1) + 2h(b_1^{-1})e_1^{(3)}e_1^{(3)} \\
+ \frac{Q(K))}{K}(2\lambda_1^2 + 2\kappa^2 + 1)\Big] + \frac{1}{3}S_{33}\Big[-h(b_1)e_3^{(1)}e_3^{(1)} + h(1) - h(b_1^{-1})e_3^{(3)}e_3^{(3)} \\
- \frac{Q(K)}{K}(\lambda_1^{-2} - 1)\Big] + \frac{1}{3}S_{13}\Big[h(b_1)e_1^{(1)}e_3^{(1)} + h(b_1^{-1})e_1^{(3)}e_3^{(3)} \\
+ \frac{Q(K)}{K}\lambda^{-1}\kappa\Big] = 0,
\end{aligned}
$$

$$
\begin{aligned}
(3.29)\quad 2\mu_0 D_{33} = \frac{1}{3}S_{11}\Big[-h(b_1)e_1^{(1)}e_1^{(1)} + h(1) - h(b_1^{-1})e_1^{(3)}e_1^{(3)} \\
- \frac{Q(K)}{K}(\lambda_1^2 + \kappa^2 - 1)\Big] + \frac{1}{3}S_{33}\Big[2h(b_1)c_3^{(1)}e_3^{(1)} + h(1) + 2h(b_1^{-1})e_3^{(3)}e_3^{(3)} \\
+ \frac{Q(K)}{K}(2\lambda_1^{-2} + 1)\Big] + \frac{1}{3}S_{13}\Big[h(b_1)e_1^{(1)}e_3^{(1)} + h(b_1^{-1})e_1^{(3)}e_3^{(3)} \\
+ \frac{Q(K)}{K}\lambda^{-1}\kappa\Big] = 0.
\end{aligned}
$$

Equations (3.28) and (3.29) provide two relations to eliminate $S_{11}$ and $S_{33}$ in terms of $S_{13}$, so that (3.27) becomes a relation between $D_{13}$ and $S_{13}$. The latter relation, expressed in the form $2\mu_0 D_{13}/S_{13} = \eta_s/\eta_0$, describes the evolution of the normalised shear fluidity in terms of the shear strain $\kappa$. In the limit, as $\kappa \to \infty$ with $\lambda_1$ finite, then $b_1 \sim \kappa^2$ and $K \sim \kappa^2$, and, further, $\mathbf{e}^{(1)} \to (1,0,0)$ and $\mathbf{e}^{(3)} \to (0,0,1)$, so Eq. (3.27) implies that

$$
(3.30)\qquad \frac{\eta_s}{\eta_0} \to \frac{1}{2}h(0) + \frac{1}{2}h(\infty) + \frac{1}{2}Q(\infty) = E_s\,,
$$

where $E_s$ is the shear enhancement factor.

The two relations (3.9) and (3.30) express the three limit values of the response functions, $h(0)$, $h(\infty)$ and $Q(\infty)$, in terms of the two enhancement factors

for compression and shear (the other limit value of the function $Q$, at $K = 3$, is defined by Eq. (3.5)). In order to determine uniquely the three limit values we derive a third equation by following STAROSZCZYK and MORLAND [18], who derived a set of equalities and inequalities which should be satisfied by instantaneous directional viscosities $\mu_{ij}$ (reciprocal directional fluidities $\eta_{ij}$ defined by Eq. (3.4), $\mu_{ij} = \eta_{ij}^{-1}$, $i, j = 1, 2, 3$, $i \neq j$). Their relations are based on the assumption that the alignment of ice crystal $c$-axes towards the direction of compression (and away from the direction of extension) depends on the relative magnitudes of the three principal stretches $\lambda_r$ $(r = 1, 2, 3)$. The smaller a given principal stretch is compared to the other two stretches, the stronger is the alignment of $c$-axes towards the direction of this stretch and, therefore, the easier is the crystal basal gliding on the plane normal to this principal stretch axis (that is, the smaller is the corresponding shear viscosity). For any ordering of stretches $\lambda_r$, say $\lambda_1 \geq \lambda_2 \geq \lambda_3$, there are six distinct sets of relative values of $\lambda_r$, and for each of them corresponding relations order $\mu_{12}$, $\mu_{13}$ and $\mu_{23}$ in the co-ordinate frame of the principal stretch axes $\lambda_r$. By using the viscosity relation corresponding to the plane flow, that is when $\lambda_2 = b_2 = 1$, and hence $b_3 = b_1^{-1}$ and $K = b_1 + 1 + b_1^{-1}$, it is possible to relate $Q(K)$ to $h(b_r)$ explicitly; namely by

$$Q(K) = -\frac{K}{b_1 - b_1^{-1}}[h(b_1) - h(b_1^{-1})], \tag{3.31}$$

where

$$2b_1 = K - 1 + \sqrt{(K-1)^2 - 4}\ , \geq 2. \tag{3.32}$$

The limit of (3.31) as $b_1 \to 1$, $K \to 3$, combined with the normalisation $(3.5)_2$, yields

$$h(1) - h'(1) = 1, \tag{3.33}$$

which is a restriction on $h(b_r)$ at $b = 1$. Further, the limit of (3.31) as $b_1 \to \infty$, when $K \sim b_1$, provides the relation

$$h(0) - h(\infty) - Q(\infty) = 0. \tag{3.34}$$

The system of three linear equations (3.9), (3.30) and (3.34) for $h(0)$, $h(\infty)$ and $Q(\infty)$ has a solution

$$h(0) = E_s\,, \quad h(\infty) = 6E_a - 5E_s\,, \quad Q(\infty) = 6(E_s - E_a), \tag{3.35}$$

which, together with the relation (3.33), defines the general properties which the response functions $h(b_r)$ and $Q(K)$ should satisfy in order that the reduced constitutive model (3.2) yields the limit responses observed in uniaxial compression and simple shear tests. More specific properties of the response functions

should, ideally, be inferred from experimental results covering the whole range of axial and shear deformations which an ice sample undergoes as it develops anisotropy from its initial isotropic state, instead of using only the limit viscosities represented by the enhancement factors $E_a$ and $E_s$, as has been done here. Unfortunately, such detailed experimental data are not available yet, therefore we adopt simple monotonic response functions satisfying (3.33) and (3.35) to explore the behaviour of ice as predicted by the orthotropic law (3.2).

## 4. Illustrations

For illustration purposes, the following response function $h(b_r)$ is adopted to investigate the creep behaviour of ice in uniaxial unconfined compression and simple shearing:

$$h(b_r) = h(\infty) - [h(\infty) - h(0)] \exp(-\alpha b_r^m), \quad \alpha > 0, \quad m > 0, \tag{4.1}$$

where $m$ is a free parameter, and $\alpha$ is determined by the restriction (3.33). The other response function, $Q(K)$, is related to $h(b_r)$ by Eq. (3.31). Two kinds of ice are considered: so-called *warm ice* and *cold ice*. The former is the ice which is near the melting point, and the creep behaviour of such ice has been extensively tested at various stress levels by BUDD and JACKA [3]. Their results have shown that warm ice softens very considerably under both the compression and shear, and for large deformations the compression and shear enhancement factors approach the respective values of $E_a \approx 3$ and $E_s \approx 8$. However, it has turned out that in polar ice sheets the creep response of ice to compressive stresses is different from that observed for ice near melting, and its viscosity increases with axial deformation (which means that the enhancement factor for compression is less than unity). Recently, MANGENEY *et al.* [10] suggested the value $E_s \approx 1/3$ for ice near the bottom of the Greenland ice cap, evaluated on the basis of the data provided by THORSTEINSSON *et al.* [21]. The shear enhancement factor for ice at the bottom of the Greenland ice sheet near its divide (centre) has been calculated to be $E_s \approx 2.5$, though it seems that further away from the divide (where shear strains are much larger than at the divide) a higher value is more relevant. Hence, the chosen enhancement factors $E_a$ and $E_s$ for warm and cold ice and the related limit values of the response functions $h$ and $Q$, defined by (3.4), are:

$$E_a = 3, \quad E_s = 8 : \quad h(0) = 8, \quad h(\infty) = -22, \quad Q(\infty) = 30, \tag{4.2}$$

$$E_a = 1/3, \quad E_s = 5 : \quad h(0) = 5, \quad h(\infty) = -23, \quad Q(\infty) = 28. \tag{4.3}$$

Plots of the selected response functions $h(b_r)$ for cold ice (for warm ice they are very similar) are presented in Fig. 1, in which labels indicate the curves

corresponding to the values of the free parameter $m$ in (4.1). The same labelling is applied in subsequent plots illustrating the creep behaviour of ice.

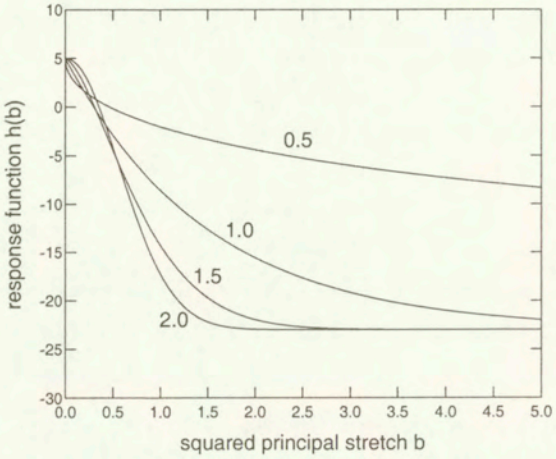


FIG. 1. Adopted forms of the fabric response function $h(b_r)$.

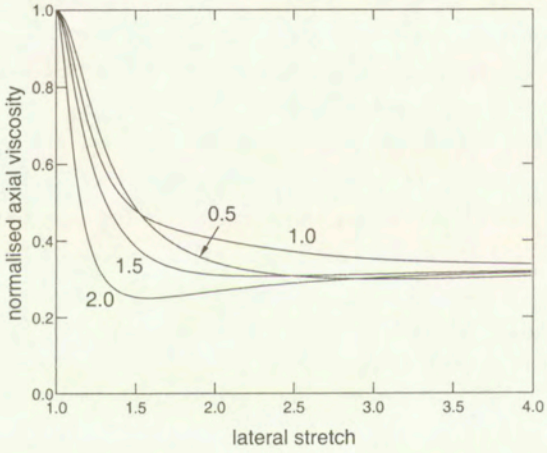


FIG. 2. Evolution of the normalized axial viscosity with increasing stretch $\lambda_1$ in uniaxial compression for different response functions $h(b_r)$ (warm ice).

The results of simulations carried out for warm ice are shown in Figs. 2 and 3. The response of ice to uniaxial compression is illustrated in Fig. 2, in which the evolution of the dimensionless axial viscosity $S_{11}/(2\mu_0 D_{11})$, the reciprocal of the axial fluidity described by Eq. (3.8), is shown for different values of the parameter $m$ in the response function $h(b_r)$. Comparing these results with those given by the stress – strain-rate formulation of the constitutive law (STAROSZCZYK and MORLAND [18]), in which analogous response functions have been applied, we

note that the present model predicts much faster softening of ice (decrease in viscosity with increasing deformation). The results of simple shear simulations are plotted in Fig. 3, illustrating the evolution of shear viscosity $S_{13}/(2\mu_0 D_{13})$, the reciprocal of the shear fluidity calculated from the relations (3.27) – (3.29). Comparison of these results with those obtained from the constitutive model [18] shows again that the inverse constitutive law predicts much faster softening of ice during its shearing, that is the limit shear viscosity defined by the enhancement factor $E_s$ is now much faster approached as the shear deformation, started from an initially isotropic state of ice, proceeds.

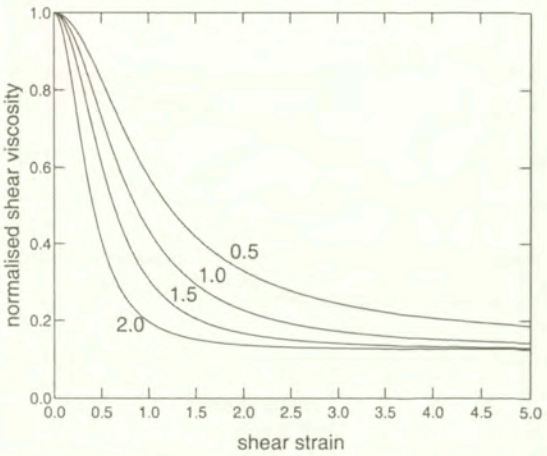


FIG. 3. Evolution of the normalised shear viscosity with increasing strain $\kappa$ in simple shear started from an isotropic state for different response functions $h(b_r)$ (warm ice).

The creep behaviour of cold ice is illustrated in Figs. 4 to 7. Figure 4 shows the evolution of the axial viscosity for different values of the free parameter $m$ in the function (4.1). It is clearly seen that the value of this parameter, particularly for $m \lesssim 1.5$, considerably affects the predicted response of cold ice to compressive stresses. Such sensitivity of the results to the adopted form of the response function, which is an undesirable feature of the constitutive model significantly restricting its flexibility, has not been observed in the case of the stress – strain-rate formulation [18], as shown by the results of simulations for cold ice presented by STAROSZCZYK and GAGLIARDINI [17]. Figure 5 demonstrates the evolution of the normalised shear viscosity of cold ice with increasing strain $\kappa$ started from the isotropic state ($\lambda_1 = \lambda_2 = 1$). Contrary to the uniaxial compression, the results for simple shearing change smoothly with varying values of the free parameter $m$ in the response function (4.1). Comparison of the shear viscosities yielded by the inverse model proposed here with the results predicted by the model [18] and presented in [17], shows that, alike the case of warm ice, the limit shear viscosity

for indefinite shear strain is now approached faster. Additionally, we note that the present constitutive theory leads to the monotonic softening of cold ice with shear strain $\kappa$ increasing from zero at the isotropic state, while the previous stress - strain-rate formulation [18] predicts initial hardening of ice, with maximum shear viscosities occurring at strains $\kappa \sim 1$, followed then by a progressive decrease in ice viscosity until the limit value, defined by the shear enhancement factor, is reached at large strains (STAROSZCZYK and GAGLIARDINI [17]).

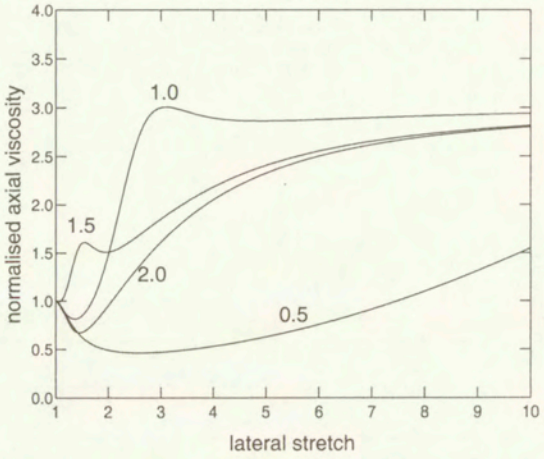


FIG. 4. Evolution of the normalised axial viscosity with increasing stretch $\lambda_1$ in uniaxial compression for different response functions $h(b_r)$ (cold ice).

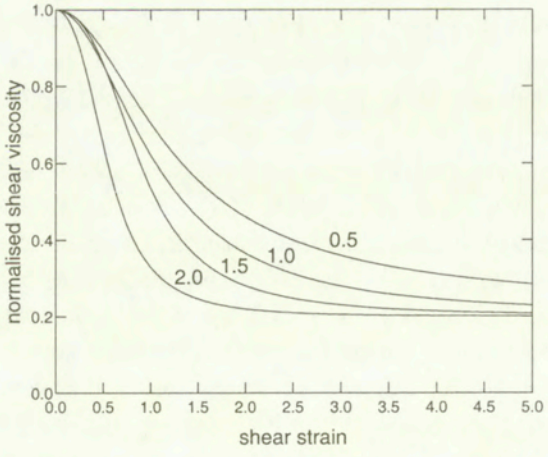


FIG. 5. Evolution of the normalised shear viscosity with increasing strain $\kappa$ in simple shear started from an isotropic state for different response functions $h(b_r)$ (cold ice).

Finally, in Figs. 6 and 7 we illustrate the behaviour of cold ice in simple shearing started from anisotropic states induced by an initial plane compression along the $x_3$ axis, defined by the stretches $\lambda_2 = 1$ and $\lambda_3 \leq 1$. Figure 6 shows, for different values of the free parameter $m$ in the response function $h(b_r)$, the variation of the dimensionless shear viscosity $S_{13}/(2\mu_0 D_{13})$ with the strain $\kappa$ for ice that has been axially pre-compressed to the stretch $\lambda_3 = \lambda_1^{-1} = 0.5$. Corresponding to the previous plot is Fig. 7, in which, for the function $h(b_r)$ with $m = 1$, the evolution of shear viscosity in simple shearing started from different anisotropic states defined by the axial stretches $\lambda_3$ is presented.

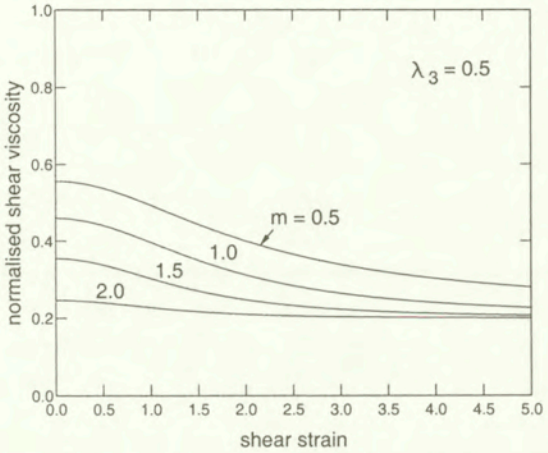


FIG. 6. Evolution of the normalised shear viscosity with increasing strain $\kappa$ in simple shear started from an anisotropic state defined by $\lambda_3 = 0.5$ for different response functions $h(b_r)$ (cold ice).

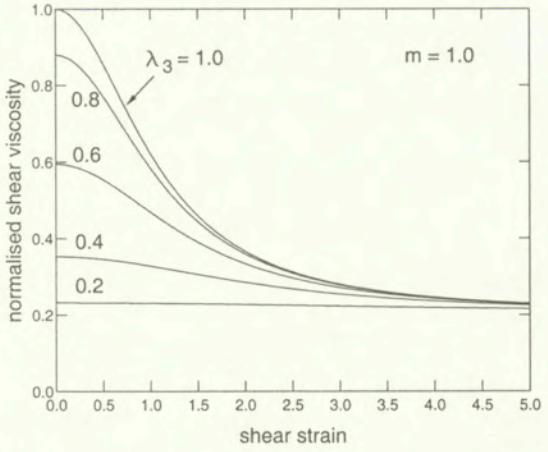


FIG. 7. Evolution of the normalised shear viscosity with increasing strain $\kappa$ in simple shear started from different anisotropic states defined by $\lambda_3$ for the response function $h(b_r)$ with $m = 1.0$ (cold ice).

## 5. Conclusions

In the paper an orthotropic constitutive law for viscous flow of ice has been formulated. The law expresses the strain-rate in terms of the deviatoric Cauchy stress, current deformation, and three structure tensors describing the evolving symmetric properties of the material. Since the results of laboratory tests on ice which have been conducted so far are insufficient to correlate the theory with experiment, simple forms of the response functions have been adopted in order to explore the predictions of the proposed theoretical model. The results of numerical simulations for maintained uniaxial compression and simple shear have been compared with the results given by the analogous stress – strain-rate model (STAROSZCZYK and MORLAND [18]). It has been found that the present strain-rate – stress formulation predicts much faster softening of the material during simple shear for both the warm and cold ice, as well as during uniaxial compression of warm ice. The results for the response of cold ice to uniaxial compression have shown that the present model is more sensitive to the specific forms of the response functions, which renders it less flexible than the former stress – strain-rate form of the law [18]. Before more definite conclusions have been drawn, however, the model response functions need to be correlated with the detailed experimental data once they are available, since at the moment these functions have been constructed only on the basis of the limit viscosities measured for indefinite deformations.

The proposed constitutive model can be used to describe the phenomenon of induced anisotropy in other materials, for which the current response is instantaneously viscous. It also seems that it is relatively simple to incorporate in the model other micro-mechanisms occurring in polycrystalline materials, for instance the process of dynamic (migration) recrystallisation, whose inclusion in discrete-grain or micro-macroscopic models is much more complex than in the case of the continuum approach pursued in this work.

## References

1. N. AZUMA, *A flow law for anisotropic ice and its application to ice sheets*, Earth Planet. Sci. Lett., **128**, 601–614, 1994.

2. J. P. BOEHLER, *Representations for isotropic and anisotropic non-polynomial tensor functions*, [In:] J. P. BOEHLER [Ed.], *Applications of tensor functions in olid mechanics*, 31–53, Springer, Wien 1987.

3. W. F. BUDD and T. H. JACKA, *A review of ice rheology for ice sheet modelling*, Cold Reg. Sci. Technol., **16**, 107–144, 1989.

4. O. CASTELNAU, P. DUVAL, R. A. LEBENSOHN and G. R. CANOVA, *Viscoplastic modeling of texture development in polycrystalline ice with a self-consistent approach: Comparison with bound estimates*, J. Geophys. Res., **101**, (B6), 13851–13868, 1996.

5. O. GAGLIARDINI and J. MEYSSONNIER, *Analytical derivations for the behaviour and fabric evolution of a linear orthotropic ice polycrystal*, J. Geophys. Res., **104**, (B8), 17797–17809, 1999.

6. G. GÖDERT and K. HUTTER, *Induced anisotropy in large ice shields: Theory and its homogenization*, Continuum Mech. Thermodyn., **10**, 5, 293–318, 1998.

7. A. J. GOW and T. C. WILLIAMSON, *Rheological implications of the internal structure and crystal fabrics of the West Antarctic ice sheet as revealed by deep core drilling at Byrd Station*, Geol. Soc. Am. Bull., **87**, 12, 1665–1677, 1976.

8. L. LLIBOUTRY, *Anisotropic, transversely isotropic nonlinear viscosity of rock ice and rheological parameters inferred from homogenization*, Int. J. Plast., **9**, 5, 619–632, 1993.

9. L. LLIBOUTRY and P. DUVAL, *Various isotropic and anisotropic ices found in glaciers and polar ice caps and their corresponding rheologies*, Ann. Gheophys., **3**, 2, 207–224, 1985.

10. A. MANGENEY, F. CALIFANO and O. CASTELNAU, *Isothermal flow of an anisotropic ice sheet in the vicinity of an ice divide*, J. Geophys. Res., **101**, (B12), 28189–28204, 1996.

11. A. MANGENEY, F. CALIFANO and K. HUTTER, *A numerical study of anisotropic, low Reynolds number, free surface flow for ice sheet modeling*, J. Geophys. Res., **102**, (B10), 22749–22764, 1997.

12. J. MEYSSONNIER and A. PHILIP, *A model for tangent viscous behaviour of anisotropic polar ice*, Ann. Glaciol., **23**, 253–261, 1996.

13. L. W. MORLAND and R. STAROSZCZYK, *Viscous response of polar ice with evolving fabric*, Continuum Mech. Thermodyn., **10**, 3, 135–152, 1998.

14. W. S. B. PATERSON, *The physics of glaciers*, Pergamon Press, 2nd, Oxford 1981.

15. D. S. RUSSEL-HEAD and W. F. BUDD, *Ice-sheet flow properties derived from bore-hole shear measurements combined with ice-core studies*, J. Glaciol., **24**, 90, 117–130, 1979.

16. A. J. M. SPENCER, *Continuum Mechanics*, Longman, Harlow 1980.

17. R. STAROSZCZYK and O. GAGLIARDINI, *Two orthotropic models for the strain-induced anisotropy of polar ice*, J. Glaciol., **45**, 151, 485–494, 1999.

18. R. STAROSZCZYK and L. W. MORLAND, *Orthotropic viscous response of polar ice*, J. Engng. Math., **37**, 1–3, 191–209, 2000.

19. R. STAROSZCZYK and L. W. MORLAND, *Plane ice-sheet flow with evolving orthotropic fabric*, Ann. Glaciol., **30**, 93–101, 2000.

20. B. SVENDSEN and K. HUTTER, *A continuum approach for modelling induced anisotropy in glaciers and ice sheets*, Ann. Glaciol., **23**, 262–269, 1996.

21. T. THORSTEINSSON, J. KIPFSTUHL and H. MILLER, *Textures and fabrics in the GRIP ice core*, J. Geophys. Res., **102**, (C12), 26583–26599, 1997.

22. C. J. VAN der VEEN and I. M. WHILLANS, *Development of fabric in ice*, Cold Reg. Sci. Technol., **22**, 2, 171–195, 1994.

*Received September 20, 2000.*

**INSTITUTE OF FUNDAMENTAL TECHNOLOGICAL RESEARCH**
is publishing the following periodicals:

ARCHIVES OF MECHANICS – bimontly (in English)
ARCHIVES OF ACOUSTICS – quarterly (in English)
ARCHIVES OF CIVIL ENGINEERING – quarterly (in English)
ENGINEERING TRANSACTIONS – quarterly (in English)
COMPUTER ASSISTED MECHANICS AND ENGINEERING SCIENCES – quarterly (in English)
JOURNAL OF TECHNICAL PHYSICS – quarterly (in English)

Subscription orders for the journals edited by IFTR may be sent directly to the
Editorial Office
Institute of Fundamental Technological Research,
Świętokrzyska 21, p. 508,
00-049 WARSZAWA, Poland.

## DIRECTIONS FOR THE AUTHORS

The journal *ARCHIVES OF MECHANICS (ARCHIWUM MECHANIKI STOSOWANEJ)* deals with the printing of original papers which should not appear in other periodicals.

As a rule, the volume of a paper should not exceed 40 000 typographic signs, that is about 20 type-written pages, format: 210×297 mm, leaded. The papers should be submitted in two copies. They must be set in accordance with the norms established by the Editorial Office. Special importance is attached to the following directions:

1. The title of the paper should be as short as possible.

2. The text should be preceded by a brief introduction; it is also desirable that a list of notations used in the paper should be given.

3. The formula number consists of two figures: the first represents the section number and the other the formula number in that section. Thus the division into subsections does not influence the numbering of formulae. Only such formulae should be numbered to which the author refers throughout the paper, and also the resulting formulae. The formula number should be written on the left-hand side of the formula; round brackets are necessary to avoid any misunderstanding. For instance, if the author refers to the third formula of the set (2.1), a subscript should be added to denote the formula, viz. $(2.1)_3$.

4. All the notations should be written very distinctly. Special care must be taken to write small and capital letters as precisely as possible. Semi-bold type should be underlined in black pencil. Explanations should be given on the margin of the manuscript in case of special type face.

5. It has been established to denote vectors by semi-bold type. Trigonometric functions are denoted by sin, cos, tg and ctg, inverse functions – by arc sin, arc cos, arc tg and arc ctg; hyperbolic functions are denoted by sh, ch, th and cth, inverse functions – by Arsh, Arch, Arth and Arcth.

6. Figures in square brackets denote reference titles. Items appearing in the reference list should include the initials of the first name of the author and his surname, also the full title of the paper (in the language of the original paper); moreover;

a) In the case of books, the publisher's name, the place and year of publication should be given, e.g.,

5. S. Ziemba, *Vibration analysis*, PWN, Warszawa 1970;

b) In the case of a periodical, the full title of the periodical, consecutive volume number, current issue number, pp. from ... to ..., year of publication should be mentioned; the annual volume number must be marked in black pencil so as to distinguish it from the current issue number, e.g.,

6. M. Sokołowski, *A thermoelastic problem for a strip with discontinuous boundary conditions*, Arch. Mech., **13**, 3, 337–354, 1961.

7. The authors should enclose a summary of the paper. The volume of the summary is to be about 100 words.

8. The authors are kindly requested to enclose the figures prepared on diskettes (format PCX, BitMap or PostScript).

Upon receipt of the paper, the Editorial Office forwards it to the reviewer. His opinion is the basis for the Editorial Committee to determine whether the paper can be accepted for publication or not.

The printing of the paper completed, the author receives 25 copies of reprints free of charge. The authors wishing to get more copies should advise the Editorial Office accordingly, not later than the date of obtaining the galley proofs.

**The papers submitted for publication in the journal should be written in English. No royalty is paid to the authors.**

**Please send us, in addition to the typescript, the same text prepared on a diskette (flopy disk) 3 1/2″ as an ASCII file, preferably in the TEX or LATEX format in Dos or Unix format.**

*EDITORIAL COMMITTEE*
*ARCHIVES OF MECHANICS*
*(ARCHIWUM MECHANIKI STOSOWANEJ)*

Archives of Mechanics

## Contents of issue 1 vol. 53

3 O. GAGLIARDINI, M. ARMINJON and D. IMBAULT, *An inhomogeneous variational model applied to predict the behaviour of isotropic polycrystalline ice*

23 T. LIPNIACKI, *On quantum turbulence in superfluid $^4He$*

45 J. RYCHLEWSKI, *A qualitative approach to Hooke's tensors. Part II*

65 R. STAROSZCZYK, *An orthotropic constitutive model for secondary creep of ice*

Arch. Mech., **53**, nr 1, str. 1–88, Warszawa 2001